Title
Molecular and Functional Characterization of the Developing Respiratory Motor Circuit

Author
Han, Albert Yoon-Kyu

Publication Date
2015

Peer reviewed|Thesis/dissertation

UNIVERSITY OF CALIFORNIA

Los Angeles

Molecular and Functional Characterization of the Developing Respiratory Motor Circuit

A dissertation submitted in partial satisfaction of the requirements for the degree Doctor of Philosophy in Neuroscience

by

Albert Yoon-Kyu Han

2015

ABSTRACT OF THE DISSERTATION

Molecular and Functional Characterization of the

Developing Respiratory Motor Circuit

by

Albert Yoon-Kyu Han

Doctor of Philosophy in Neuroscience

University of California, Los Angeles, 2015

Professor Bennett Novitch, Chair

The faithful and sophisticated control of motor neurons (MNs) allows for our ability to walk, chew, breathe, and speak. This dissertation is focused on the characterization of MNs and the intricate circuitry that are involved in the control of these MNs that surround the airways. The relevance of this study goes beyond satisfying our curiosity of the physiology of breathing. This knowledge is critical in their application in respiratory medicine and speech rehabilitation – as the same set of MNs generate rudimentary vocal sounds in rodents and may provide us with a greater understanding about speech motor pathways in humans.

The dissertation begins with a literature review of principles of circuit assembly predominantly centered in the spinal cord. In Chapter 2, I define the molecular organization of the cranial MNs in the brainstem. Unique transcription factors and guidance cues including Foxp1, Pou3f1, Etv4, and Npn2 label specific cranial motor pools that match previously described motor populations identified by classic retrograde labeling. This molecular definition of cranial motor pools opens up new doors for us to understand their origins to harness the potential for rehabilitation when these MNs are diseased or injured.

In Chapter 3, I demonstrate that the respiratory drive can extend to brachial limb-innervating MNs, a feature normally suppressed by Foxp1. In the absence of Foxp1, the limb-innervating MNs exhibit molecular and anatomical characteristics that resemble that of the thoracic respiratory MNs. The findings of this study provide another compelling evidence that the respiratory motor circuit can integrate MNs out of their usual field of innervation to harbor ectopic respiratory MNs – similar to the respiratory drive crossing the midline in the crossed phrenic phenomenon.

In Chapter 4, through genetic manipulation I show that Pou3f1, a marker for phrenic and other respiratory MN populations, is essential for proper the phrenic nerve branch projection and intercostal cell fate specification. Finally in Chapter 5, I summarize the key findings of my dissertation and discuss the limitations as well as remaining questions. Together, the results presented in my dissertation have a significant impact on our understanding of the respiratory motor pathways, which could be applied for the regeneration of diseased cells or rehabilitation efforts to accelerate the recovery of motor circuitry involved in breathing, speech, and language.

The dissertation of Albert Yoon-Kyu Han is approved.

Jack Feldman

Kelsey Martin

Carlos Portera-Cailliau

V. Reggie Edgerton

Bennett Novitch, Committee Chair

University of California, Los Angeles

2015

DEDICATION PAGE

So the other disciples told him, "We have seen the Lord."

But he said to them, "Unless I see in his hands the mark of the nails,

and place my finger into the mark of the nails,

and place my hand into his side, I will never believe."

John 20:25 (ESV)

To my wife, Rana, and my son, Thomas Taeyong Han

To my parents, Kwanhee and Gyewon Han

TABLE OF CONTENTS

LIST OF FIGURES AND TABLES

ACKNOWLEDGEMENTS

The third chapter in this dissertation is an article currently in preparation for publication, which was authored by Han AY, Kam K, Feldman JL, and Novitch BG, entitled "Respiratory conversion of brachial motor neurons in the absence of Foxp1," and I am indebted to countless individuals who contributed to my dissertation study.

First and foremost, none of this could have been possible without my advisor, Dr. Bennett Novitch. I am very grateful for his dedication, enthusiasm, wealth of knowledge and years of mentorship that shaped me into a scientist. It was through his patience and generosity that I could begin and complete my graduate study. I am also indebted to my collaborating advisor Dr. Jack Feldman, who has taken me in as one of his own- providing me with inspiration and the optimal experiments to study inspiration.

I am also thankful for the scientific feedback and guidance from my committee members- Dr. Carlos Portera-Cailliau, Dr. Jack Feldman, Dr. Kelsey Martin, and Dr. Reggie Edgerton. I was very fortunate to receive advice and support at critical moments in my training, which always steered me into the right direction. I will forever remember their advice as I complete my medical training and beyond. I am especially grateful to Dr. Carlos Portera-Cailliau and Dr. Kelsey Martin whom were generous of their time and in their mentorship as mentors and directors of the Medical Scientist Training Program.

I was extremely privileged to be part of an extraordinary team of many talents during my training. I will remember the help I received from the original four graduate students of the Novitch Lab who helped me get on my feet: Dr. David Rousso, Dr. Katrina Adams, Dr. Zachary Gaber, and Dr. Jennifer Kong. Their peer and scholastic

support kept me motivated during graduate school. I also thank the support I received from other members of the lab: Shanna Swartwood, Amy Hurwitz, Dr. Caroline Pearson, Destaye Moore, Dr. Ken Yamauchi, Jessie Bluth, Jack Hale, Lorenzo del Castillo, and Dr. Momoko Watanabe. In addition, I received tremendous help from Dr. Samantha Butler and her lab members- Supraja Varadarajan, Madeline Andrews, Dan Sivalingam, and Dr. Sandeep Gupta. I am also indebted to many members of the Feldman Lab for teaching me in vivo/in vitro techniques and even collecting data for my studies- Dr. Kaiwen Kam, Dr. Victor Janczewski, Dr. Cindy Yang, Dr. Robert Huckstepp, Dr. David Sherman, Raquel Abreu, Dr. Max Shao, and Grace Li. Last but not least, I had the greatest pleasure working with my undergraduate research assistant Eric Wang. He has contributed an enormous amount to this study and personally helped me to become a better teacher and a mentor.

My interest in science is deeply rooted in my early exposure to the fascinating laws of nature by my parents who are both scientists, Drs. Kwanhee and Gyewon Han. I appreciate their unending love and support during my scientific training. I am also thankful to my best friend and the love of my life, Rana, who I met and married during graduate school. She has been patient with my work schedule and has made tremendous sacrifices so I could complete my studies. I am personally indebted to members of the Grace Stewards for Christ-especially the leaders Dr. Ki-Hyuk Shin and Dr. Sung-Ock Sohn, who are both members of the faculty at UCLA and have shown to me that science and spirituality can be pursued together. I also thank the brothers and sisters of the GSC, Dr. Steve Suh and Jinhee Suh, Dr. Areum Han, and Bumcheol Lee. While the lab has been my second home, the University Presbyterian Church has been the home for my

soul- I appreciate Pastor Soon, SMN Esther, Noah Park, and other brothers and sisters in Christ who helped me to stay spiritually healthy during the times of need. Finally, I thank Guang Zhang who has always been there for me as a friend to share my ups and downs in life since sixteen years ago (and hopefully sixty more years to come). It was due to the help of these many individuals that I could complete my dissertation.

VITA

Albert Yoon-Kyu HAN
(Yoon Kyu HAN)

EDUCATION

08/2007 to 06/2017	David Geffen School of Medicine at UCLA Los Angeles, California Medical Scientist Training Program Interdepartmental Ph.D. Program for Neuroscience
08/2003 to 05/2007	University of California, Berkeley Berkeley, California B.A. in Computer Science, 2007 Highest Honors in Computer Science Highest Distinction in General Scholarship

HONORS AND AWARDS

2013	NIH National Research Service Award Pre-doctoral Fellowship (F31)
2012	Neural Microcircuits Training Program (T32) Broad Stem Cell Research Center Travel Supplemental Award
2011	California Institute for Regenerative Medicine ISSCR Scholarship
2009	Oliver Goldsmith, MD, Scholarship
2009	HHMI Research Fellowship for Medical Students
2008	Korean-American Medical Association Scholarship
2007	Phi Beta Kappa, Upsilon Pi Epsilon
2006	Haas Scholars Program

RESEARCH EXPERIENCE

06/2010 to present	Graduate Student University of California, Los Angeles Laboratory: Bennett G. Novitch, PhD Project: Molecular and functional characterization of the developing respiratory motor circuit
09/2009 to 06/2010	HHMI Medical Student Research Fellow University of California, Los Angeles Laboratory: Mirella Dapretto, PhD

	Project: Neural basis of native and non-native speech perception in children using fMRI
03/2005 to 07/2007	Undergraduate Researcher/Haas Scholar University of California, Berkeley Laboratory: Shaowen Bao, PhD Project: Plasticity of the auditory cortex induced by sensory stimuli

WORK EXPERIENCE

08/2009 to 08/2010	Medical Student Tutor/Learning Skills Counselor David Geffen School of Medicine at UCLA
07/2008 to 06/2010	Medical Student Volunteer Student Founder, Student Chief (07/2008-03/2010) UCLA-Koreatown Clinic, UCLA
08/2006 to 12/2006	Assignment Grader for CS61A Department of Electrical Engineering and Computer Sciences University of California, Berkeley
01/2005 to 05/2007	Student Tutor (computer science and general chemistry) Student Learning Center University of California, Berkeley

PUBLICATIONS

1. **Han AY**, Kam K, Feldman JL, Novitch BG. Respiratory conversion of brachial motor neurons by the removal of Foxp1. (in preparation)
2. **Han YK**, Köver H, Insanally MN, Semerdjian JH, Bao S. Early experience impairs perceptual discrimination. *Nat Neurosci.* 2007 Sep; 10(9):1191-7.

PRESENTATIONS AND ABSTRACTS

1. **Han AY**. Molecular and Functional Characterization of the Developing Respiratory Motor Circuit. The 8th Annual Dynamics of Neural Microcircuits Symposium at UCLA. Invited symposium speaker.
2. **Han YK**, Wang EY, Novitch BG. Identification of Molecules Important for the Development of Respiratory Motor Circuits Using Microarray Analysis. Poster presented at: 10th Annual Meeting of the International Society for Stem Cell Research; 2012 June 13-16; Yokohama, Japan.
3. **Han YK**, Wilson SM, McNealy K, Shih V, Iacoboni M, Dapretto M. Neural Basis of Phoneme Perception in Early Adolescence and Adulthood. Poster presented at: 16th Annual Meeting of the Organization for Human Brain Mapping; 2010 June 5-10; Barcelona, Spain.

4. Kim MJ, Ra H, **Han YK**, Jo AM. Sociodemographic predictors of travel distance to a free UCLA student-staffed clinic. Poster presented at: 26th Annual UCLA Multi-Campus Family Medicine Research Forum; 2010 May 12; Los Angeles, CA.
5. Jung M, Kim J, **Han YK**, Jo AM. Difficulties of seeking medical care among indigent Korean immigrants. Poster presented at: 26th Annual UCLA Multi-Campus Family Medicine Research Forum; 2010 May 12; Los Angeles, CA.
6. **Han YK**, Wilson SM, McNealy K, Iacoboni M, Dapretto M. Left Premotor and Inferior Parietal Cortex Activity in Response to Non-Native Speech Sounds Increases from Childhood to Early Adolescence. Poster presented at: Language: Development & Aging. Cognitive Neuroscience Society 2010 Annual Meeting; 2010 April 17-20; Montréal, QC, Canada.
7. **Han YK**, Choi S, Kim K, Jung M, Son JB, Jo AM. Understanding the health status and needs of indigent immigrants in the Los Angeles area. Paper presented at: 70th Annual Meeting of the Society for Applied Anthropology; 2010 March 24-27; Mérida, México.
8. Jo AM, Yoon DJ, **Han YK**, Lee C, Lee CK, Lee ES, Dowling PT. Working together toward a better community health: Developing and establishing a free community health center in Koreatown. Poster presented at: 25th Annual UCLA Multi-Campus Family Medicine Research Forum; 2009 May 12; Los Angeles, CA.
9. **Han YK**, Son JB, Youn L, Choli S, Jo AM. Understanding health and health care needs of patients accessing UCLA-KRC Community Health Center. Poster presented at: 25th Annual UCLA Multi-Campus Family Medicine Research Forum; 2009 May 12; Los Angeles, CA.

CHAPTER ONE – Mechanisms of motor circuit assembly in the central nervous system

Networks of neural activity in the central nervous system orchestrate our cognitive and motor behaviors. Motor programs initiated from supraspinal areas descend to the lower motor neurons in the brainstem and the spinal cord, which is then modulated by an overbearing sensorimotor feedback. As the final effector of motor control in the central nervous system, this circuitry grounds upon a precise matching between premotor inputs to motor neurons and motor neurons to their muscle target.

I began my work to understand principles of circuit organization in the respiratory motor system, as this circuit has a defined input and output with minimal feedback from the locomotor pathways. At the core of the respiratory motor circuitry, the motor neurons arise from the progenitor domains in the ventricular zone, and they migrate out laterally to form nuclear or columnar organization in the brainstem and the spinal cord, respectively. Dysfunctions or injuries to the motor system have a devastating effect on movement and may result in death. This profound clinical relevance has fueled intense investigation to understand the causes of pathological conditions that impact breathing. In this Chapter, I summarize some of the current state of knowledge regarding the respiratory motor neuron development and the microcircuits controlling this pathway. I propose my two hypotheses- 1. Cranial respiratory motor neurons show conserved molecular organization between mice and humans; 2. The respiratory drive can extend in the rostrocaudal dimension beyond its usual territory. In the remaining chapters, I demonstrate the evidence that support these hypotheses.

INTRODUCTION

Motor neurons (MNs) provide the final output to muscles, which allows us to walk, talk, and express our ideas through written language. MN activity is modulated by intricate microcircuits of interneurons that not only initiates the signal but modulates it by adjusting the strength and the duration of the MNs activity. When either the microcircuit modulating the activity of MNs is disturbed as in Parkinson's disease or presents a disease in the MNs themselves as in amyotrophic lateral sclerosis, the quality of life is severely diminished if not ended. Furthermore, injury to the connections between the premotor microcircuits and the MNs as in spinal cord injury (SCI) can also be devastating to the patient. Indeed, the most frequent class of SCI is incomplete tetraplegia resulting from injuries at the level of the cervical spinal cord, and the most frequent cause of death is pneumonia due to their weakened respiratory motor pathways and their dependence on ventilators (National Spinal Cord Injury Statistical Center, 2011).

Genesis of cranial and spinal motor neurons

In the developing neural tube, multiple morphogens are maintained in a gradient that allows for the identification of an exact location in a three-dimensional space. Two of the most well characterized morphogens are sonic hedgehog (Shh) and the family of bone morphogenetic proteins (BMPs), that are secreted from the floor plate and roof plate of the neural tube, respectively (Jessell, 2000). The level of Shh and BMP creates tiered domains of progenitors in the developing neural tube **(Fig 1-1A)**. One of the domains express oligodendrocyte lineage transcription factor (Olig2), which is named the pMN domain (Novitch, Chen, & Jessell, 2001). All somatic motor neurons emerge from the

pMN domain, where Isl1^{+} branchiomotor and visceral motor neurons of the brainstem arise from the p3 domain **(Fig 1-1B)** (Guthrie, 2007).

In the brainstem, the locations of cranial nuclei are found in the vicinity of outlets of cranial motor nerves. In terrestrial animals, including humans, mice and birds, twelve cranial nerves emerge from the hindbrain region numbered according to the rostral-caudal position from which they emerge **(Fig 1-1D)** (Guthrie, 2007). Among the twelve, cranial nerves III through XII (CNII – CN XII) contain efferent projections from cranial motor neurons towards muscles of the head and neck. Cranial MNs are classified into one of three subtypes- visceral motor, somatic motor, and branchiomotor neurons according to their cell morphology, axonal trajectory, and gene expression patterns **(Fig 1-2C)** (Cordes, 2001). Visceral MNs innervate parasympathetic ganglia of the autonomic nervous system, whereas somatic MNs and branchiomotor neurons (brMNs) innervate skeletal muscles (Chandrasekhar, 2004). Somatic MNs project to muscle derived from paraxial and prechordal mesoderm, which include tongue and ocular muscles innervated by the hypoglossal nerve (XII) and the oculomotor (III), trochlear (IV), and abducens (VI) nerve, respectively.[1] BrMNs innervate muscles of the four branchial arches, which are the evolutionary remnants of the bony structures that support gills in early vertebrates such as fish. Muscles of mastication within the first branchial arch are controlled by the trigeminal motor nucleus (nV). Facial muscles involved in expression of emotion are located in the second branchial arch and are innervated by the facial motor nucleus (nVII) **(Fig 1-1C)**. The muscles of branchial arches 3 and 4, which are involved in deglutition

[1] Roman numerals are used here to denote the cranial nerve, whereas roman numerals followed by the letter "n" denote the motor nucleus that projects out into the cranial nerve (VII vs. nVII)

and vocalization, are innervated by the axons of the nucleus ambiguus, which travel through IX, X, and XI **(Table 1-1)** (Jurgens, 2002; Wetzel, Kelley, & Campbell, 1980).

Cranial motor neurons require much more time for proper maturation compared to spinal motor neurons. For example, on e10 and e11, neuroblasts that will later become facial MNs leave the p3 progenitor domain and migrate caudally and laterally to the ventral surface of the hindbrain (Pierce, 1973). By e15, most branchiomotor neurons have arrived at the facial nucleus, and their motor axons have arrived at target muscles (Ashwell & Watson, 1983). Functional innervation of peripheral targets by facial MNs is thought to occur by e15, due to the presence acetylcholinesterase activity in auricular musculature, one of the several muscles innervated by the facial motor nucleus. The number of facial MNs peaks on e17 and is followed by a rapid two-day decay that results in a loss of 68% by e19. Neuronal degeneration continues, but at a much slower rate, throughout embryonic and postnatal development until P10, at which the facial motor nucleus arrives at a stable population number (Ashwell & Watson, 1983).

Organization of spinal motor neurons

Spinal motor neurons are organized in distinct longitudinal columns through the rostrocaudal axes. There are at least four motor columns in the spinal cord **(Fig 1-2A)**. At the brachial and lumbar levels, four motor columns exist: 1) the lateral motor column (LMC) innervates the limb muscles; 2) the medial motor column (MMC; or formerly known as MMCm) innervates the axial muscles; 3) the hypaxial motor column (HMC; formerly known as MMCl) innervates the muscles of the body wall; and 4) the preganglionic motor column (PGC) innervates the sympathetic ganglia **(Fig 1-2B, D)**.

Foxp1 is known to express at high levels in the LMC and low levels in the PGC (Dasen, De Camilli, Wang, Tucker, & Jessell, 2008; Rousso, Gaber, Wellik, Morrisey, & Novitch, 2008). The motor columns can largely be distinguished by the LIM-homeodomain protein Lhx3. Up till recently, the HMC had been identified by the presence of general motor neuron markers such as Hb9 and Isl1, but with the absence of the expression of Foxp1 and Lhx3. Recent studies identified additional markers of phrenic MNs including POU domain class 3 transcription factor 1 (a.k.a. Oct6 and SCIP), pleiotrophin (Ptn) and others adhesion molecules which show that the phrenic may be a unique motor column in the spinal cord (Machado et al., 2014; Philippidou, Walsh, Aubin, Jeannotte, & Dasen, 2012). Motor columns can be further subdivided into motor pools that innervate muscles of similar function and/or anatomical location (Jessell, 2000; Livet et al., 2002; Vrieseling & Arber, 2006).

Signaling and adhesion molecules in motor circuit assembly

Cell recognition molecules have traditionally been thought as the critical players that allow for specificity in synaptic connectivity. Indeed, adhesion molecules are critical for the clustering of MNs into distinct clusters of motor pools (Astick, Tubby, Mubarak, Guthrie, & Price, 2014; Price, 2012). However, these molecules can also appropriately guide axons to their targets and assist in formation of specific synapses in an activity-independent manner (Sanes & Yamagata, 2009; Shen & Scheiffele, 2010; Williams, de Wit, & Ghosh, 2010). One of the most well studied circuits for determining the mechanisms of circuit assembly of the motor system is the monosynaptic segmental reflex circuit that involves direct and indirect proprioceptive feedback to the motor

neuron from the muscle spindles. Ets variant 4 (Etv4; a.k.a. Pea3) is specifically expressed by caudal cervical motor pools that innervate latissimus dorsi (LD), cutaneous maximus (CM), and pectoralis minor (Pec_{min}) in rostrocaudal order (Caruso et al., 2014; Lamballe et al., 2011). When Etv4 is removed, motor pools fail to acquire certain motor neuron properties including the dendritic patterning and selectivity of proprioceptive afferent connectivity (Vrieseling & Arber, 2006). In addition, a secreted repellent molecule Sema3E was associated with Etv4-expressing motor pool. It was determined that one of the key assignments of molecular mechanism underlying proper reflex circuit is governed by semaphorin and plexin signaling (Pecho-Vrieseling, Sigrist, Yoshida, Jessell, & Arber, 2009). In addition, similar findings were observed for hindlimb motor pools in which attenuation of Plexin activity resulted in aberrant monosynaptic circuit formation (Fukuhara et al., 2013).

Utilization of the positional template in motor circuit assembly

The position of MN soma has an enormous contribution to circuit assembly as well. Similar to the establishment of Shh and other morphogen gradients in early development, other secreted or membrane bound axon guidance cues have been demonstrated to exist in gradients in the developing neural tube (Zlatic, Li, Strigini, Grueber, & Bate, 2009). The premotor interneurons involved in agonist-antagonist muscle control can be identified by their time of neurogenesis and positioned topographically (Tripodi, Stepien, & Arber, 2011). Using conditional Foxp1 removal from motor neurons, it was also found that removal of Foxp1 results in "scrambling" of hindlimb motor neuron identity, which result in aberrant connections of proprioceptive

afferent inputs projecting to predetermined positions in the spinal cord despite the wrong identity and sometimes even in the absence of motor neurons (Surmeli, Akay, Ippolito, Tucker, & Jessell, 2011).

Descending respiratory motor control to motor neurons

In contrast to the segmental reflex circuit, there is a considerable lack of understanding of how the respiratory motor circuit is formed despite the fact that the respiratory motor circuit provides a very unique and defined system to study circuit assembly. Respiratory muscles receive spinal motor input from medulla to the lumbar spinal cord **(Fig 1-3D)**. In the brainstem, two distinct oscillators are found (Feldman, Del Negro, & Gray, 2013). These are the Pre-Bötzinger Complex (preBötC) and retrotrapezoid nucleus and parafacial respiratory group **(Fig 1-3A).** The respiratory interneurons found in the preBötC are Dbx1-lineage, and they express somatostatin (SST), solute carrier family 17, member 6 (Slc16a6; other name: vGlut2), and neurokinin 1 receptor (NK1R) (Gray et al., 2010). The preBötC among other neurons involved in respiratory modulation project to the interneurons in the medulla named the ventral respiratory group (VRG). The VRG is the group of neurons that provide direct projection to the phrenic and other respiratory motor neurons of the spinal cord. Several molecules have been identified in the VRG of the rat, including parvalbumin, enkephalin and reelin **(Fig 1-3B)** (Alheid, Gray, Jiang, Feldman, & McCrimmon, 2002; McCrimmon et al., 2001; Stornetta, Sevigny, & Guyenet, 2003; Tan et al., 2012). However, their contribution in the circuit assembly are yet unclear.

The anatomical blueprint of the connection between VRG and respiratory motor neurons have been well-characterized by tracing studies in several different ways. The first demonstration of the monosynaptic connection between VRG and phrenic MNs was performed by Jack Feldman. In the cat, injection of tritiated amino acids in the VRG revealed a bilateral connection to lamina IX of the spinal cord at the C4 to C6 level and a primarily contralateral projection to laminae VIIII and IX in the thoracic spinal cord **(Fig 1-3B)** (Feldman, Loewy, & Speck, 1985). In the rat and the rabbit, slight ipsilateral dominance is exhibited, whereas there is a contralateral dominance of that in the cat (Ellenberger, Vera, Haselton, Haselton, & Schneiderman, 1990). In addition, a small portion of VRG axons cross at the segmental level (H. G. Goshgarian, Ellenberger, & Feldman, 1991). The descending pathway for the phrenic premotor axons is via the lateral funiculus and the ventral funiculus; the descending fibers to the intercostal MNs in the thoracic is restricted to the ventral funiculus (Dick, Jodkowski, Viana, & Berger, 1988; Feldman et al., 1985; Sasaki & Uchino, 1995). For abdominal MNs, expiratory bulbospinal neurons provide the temporal pattern while other inputs determine the degree in which the muscles are activated (Road, Ford, & Kirkwood, 2013).

The bulbospinal pathway providing premotor control of phrenic MN activity therefore has a monosynaptic component directly to motor neuron dendrites and cell soma from electron microscopy (Ellenberger, Feldman, & Goshgarian, 1990). In transneuronal tracing, the majority of the excitatory inspiratory premotor neurons were found in DRG and rVRG (Cohen, 1981; Dobbins & Feldman, 1994; Lois, 2008; Miller, Bianchi, & Bishop, 1997). cVRG is known to be involved in expiration, and it was least connected to the diaphragm among the known respiratory groups (Arita, Kogo, &

Koshiya, 1987; Lois, 2008). The existing cVRG connection is by polysynaptic connection via respiratory interneurons in cervical levels to the diaphragm (Feldman et al., 1985; Lois, 2008). The cells in the DRG and VRG have larger cell volumes compared to those in the BOT and preBötC as more cellular metabolic demands are needed to support long descending axons down the spinal cord (Lois, 2008).

There is considerable flexibility of the organization of the respiratory motor circuit, as the direct and indirect connections between the respiratory premotor areas and the respiratory MNs can change with injury or during development. In the rat, the direct monosynaptic respiratory drive and the polysynaptic respiratory drive compete upon birth, and eventually direct respiratory drive begins to dominate after P3 (Fig 1-3C) (Juvin & Morin, 2005). Furthermore, with hemisection of the rostral spinal cord, the respiratory drive can cross to the contralateral side within the spinal cord which is latent in uninjured animals (See Chapter 5 for detailed discussion) (Harry G. Goshgarian, 2009).

CONCLUSION

The respiratory motor circuit has multiple components that allow for proper breathing – the rhythm generator, relay circuit, feedback circuit, respiratory motor neurons, and respiratory muscles. My dissertation attempts to focus on the developmental origins and organization of the respiratory motor neurons as well as how the circuit assembly changes in light of cell fate transformation. In Chapter 2, I characterize some of the cranial motor neurons using known markers for spinal motor neurons and identify that Pou3f1 is expressed by subpopulations of motor neurons that have inspiratory-related activity as confirmed their anatomy. In Chapter 3, I provide the evidence that molecular matching process underlies the specificity in respiratory premotor input with respiratory motor neurons using Foxp1 conditional mutants that allow for transformation of limb-innervating motor neurons to hypaxial motor neurons. In Chapter 4, I show that Pou3f1 is expressed by inspiratory MNs in the cord, and it is necessary for proper innervation of the diaphragm the major inspiratory muscle. I conclude this dissertation with potentials for understanding congenital conditions as well as developing new therapy by understanding the molecular mechanisms that govern the assembly of respiratory motor circuitry.

FIGURES

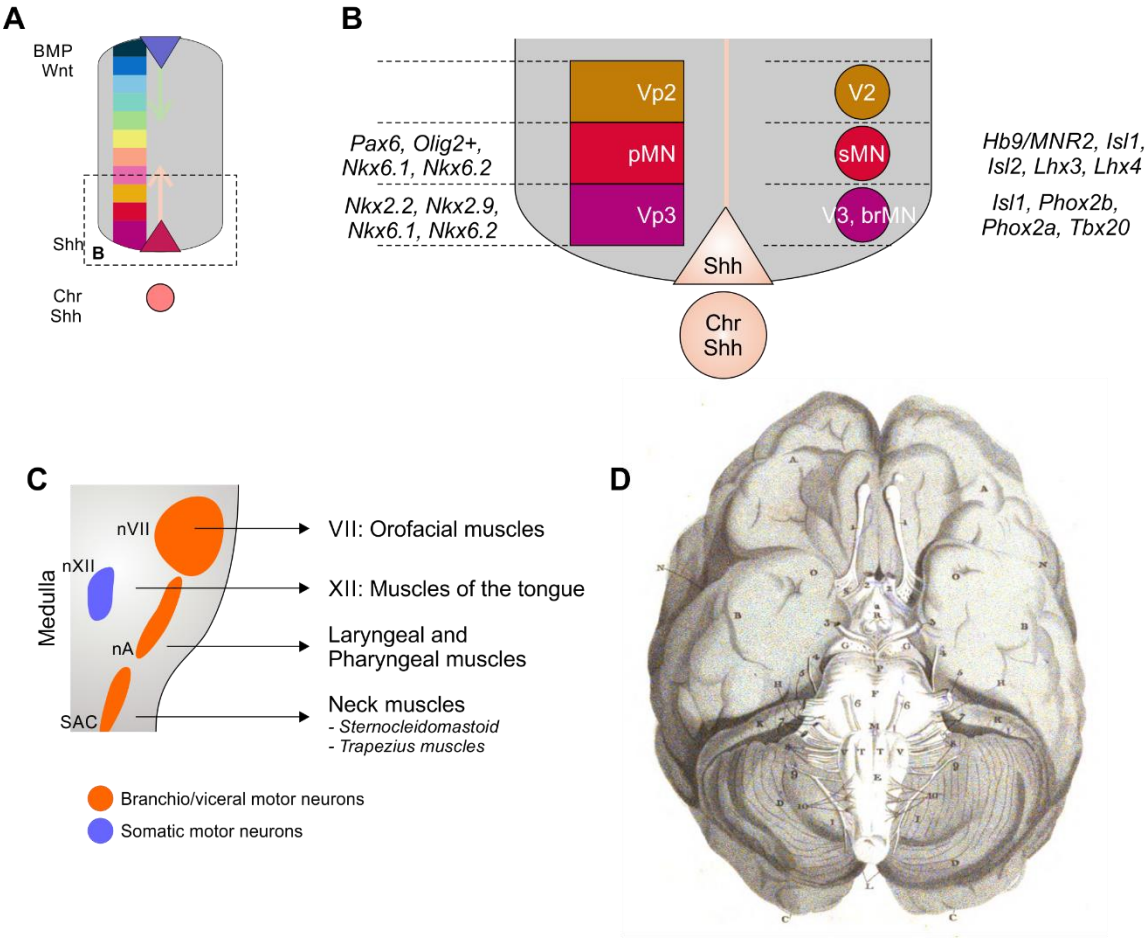

Figure 1-1. Motor neuron genesis in the central nervous system

(A) Gradients of families of morphogens (BMP, Wnt, Shh, and Chr) present in the developing neural tube. Adapted from Gómez-Skarmeta et al. (Gomez-Skarmeta, Campuzano, & Modolell, 2003) .

(B) Progenitor identity and subsequent motor neuron identity based on classification of motor neurons.

(C) Summary of motor neuron class of cranial motor neurons involved in movement of the face, tongue, and larynx

(D) Gross anatomy of the brain viewed from the ventral side aspect of the brainstem. Adapted from Bell C (Bell, 1802).

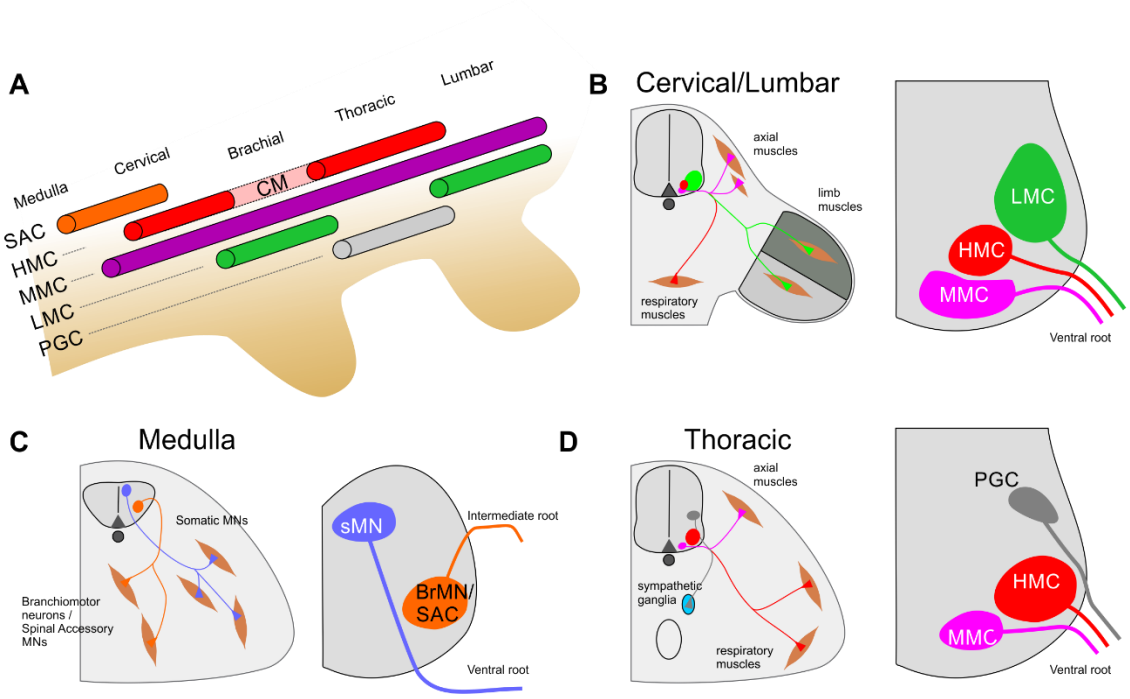

Figure 1-2. Columnar organization of the spinal motor neurons

(A) Columnar organization from medulla to lumbar spinal cord with individual motor columns illustrated in different colors.

(B) Cervical and lumbar spinal cord columnar organization in a cross sectional diagram.

(C) Organization and ventral root exits of spinal accessory motor column present in the rostral cervical spinal cord that is continuous with branchiomotor populations in the medulla.

(D) Thoracic spinal cord columnar organization in a cross sectional diagram.

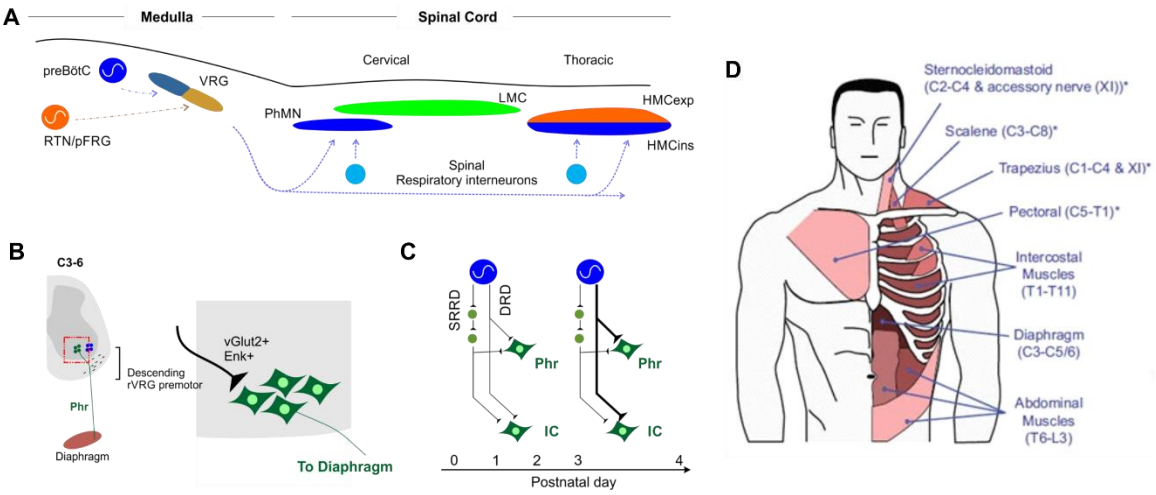

Figure 1-3. Summary of the respiratory motor circuit

(A) Diagram illustrating the medullary oscillators, the premotor interneurons, and motor neurons that are part of the respiratory motor circuit.

(B) Projection pattern and nature of the respiratory premotor fibers descending into the spinal cord.

(C) Postnatal competition of direct innervation and indirect extension of the respiratory drive in the developing rat. Adapted from Juvin et al. (Juvin & Morin, 2005).

(D) Summary of the muscles of respiration of the body. Figure from Lane. (Lane, 2011).

Table 1-1. The cranial motor neurons in the human brainstem

Adapted from Guthrie et al (Guthrie, 2007).

Nerve	Subtype	Nucleus	Target muscles or ganglia
III	Somatic motor	Oculomotor	Superior, inferior and medial recti muscles; inferior oblique, levator palpebrae superioris
	Visceral motor	Edinger-Westphal	Ciliary ganglion
IV	Somatic motor	Trochlear	Superior oblique
V	Branchiomotor	Trigeminal motor	Muscles of mastication, tensor tympani, anterior belly of digastric, others
VI	Somatic motor	Abducens	Lateral rectus muscle
VII	Branchiomotor	Facial motor	Muscles of facial expression, stapedius, posterior belly of digastric
	Visceral motor	Superior salivatory	Pterygopalatine/sphenopalatine ganglion, submandibular ganglion
IX	Branchiomotor	Nucleus ambiguus	Stylopharyngeus muscle
	Visceral motor	Inferior salivatory	Otic ganglion
X	Branchiomotor	Nucleus ambiguus	Laryngeal and pharyngeal muscles
	Visceral motor	Dorsal motor	Non-striated muscle of thoracic and abdominal viscera
Cranial XI	Branchiomotor	Nucleus ambiguus	Laryngeal and pharyngeal muscles
Spinal XI	Branchiomotor	Accessory nucleus, cervical spinal cord	Sternocleidomastoid and trapezius muscles
XII	Somatic motor	Hypoglossal	Tongue muscles

REFERENCES

Alheid, G. F., Gray, P. A., Jiang, M. C., Feldman, J. L., & McCrimmon, D. R. (2002). Parvalbumin in respiratory neurons of the ventrolateral medulla of the adult rat. *J Neurocytol, 31*(8-9), 693-717.

Arita, H., Kogo, N., & Koshiya, N. (1987). Morphological and physiological properties of caudal medullary expiratory neurons of the cat. *Brain Res, 401*(2), 258-266.

Ashwell, K. W. (1982). The adult mouse facial nerve nucleus: morphology and musculotopic organization. *J Anat, 135*(Pt 3), 531-538.

Ashwell, K. W., & Watson, C. R. (1983). The development of facial motoneurones in the mouse--neuronal death and the innervation of the facial muscles. *J Embryol Exp Morphol, 77*, 117-141.

Astick, M., Tubby, K., Mubarak, W. M., Guthrie, S., & Price, S. R. (2014). Central topography of cranial motor nuclei controlled by differential cadherin expression. *Curr Biol, 24*(21), 2541-2547. doi: 10.1016/j.cub.2014.08.067

Bailey, E. F., & Fregosi, R. F. (2004). Coordination of intrinsic and extrinsic tongue muscles during spontaneous breathing in the rat. *J Appl Physiol (1985), 96*(2), 440-449. doi: 10.1152/japplphysiol.00733.2003

Bell, C. (1802). *The anatomy of the brain explained in a series of engravings*. London: T.N. Longman and O. Rees, and T. Cadell and W. Davies.

Bermingham, J. R., Jr., Scherer, S. S., O'Connell, S., Arroyo, E., Kalla, K. A., Powell, F. L., & Rosenfeld, M. G. (1996). Tst-1/Oct-6/SCIP regulates a unique step in peripheral myelination and is required for normal respiration. *Genes Dev, 10*(14), 1751-1762.

Bieger, D., & Hopkins, D. A. (1987). Viscerotopic representation of the upper alimentary tract in the medulla oblongata in the rat: the nucleus ambiguus. *J Comp Neurol, 262*(4), 546-562. doi: 10.1002/cne.902620408

Caruso, N., Herberth, B., Lamballe, F., Arce-Gorvel, V., Maina, F., & Helmbacher, F. (2014). Plasticity versus specificity in RTK signalling modalities for distinct biological outcomes in motor neurons. *BMC Biology, 12*, 56. doi: 10.1186/s12915-014-0056-6

Cattaneo, L., & Pavesi, G. (2014). The facial motor system. *Neurosci Biobehav Rev, 38*, 135-159. doi: 10.1016/j.neubiorev.2013.11.002

Chandrasekhar, A. (2004). Turning Heads: Development of Vertebrate Branchiomotor Neurons. *Developmental dynamics : an official publication of the American Association of Anatomists, 229*(1), 143-161. doi: 10.1002/dvdy.10444

Chen, H., Bagri, A., Zupicich, J. A., Zou, Y., Stoeckli, E., Pleasure, S. J., . . . Tessier-Lavigne, M. (2000). Neuropilin-2 regulates the development of selective cranial and sensory nerves and hippocampal mossy fiber projections. *Neuron, 25*(1), 43-56.

Cohen, M. I. (1981). Central determinants of respiratory rhythm. *Annu Rev Physiol, 43*, 91-104. doi: 10.1146/annurev.ph.43.030181.000515

Cordes, S. P. (2001). Molecular genetics of cranial nerve development in mouse. *Nat Rev Neurosci, 2*(9), 611-623. doi: 10.1038/35090039

Dasen, J. S., De Camilli, A., Wang, B., Tucker, P. W., & Jessell, T. M. (2008). Hox repertoires for motor neuron diversity and connectivity gated by a single accessory factor, FoxP1. *Cell, 134*(2), 304-316. doi: 10.1016/j.cell.2008.06.019

Dick, T. E., Jodkowski, J. S., Viana, F., & Berger, A. J. (1988). Projections and terminations of single respiratory axons in the cervical spinal cord of cat. *Brain Res, 449*(1-2), 201-212.

Dobbins, E. G., & Feldman, J. L. (1994). Brainstem network controlling descending drive to phrenic motoneurons in rat. *J Comp Neurol, 347*(1), 64-86. doi: 10.1002/cne.903470106

Dobbins, E. G., & Feldman, J. L. (1995). Differential innervation of protruder and retractor muscles of the tongue in rat. *J Comp Neurol, 357*(3), 376-394. doi: 10.1002/cne.903570305

Ellenberger, H. H., Feldman, J. L., & Goshgarian, H. G. (1990). Ventral respiratory group projections to phrenic motoneurons: electron microscopic evidence for monosynaptic connections. *J Comp Neurol, 302*(4), 707-714. doi: 10.1002/cne.903020403

Ellenberger, H. H., Vera, P. L., Haselton, J. R., Haselton, C. L., & Schneiderman, N. (1990). Brainstem projections to the phrenic nucleus: an anterograde and retrograde HRP study in the rabbit. *Brain Res Bull, 24*(2), 163-174.

Ensini, M., Tsuchida, T. N., Belting, H. G., & Jessell, T. M. (1998). The control of rostrocaudal pattern in the developing spinal cord: specification of motor neuron subtype identity is initiated by signals from paraxial mesoderm. *Development, 125*(6), 969-982.

Feldman, J. L., Del Negro, C. A., & Gray, P. A. (2013). Understanding the rhythm of breathing: so near, yet so far. *Annu Rev Physiol, 75*, 423-452. doi: 10.1146/annurev-physiol-040510-130049

Feldman, J. L., Loewy, A. D., & Speck, D. F. (1985). Projections from the ventral respiratory group to phrenic and intercostal motoneurons in cat: an autoradiographic study. *J Neurosci, 5*(8), 1993-2000.

Fukuhara, K., Imai, F., Ladle, D. R., Katayama, K., Leslie, J. R., Arber, S., . . . Yoshida, Y. (2013). Specificity of monosynaptic sensory-motor connections imposed by repellent Sema3E-PlexinD1 signaling. *Cell Rep, 5*(3), 748-758. doi: 10.1016/j.celrep.2013.10.005

Giger, R. J., Cloutier, J. F., Sahay, A., Prinjha, R. K., Levengood, D. V., Moore, S. E., . . . Geppert, M. (2000). Neuropilin-2 is required in vivo for selective axon guidance responses to secreted semaphorins. *Neuron, 25*(1), 29-41.

Gomez-Skarmeta, J. L., Campuzano, S., & Modolell, J. (2003). Half a century of neural prepatterning: the story of a few bristles and many genes. *Nat Rev Neurosci, 4*(7), 587-598. doi: 10.1038/nrn1142

Goshgarian, H. G. (2009). The Crossed Phrenic Phenomenon and Recovery of Function Following Spinal Cord Injury. *Respiratory physiology & neurobiology, 169*(2), 85-93. doi: 10.1016/j.resp.2009.06.005

Goshgarian, H. G., Ellenberger, H. H., & Feldman, J. L. (1991). Decussation of bulbospinal respiratory axons at the level of the phrenic nuclei in adult rats: a possible substrate for the crossed phrenic phenomenon. *Exp Neurol, 111*(1), 135-139.

Gray, P. A., Hayes, J. A., Ling, G. Y., Llona, I., Tupal, S., Picardo, M. C., . . . Del Negro, C. A. (2010). Developmental origin of preBotzinger complex respiratory neurons. *J Neurosci, 30*(44), 14883-14895. doi: 10.1523/jneurosci.4031-10.2010

Guidato, S., Barrett, C., & Guthrie, S. (2003). Patterning of motor neurons by retinoic acid in the chick embryo hindbrain in vitro. *Mol Cell Neurosci, 23*(1), 81-95.

Guthrie, S. (2007). Patterning and axon guidance of cranial motor neurons. *Nat Rev Neurosci, 8*(11), 859-871. doi: 10.1038/nrn2254

Ho, R. H., Wu, W., & Elde, R. (1993). Pre-pro-somatostatin mRNA in the developing rat spinal cord with special reference to ventral horn motoneurons. *Neurosci Lett, 163*(2), 125-128.

Hwang, J. C., St John, W. M., & Bartlett, D., Jr. (1983). Respiratory-related hypoglossal nerve activity: influence of anesthetics. *J Appl Physiol Respir Environ Exerc Physiol, 55*(3), 785-792.

Jarrar, W., Dias, J. M., Ericson, J., Arnold, H. H., & Holz, A. (2015). Nkx2.2 and nkx2.9 are the key regulators to determine cell fate of branchial and visceral motor neurons in caudal hindbrain. *PLoS One, 10*(4), e0124408. doi: 10.1371/journal.pone.0124408

Jessell, T. M. (2000). Neuronal specification in the spinal cord: inductive signals and transcriptional codes. *Nat Rev Genet, 1*(1), 20-29. doi: 10.1038/35049541

Ji, S. J., Zhuang, B., Falco, C., Schneider, A., Schuster-Gossler, K., Gossler, A., & Sockanathan, S. (2006). Mesodermal and neuronal retinoids regulate the induction and maintenance of limb innervating spinal motor neurons. *Dev Biol, 297*(1), 249-261. doi: 10.1016/j.ydbio.2006.05.015

Jurgens, U. (2002). Neural pathways underlying vocal control. *Neurosci Biobehav Rev, 26*(2), 235-258.

Juvin, L., & Morin, D. (2005). Descending respiratory polysynaptic inputs to cervical and thoracic motoneurons diminish during early postnatal maturation in rat spinal cord. *Eur J Neurosci, 21*(3), 808-813. doi: 10.1111/j.1460-9568.2005.03910.x

Kleinfeld, D., Deschenes, M., Wang, F., & Moore, J. D. (2014). More than a rhythm of life: breathing as a binder of orofacial sensation. *Nat Neurosci, 17*(5), 647-651. doi: 10.1038/nn.3693

Lamballe, F., Genestine, M., Caruso, N., Arce, V., Richelme, S., Helmbacher, F., & Maina, F. (2011). Pool-specific regulation of motor neuron survival by neurotrophic support. *J Neurosci, 31*(31), 11144-11158. doi: 10.1523/jneurosci.2198-11.2011

Lane, M. A. (2011). Spinal respiratory motoneurons and interneurons. *Respir Physiol Neurobiol, 179*(1), 3-13. doi: 10.1016/j.resp.2011.07.004

Lee, B. H., Lynn, R. B., Lee, H. S., Miselis, R. R., & Altschuler, S. M. (1992). Calcitonin gene-related peptide in nucleus ambiguus motoneurons in rat: viscerotopic organization. *J Comp Neurol, 320*(4), 531-543. doi: 10.1002/cne.903200410

Livet, J., Sigrist, M., Stroebel, S., De Paola, V., Price, S. R., Henderson, C. E., . . . Arber, S. (2002). ETS gene Pea3 controls the central position and terminal arborization of specific motor neuron pools. *Neuron, 35*(5), 877-892.

Lois, J. H. (2008). *Central Respiratory Circuits That Control Diaphragm Function In Cat Revealed By Transneuronal Tracing.* (M.S.), University of Pittsburgh,, Pittsburgh, PA. Retrieved from Access for Pitt-affiliated users only http://etd.library.pitt.edu/ETD/available/etd-08052008-090917/

Machado, C. B., Kanning, K. C., Kreis, P., Stevenson, D., Crossley, M., Nowak, M., . . . Lieberam, I. (2014). Reconstruction of phrenic neuron identity in embryonic stem cell-derived motor neurons. *Development, 141*(4), 784-794. doi: 10.1242/dev.097188

Maden, M., Sonneveld, E., van der Saag, P. T., & Gale, E. (1998). The distribution of endogenous retinoic acid in the chick embryo: implications for developmental mechanisms. *Development, 125*(21), 4133-4144.

McClung, J. R., & Goldberg, S. J. (2000). Functional anatomy of the hypoglossal innervated muscles of the rat tongue: a model for elongation and protrusion of the mammalian tongue. *Anat Rec, 260*(4), 378-386.

McCrimmon, D. R., Alheid, G. F., Ptak, K., Gray, P. A., Zummo, G., Escobar, S., & Feldman, J. L. (2001). Distribution of calcium binding proteins, sodium channels and persistent sodium current in the rat ventral respiratory group. *Respiratory Research, 2*(Suppl 1), 2.2-2.2. doi: 10.1186/rr96

Megirian, D., Hinrichsen, C. F., & Sherrey, J. H. (1985). Respiratory roles of genioglossus, sternothyroid, and sternohyoid muscles during sleep. *Exp Neurol, 90*(1), 118-128.

Miller, A. D., Bianchi, A. L., & Bishop, B. (1997). *Neural control of the respiratory muscles*. Boca Raton: CRC Press.

Moore, J. D., Deschenes, M., Furuta, T., Huber, D., Smear, M. C., Demers, M., & Kleinfeld, D. (2013). Hierarchy of orofacial rhythms revealed through whisking and breathing. *Nature, 497*(7448), 205-210. doi: 10.1038/nature12076

Moore, J. D., Kleinfeld, D., & Wang, F. (2014). How the brainstem controls orofacial behaviors comprised of rhythmic actions. *Trends Neurosci, 37*(7), 370-380. doi: 10.1016/j.tins.2014.05.001

Muller, F., & O'Rahilly, R. (2011). The initial appearance of the cranial nerves and related neuronal migration in staged human embryos. *Cells Tissues Organs, 193*(4), 215-238. doi: 10.1159/000320026

National Spinal Cord Injury Statistical Center. (2011). Spinal cord injury facts and figures at a glance. *J Spinal Cord Med, 34*(6), 620-621. doi: 10.1179/204577211x13218754005537

Novitch, B. G., Chen, A. I., & Jessell, T. M. (2001). Coordinate regulation of motor neuron subtype identity and pan-neuronal properties by the bHLH repressor Olig2. *Neuron, 31*(5), 773-789.

Onimaru, H., Kumagawa, Y., & Homma, I. (2006). Respiration-related rhythmic activity in the rostral medulla of newborn rats. *J Neurophysiol, 96*(1), 55-61. doi: 10.1152/jn.01175.2005

Pecho-Vrieseling, E., Sigrist, M., Yoshida, Y., Jessell, T. M., & Arber, S. (2009). Specificity of sensory-motor connections encoded by Sema3e-Plxnd1 recognition. *Nature, 459*(7248), 842-846. doi: 10.1038/nature08000

Philippidou, P., Walsh, C. M., Aubin, J., Jeannotte, L., & Dasen, J. S. (2012). Sustained Hox5 gene activity is required for respiratory motor neuron development. *Nat Neurosci, 15*(12), 1636-1644. doi: 10.1038/nn.3242

Pierce, E. T. (1973). Time of origin of neurons in the brain stem of the mouse. *Prog Brain Res, 40*(0), 53-65. doi: 10.1016/s0079-6123(08)60679-2

Price, S. R. (2012). Cell adhesion and migration in the organization of spinal motor neurons. *Cell Adh Migr, 6*(5), 385-389. doi: 10.4161/cam.21044

Road, J. D., Ford, T. W., & Kirkwood, P. A. (2013). Connections between expiratory bulbospinal neurons and expiratory motoneurons in thoracic and upper lumbar segments of the spinal cord. *J Neurophysiol, 109*(7), 1837-1851. doi: 10.1152/jn.01008.2012

Rousso, D. L., Gaber, Z. B., Wellik, D., Morrisey, E. E., & Novitch, B. G. (2008). Coordinated actions of the forkhead protein Foxp1 and Hox proteins in the columnar organization of spinal motor neurons. *Neuron, 59*(2), 226-240. doi: 10.1016/j.neuron.2008.06.025

Saboisky, J. P., Butler, J. E., Fogel, R. B., Taylor, J. L., Trinder, J. A., White, D. P., & Gandevia, S. C. (2006). Tonic and phasic respiratory drives to human genioglossus motoneurons during breathing. *J Neurophysiol, 95*(4), 2213-2221. doi: 10.1152/jn.00940.2005

Sanes, J. R., & Yamagata, M. (2009). Many paths to synaptic specificity. *Annu Rev Cell Dev Biol, 25*, 161-195. doi: 10.1146/annurev.cellbio.24.110707.175402

Sasaki, S., & Uchino, H. (1995). An electrophysiological demonstration of axonal projections of single ventral inspiratory neurons to the phrenic nucleus of the cat. *Brain Res, 701*(1-2), 108-116.

Schwartz, J. P., Taniwaki, T., Messing, A., & Brenner, M. (1996). Somatostatin as a trophic factor. Analysis of transgenic mice overexpressing somatostatin in astrocytes. *Ann N Y Acad Sci, 780*, 29-35.

Seroogy, K. B., Bayliss, D. A., Szymeczek, C. L., Hokfelt, T., & Millhorn, D. E. (1991). Transient expression of somatostatin messenger RNA and peptide in the hypoglossal nucleus of the neonatal rat. *Brain Res Dev Brain Res, 60*(2), 241-252.

Shen, K., & Scheiffele, P. (2010). Genetics and cell biology of building specific synaptic connectivity. *Annu Rev Neurosci, 33*, 473-507. doi: 10.1146/annurev.neuro.051508.135302

Stanek, E. t., Cheng, S., Takatoh, J., Han, B. X., & Wang, F. (2014). Monosynaptic premotor circuit tracing reveals neural substrates for oro-motor coordination. *Elife, 3*, e02511. doi: 10.7554/eLife.02511

Stifani, N. (2014). Motor neurons and the generation of spinal motor neuron diversity. *Frontiers in Cellular Neuroscience, 8*, 293. doi: 10.3389/fncel.2014.00293

Stornetta, R. L., Sevigny, C. P., & Guyenet, P. G. (2003). Inspiratory augmenting bulbospinal neurons express both glutamatergic and enkephalinergic phenotypes. *J Comp Neurol, 455*(1), 113-124. doi: 10.1002/cne.10486

Surmeli, G., Akay, T., Ippolito, G. C., Tucker, P. W., & Jessell, T. M. (2011). Patterns of spinal sensory-motor connectivity prescribed by a dorsoventral positional template. *Cell, 147*(3), 653-665. doi: 10.1016/j.cell.2011.10.012

Tan, W., Sherman, D., Turesson, J., Shao, X. M., Janczewski, W. A., & Feldman, J. L. (2012). Reelin demarcates a subset of pre-Botzinger complex neurons in adult rat. *J Comp Neurol, 520*(3), 606-619. doi: 10.1002/cne.22753

ten Donkelaar, H., Lammens, M., Cruysberg, J. M., & Cremers, C. J. R. (2006). Development and Developmental Disorders of the Brain Stem *Clinical Neuroembryology* (pp. 269-308): Springer Berlin Heidelberg.

Tripodi, M., Stepien, A. E., & Arber, S. (2011). Motor antagonism exposed by spatial segregation and timing of neurogenesis. *Nature, 479*(7371), 61-66. doi: 10.1038/nature10538

Vrieseling, E., & Arber, S. (2006). Target-induced transcriptional control of dendritic patterning and connectivity in motor neurons by the ETS gene Pea3. *Cell, 127*(7), 1439-1452. doi: 10.1016/j.cell.2006.10.042

Wetzel, D. M., Kelley, D. B., & Campbell, B. A. (1980). Central control of ultrasonic vocalizations in neonatal rats: I. Brain stem motor nuclei. *J Comp Physiol Psychol, 94*(4), 596-605.

Wichterle, H., Lieberam, I., Porter, J. A., & Jessell, T. M. (2002). Directed differentiation of embryonic stem cells into motor neurons. *Cell, 110*(3), 385-397.

Williams, M. E., de Wit, J., & Ghosh, A. (2010). Molecular mechanisms of synaptic specificity in developing neural circuits. *Neuron, 68*(1), 9-18. doi: 10.1016/j.neuron.2010.09.007

Yasuda, K., Nakayama, Y., Tanaka, M., Tanaka, M., Mori, R., & Furusawa, K. (2002). The distribution of respiration-related and swallowing-related motoneurons innervating the rat genioglossus muscle. *Somatosens Mot Res, 19*(1), 30-35. doi: 10.1080/08990220120113020

Yoshikawa, M., Hirabayashi, M., Ito, R., Ozaki, S., Aizawa, S., Masuda, T., . . . Shiga, T. (2015). Contribution of the Runx1 transcription factor to axonal pathfinding and muscle innervation by hypoglossal motoneurons. *Dev Neurobiol*. doi: 10.1002/dneu.22285

Zlatic, M., Li, F., Strigini, M., Grueber, W., & Bate, M. (2009). Positional cues in the Drosophila nerve cord: semaphorins pattern the dorso-ventral axis. *PLoS Biol, 7*(6), e1000135. doi: 10.1371/journal.pbio.1000135

CHAPTER TWO – Molecular characterization of the developing cranial motor neurons

The movement of the face, the neck, and the oropharynx are mediated by the cranial motor neurons (MNs) in the brainstem. The myriad muscles of the head and neck act together for many actions including expressive behaviors such as vocalization or life-sustaining involuntary behaviors as in breathing, coughing, and vomiting. Despite the importance of the functions of these MNs, their molecular origins and the organization has not yet been studied in detail. Using combined immunohistochemistry and retrograde labeling, I have identified that Foxp1 and Pou3f1 are present in motor pools that are part of the facial nucleus, the hypoglossal nucleus, and the nucleus ambiguus. Pou3f1 in the hypoglossal motor nucleus was found to be localized to the ventral half, which were also retrograde labeled by nerve branch projecting to the genioglossus. Furthermore, the expression of Foxp1 and Pou3f1 in the cranial MNs was conserved in human fetal brainstem as well. The expression of Pou3f1 in multiple respiratory- and rhythmic cranial MNs suggest that Pou3f1 may be involved in the development of some aspect of generalized rhythmic behavior in mammals.

INTRODUCTION

Proper functions of cranial motor neurons (MNs) are required for life-sustaining behaviors such as breathing, chewing, and swallowing. Among the twelve cranial nerves originating out of the brainstem, three motor nuclei are especially relevant for the movement of the orofacial muscle and airway patency – these include the nucleus ambiguus, the facial nucleus, and the hypoglossal nucleus (Bieger & Hopkins, 1987). It has been well characterized that the genioglossus muscle, innervated by the hypoglossal MNs, contract with each inspiratory phase for protrusion of the tongue (Hwang, St John, & Bartlett, 1983; Megirian, Hinrichsen, & Sherrey, 1985; Saboisky et al., 2006). Furthermore, recent *in vitro* recordings of facial MNs revealed respiratory-related movements that are synchronous with the inspiratory phase (Moore et al., 2013; Onimaru, Kumagawa, & Homma, 2006). The synchronous rhythmic activities detected in the cranial MNs demonstrate that these MNs are integrated into a shared brainstem circuitry.

In contrast to the spinal cord, two types of MNs arising from two discrete progenitor domains are present in the brainstem. Somatic MNs originate from the pMN progenitor domain that expresses Olig2+; branchiomotor neurons and visceromotor neurons arise from the p3 domain of Nkx2.2 lineage (Guthrie, 2007). Removal of Nkx2.2 and Nkx2.9 results in conversion of branchiomotor neurons (i.e. vagus and spinal accessory MNs) into somatic MNs (Jarrar, Dias, Ericson, Arnold, & Holz, 2015).

In contrast to the columnar organization of the spinal MNs, cranial MNs are organized into distinct clusters of MNs- motor nuclei. Within each motor nucleus, motor pools/sub-nucleus can exist that project to a single muscle. Classic retrograde labeling

study revealed at least six subnuclei that make up the facial nucleus: dorsomedial (DM), ventromedial (VM), dorsal intermediate (DI), ventral intermediate (VI), dorsolateral (DL), and lateral (Lat) subnuclei (Ashwell, 1982). The DM and VM innervates the anterior and posterior auricular musculature, respectively; DI innervates the orbicularis occuli; VI innervates the mentalis and platysma; and the DL and L subnuclei innervate nasolabial musculature (Ashwell, 1982). This is summarized in Figure 1A. The hypoglossal motor nuclei shows similar musculotopic innervation as described by anatomical tracing studies as summarized in Figure 1B (Dobbins & Feldman, 1995; McClung & Goldberg, 2000; Yasuda et al., 2002). Only few markers of hypoglossal motor pool have been explored. One of which is Runx1 that was found to label ventrocaudal hypoglossal MNs projecting to intrinsic and transverse tongue muscles (Yoshikawa et al., 2015). More recently, novel ways of classifying the cranial MN populations using the cadherin code have been documented (Astick et al., 2014).

In the developing spinal cord, many transcription factors and axon guidance cues have been explored for their role in proper function and assembly of the motor circuitry (Sanes & Yamagata, 2009; Stifani, 2014). While most of the MN development has been focused on spinal motor pool organization and maturation, these aspects of cranial MNs are largely unknown. In particular, would the markers- such as Foxp1, Pou3f1, Etv4, and others- that are prominently used to define spinal MN organization also present in the cranial MNs? I have not only identified discrete regions could be defined by using the combination of these markers, but also this organization is shared between human fetal developing brainstem as well.

MATERIALS AND METHODS

Animal preparation

C57/Bl6 wild type mice were used in these experiments. Each mating pair was checked for plugs in the morning, where the appearance of a plug was defined as e0.5. The pregnant dams were collected at e15.5, e16.5, e17.5, and P0. The brainstem was isolated by dissecting away any extraneous tissues in ice-cold phosphate buffered saline (PBS). The brainstem was fixed in 4% paraformaldehyde (PFA) in PBS overnight. The preparation was subsequently cryoprotected in 30% sucrose solution overnight, mounted in OCT, and sectioned at appropriate thickness depending on the age of the specimen on Superfrost slides. Human fetal tissue samples were generously provided by Katrina Adams.

Retrograde labeling experiments

For retrograde labeling experiments, we used GFP reporter driven by motor neuron-specific Hb9 promoter (Hb9::GFP) (Wichterle, Lieberam, Porter, & Jessell, 2002). e14.5 embryos was dissected to reveal the hypoglossal nerve in ice-cold DMEM/F12 oxygenated with 95%/5% oxygen/CO_2. Either horseradish peroxidase or 3000MW tetramethylrhodamine dextran was injected in the specific branches of the nerve. The injected embryo was subsequently incubated in oxygenated DMEM/F12 overnight. The preparation was fixed in PFA, cryoprotected, and mounted in OCT for cryosectioning.

Immunohistochemistry

Cryosectioned slides were blocked with antibody blocking solution (1% heat-inactivated horse serum, 0.1% sodium azide, 0.1% triton-X in PBS) for at least 30 minutes. Slides were incubated overnight with primary antibodies diluted in the antibody blocking solution. The antibodies that were used in this study were guinea pig Foxp1 (Rousso et al., 2008), goat Islet-1 (R&D Systems), rabbit Pou3f1 (generous gift from Dies Meijer), *Nkx6.1*, *Er81*, rabbit Etv4 (generous gift from Silvia Arber), and rabbit NK1R. The primary antibodies were washed off three times with 0.1% Triton-X in PBS. The slides were then incubated in secondary antibodies for four hours at room temperature. The slides were mounted in Prolong Gold (Invitrogen). The images were collected on LSM780 confocal microscopy system (Zeiss).

In situ hybridization

The slides were post-fixed in 4% PFA in PBS for 10 minutes, washed in PBS three times. The slides were acetylated for 10 minutes and washed in PBS three times. The slides were blocked in hybridization buffer for at least one hour. The anti-sense probes against mouse neuropilin-1 and somatostatin mRNA were generated using T3 RNA polymerase (Roche) and DIG labeling mix (Roche). The anti-sense RNA probes were detected by using AP probe and NBT/BCIP solution. The sequences of primers that were used for the generation of anti-sense RNA probes are listed in Table 1.

RESULTS

Overview of the cranial motor neuron organization

In order to identify the exact locations of different cranial motor nuclei in the brainstem, I used wholemount immunohistochemistry with a general motor neuron marker Isl1 that are expressed in somatic and branchial/visceral motor neurons (Guthrie, 2007). As previously described in the literature, nVII is positioned more rostrally compared to nXII with nA expressed at the same rostrocaudal levels as nXII in the sagittal view **(Fig 2-2A)**. From the transverse view, hypoglossal motor nuclei are positioned medially and facial motor nuclei laterally in the rostral medulla. The hypoglossal is positioned in the dorsomedial tegmentum of the medulla, where the fourth ventricle and central canal can be used as landmark to identify their locations. Between the levels between nXII and nVII, and nA can be seen. At least three different subdivisions of nA exists in rats when retrogradely labeled from pharynx, larynx, and the heart (Lee, Lynn, Lee, Miselis, & Altschuler, 1992). nVII can be defined as two large separated medial and lateral group as it can be seen in this view, both with equal length. There is also a shorter intermediate group. The general overall morphology is consistent with previous studies that have characterized this region (Ashwell, 1982).

Organization of the facial motor pools

In the developing facial motor nucleus, a number of transcription factors are found to mark different subdivisions. The most salient subdivision was visible when motor neurons were labeled with transcription factors that were found to be expressed in different motor columns and motor pools of the spinal cord (Rousso et al., 2008). Foxp1

is expressed by nVII MNs in the nVII-DI subnucleus, whereas Pou3f1 is expressed by nVII-L, nVII-DL, nVII-DM, and nVII-DL **(Fig 2-3A)**. Interestingly, the expression of Foxp1 and Pou3f1 were mutually exclusive. NK1R was expressed by nVII-DL at high levels, whereas it was expressed at moderate and low levels in VII-DM and VII-DL, respectively **(Fig 2-3B)**. The expression of neuropilin2 was restricted to nVII-DM, nVII-DL, and nVII-L subnuclei **(Fig 2-3C and 2-3D)**. Nkx6.1 was expressed by entire nVII nucleus, but the level seemed slightly lower in the lateral nucleus **(Fig 2-3E)**. Er81 (Etv1) expression was exclusive to the nVII-DL subnucleus **(Fig 2-3F)**. Finally, somatostatin was expressed by nVII-DM subnucleus **(Fig 2-3G and 2-3H)**.

Organization of the hypoglossal motor pools

Because of previously described musculotopic subdivision of the nXII, the same markers were used to characterize nXII. At e17.5, I have found that Foxp1 is found in intermediate nXII motor pool, whereas Pou3f1 is mostly ventral MNs **(Fig 2-4A)**. Nk1R was also expressed by the dorsal subdivision of nXII **(Fig 2-4B)**. Somatostatin was expressed by motor neurons in the far lateral cluster **(Fig 2-4C, 4D)**. Etv1 and Pea3 were not expressed in nXII at e17.5 (data not shown). In addition, neuropilin 2 was expressed by all nXII motor neurons (data not shown). Since Pou3f1 is expressed by other respiratory motor neurons, I was curious if Pou3f1 expression is restricted to the one rostrocaudal level, thus Pou3f1 expression was assessed at every 320μm. In this assessment, I found that Pou3f1 is expressed by nXII at only the caudal levels of the developing hindbrain **(Fig 2-4E-4H)**. In order to confirm that these MNs are indeed in the ventral subdivision of nXII, I injected retrograde labels from dorsal and ventral

branches of the hypoglossal nerve **(Fig 2-5A, 5B)**. Indeed, I have found that the Pou3f1+ MNs are projecting exclusively towards the ventral branch of XII and never the dorsal branch **(Fig 2-5C)**.

Motor pool organization of the developing human cranial motor nuclei

The organization of the motor system is largely conserved between mice and humans. Thus, I assessed the expression of markers that I discovered in the mouse in gestation week (GW) 8.1 human fetal brainstem. First, the facial nucleus was assessed with Pou3f1 and Foxp1 at this stage (Figure 6B). Pou3f1 is present ubiquitously in most facial MNs, and Foxp1 expression is also present in the cluster that is putative DI subnucleus **(Fig 2-6B)**. Next, the hypoglossal nucleus was assessed with the same markers. At GW8.1, Pou3f1 was found in the ventral-most nXII MNs as well **(Fig 2-6A)**. This result supports the fact that in mouse and human, the Pou3f1+ MNs are present in nXII and nVII at GW8.1, where they only occupy the ventral subdivision in nXII.

DISCUSSION

In this study, I molecularly defined the subnuclei organization of the facial nucleus and the hypoglossal nuclei using markers that were extensively used in the characterization of the developing spinal cord MNs **(Fig 2-7A, 7B)**. A number of markers show exclusive or co-expression similar to the spinal cord, and there is an enormous diversity of the cranial MNs utilizing very similar molecular machinery to build motor circuitry.

Diversity of cranial motor neuron diversity by transcriptional regulators

While in the nVII Foxp1 and Pou3f1 are expressed in a mutually exclusive manner, we have identified some Foxp1 and Pou3f1-overlapping population in nXII. Mutually exclusive expression of Foxp1/Pou3f1 and overlapping Foxp1/Pou3f1 presence evokes this kind of expression pattern in the cervical levels of the spinal cord where the phrenic MNs express Pou3f1 but not Foxp1, and forearm flexor projecting MNs show co-localization of Foxp1 and Pou3f1. It is not yet what the Semaphorin "code" or cadherin "code" that results from co-expression or mutually exclusive expression, but the differences in molecular mechanisms of target innervation and/or premotor input finding.

Role of peptides in motor neuron development

SST expression was previously described in a subpopulation of hypoglossal motor neurons of the rat where the expression of SST this population gradually diminished after birth, and disappeared by adulthood (Seroogy, Bayliss, Szymeczek, Hokfelt, & Millhorn, 1991). In addition to nXII, SST was also found to be present in spinal motor neurons of

the rat (Ho, Wu, & Elde, 1993). We also have evidence that it is present in rostral cervical HMC population that presumably innervates various neck muscles (data not shown). SST has been suggested as acting as trophic factors during development (Schwartz, Taniwaki, Messing, & Brenner, 1996). The specific expression of SST in nVII-DM and the lateral-most hypoglossal nucleus suggest that these MN population might share similar properties.

Expression of Foxp1 in cranial motor neurons

In this study, I found that Foxp1 is present in subpopulations of the facial and hypoglossal nuclei that innervates the neck and intrinsic muscles of the tongue, respectively. Foxp1 is a transcription factor critical for limb-innerving motor neuron development. In the developing spinal cord, the limb-innervating lateral motor column (LMC) and visceral preganglionic motor column (PGC) exclusively expresses Foxp1 beyond postnatal times (Rousso et al., 2008).

Retinoic acid signaling is known to mediate the generation of MNs in hindbrain and the spinal cord. The somites surrounding the developing neural tube synthesize high levels of RA (Maden, Sonneveld, van der Saag, & Gale, 1998). The high levels of RA can be mimicked by placing beads soaked in RA resulting in as large as nine times more somatic MNs in hindbrain region compared to control (Guidato, Barrett, & Guthrie, 2003). In addition, RA has a role in specification of spinal motor neurons to LMC fate by the RA released by paraxial mesoderm (Ensini, Tsuchida, Belting, & Jessell, 1998). During maturation of LMC MNs, the LMC MNs themselves express retinaldehyde dehydrogenase II (RALDH2) that synthesize RA locally for maintenance of LMC

phenotype (Ji et al., 2006). At e17.5 I was not able to detect RALDH2 expression in neither nVII nor nXII, which argues against the local synthesis of RA that might be maintaining Foxp1 expression in nVII and nXII (data not shown). However, the mechanism behind the induction of Foxp1 and the effect it has on proper wiring of neck and intrinsic muscles of the tongue is to be assessed.

Expression of Pou3f1 in respiratory-related motor neurons

Pou3f1 was previously found in multiple areas of the brainstem, however specific identity and innervating target has not been determined (Bermingham et al., 1996). I show here that the Pou3f1+ MN are found in the lateral division of the facial nucleus used in whisking. The whisking contraction of the mouse shows rhythmic behavior that is thought to be regulated by the Pre-Bötzinger Complex (preBötC) (Moore et al., 2013).

Pou3f1+ MNs were present in the nucleus ambiguus and the ventral caudal hypoglossal nucleus. A portion of the ventral caudal hypoglossal nucleus provide the innervation to the genioglossus muscle of the tongue, which acts as a protrusor that keeps the airway patent during breathing. This study did not examine the expression of Runx1 in relation to the expression of Pou3f1 (Yoshikawa et al., 2015). Analysis of co-localization of Runx1 and Pou3f1 would reveal if Pou3f1+ MNs also innervate the intrinsic muscles of the tongue. Nevertheless, the presence of Pou3f1+ multiple motor subnuclei that are involved in breathing shows that Pou3f1 may play a role in receiving of rhythmic premotor input. Recent studies have proposed that all orofacial rhythms originate from respiratory rhythm (Kleinfeld, Deschenes, Wang, & Moore, 2014; Moore et al., 2013; Moore, Kleinfeld, & Wang, 2014). Future studies should elucidate the

premotor circuitry of the respiratory-related MNs of the brainstem, which I also predict that would place medullary oscillators at the center.

Premotor circuitry innervating the hypoglossal motor neurons

The intrinsic muscles of the tongue have a different activation pattern compared to extrinsic muscles in the rat, where intrinsic muscles are quiescent at rest but becomes active following greater activation of extrinsic muscles during respiratory challenge (Bailey & Fregosi, 2004). The circuitry that provides differential respiratory modulation of intrinsic vs extrinsic tongue muscles not been well characterized, although the premotor circuitry controlling the tongue muscles have revealed key anatomical locations that might be critical for proper movement of the tongue (Dobbins & Feldman, 1995; Stanek, Cheng, Takatoh, Han, & Wang, 2014). The hypoglossal premotor neurons were also organized in functionally distinct manner, where protrude premotor neurons situated more ventromedial compared to the retractor premotor neurons (Dobbins & Feldman, 1995). The developmental lineage and molecular identity of these medullary interneurons are not yet clear.

Expression of key axon guidance molecules

In addition to a number of transcription factors, I assessed one specific type of receptor in Semaphorin signaling pathway. Neuropilin receptors are expressed widely in the developing central nervous system. Neuropilin 2 (Nrp2) was shown to be required for fasciculation and normal trajectory of oculomotor, trochlear, and facial nerves in the rat (Chen et al., 2000; Giger et al., 2000). The expression pattern reported in this chapter

shows that there may be a population of intermediate nVII MNs that might be excluded from Nrp2/Sema influence during development due to their lack of expression of Nrp2.

Conserved motor neuron topography between mice and humans

In this study, I have shown that Pou3f1 is expressed in subpopulations of nVII and nXII of the developing human fetus. The location of these motor neurons parallel my findings in the developing mouse. The human cranial motor nuclei has been shown to follow similar anatomical layout compared to the mouse, with more lateral subdivision controlling the lower half of the face and the medial subdivision the lateral half (Cattaneo & Pavesi, 2014). Extensive migration occurs during development, although all cranial nerves are visible by Carnegie Stage 16 (Muller & O'Rahilly, 2011). Future studies focused on conserved molecular mechanisms are necessary to understand the pathophysiology of the head and neck disorders that affect this region, including Möbius syndrome and congenital facial palsy (ten Donkelaar, Lammens, Cruysberg, & Cremers, 2006).

CONCLUSION

The facial and hypoglossal motor nucleus comprise of multiple motor pools that can be identified by combinations of transcription factors, axon guidance receptors, and peptide neurotransmitter expressions. While the motor circuitry that innervate the tongue and the face in human is vastly more complex than that of rodent model organisms, future studies should focus on the role of these molecules in vocalization and communication via facial expression. Recent ideas that all orofacial rhythm originates from the medullary oscillators parallel my findings of Pou3f1 in rhythmic MN populations in the brainstem. Studying the molecular mechanisms of rhythmic motor circuitry would provide an important knowledge relevant for understanding the congenital malformations of the cranial motor system as well as in developing rehabilitation approaches when there are injuries to this system.

FIGURES

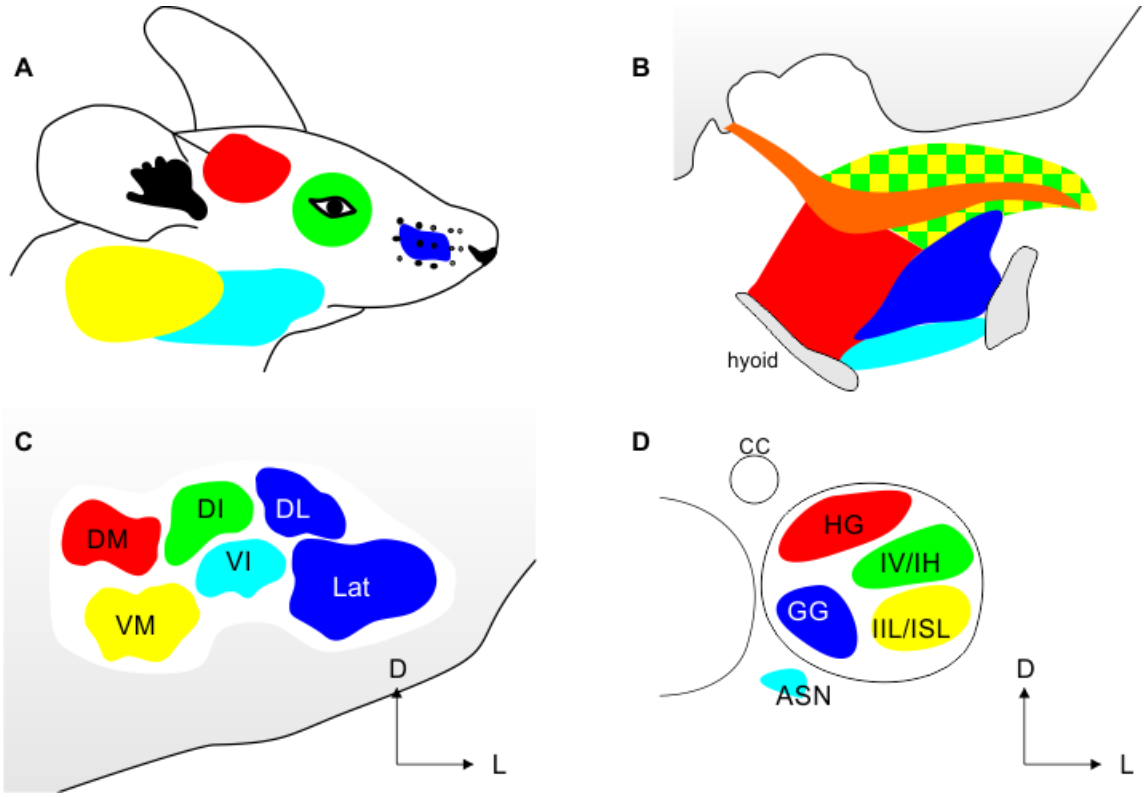

Figure 2-1. Musculotopic organization of the facial nucleus (nVII) and the hypoglossal nucleus (nXII) of the mouse

nVII is organized in six subnuclei positioned in the characteristic positions where most rostral facial muscle is innervated by most laterally positioned subnuclei (A and C). nXII is organized in subnuclei multiple subnuclei identified by retrograde labeling from different muscles of the tongue (B and D). Adapted from Ashwell (1982).

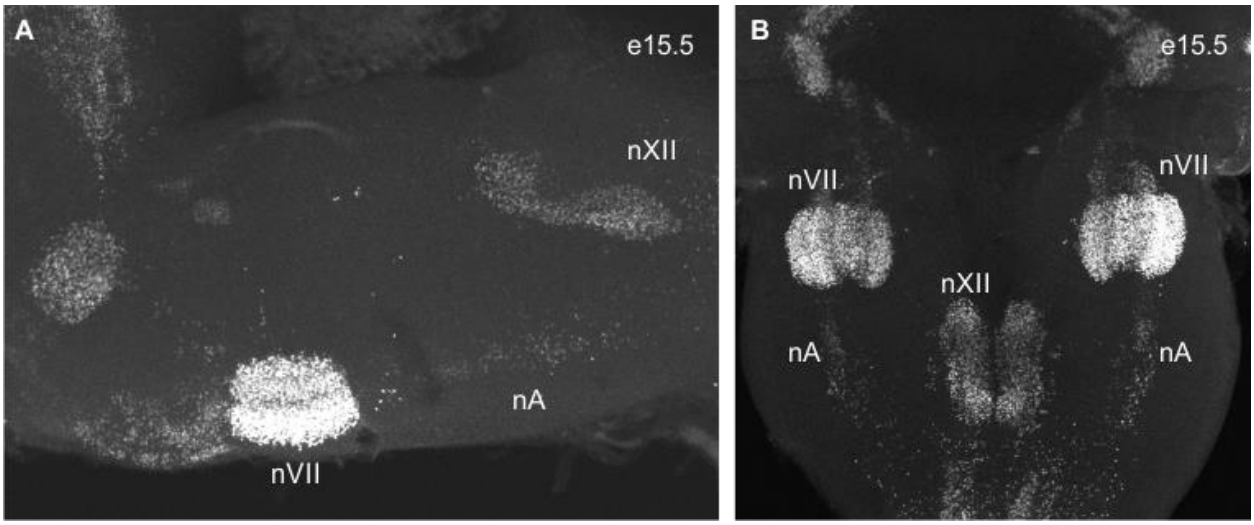

Figure 2-2. Overview of cranial motor neuron organization in the developing brainstem

Sagittal (A) and Transverse (B) views of wholemount Isl1 of e15.5 hindbrain reveals general location of the nVII, nA and nXII.

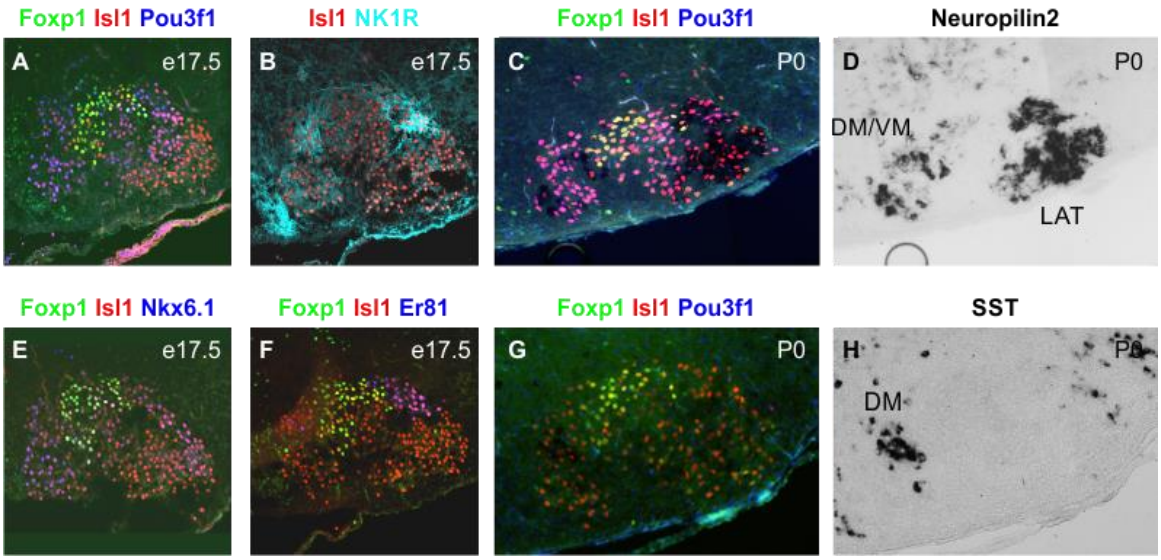

Figure 2-3. Motor pool organization of the facial motor nucleus

Foxp1 is expressed in dorsal side of nVII between two subnuclei that express Pou3f1 at high levels (A). Nk1R and Etv1 are co-localized to dorsolateral population of nVII (B and F). SST is expressed by dorsomedial most nuclei and does not co-localize with Foxp1 (G and H). Interestingly, Nrp2 do not overlap with the intermediate nucleus as well (C and D).

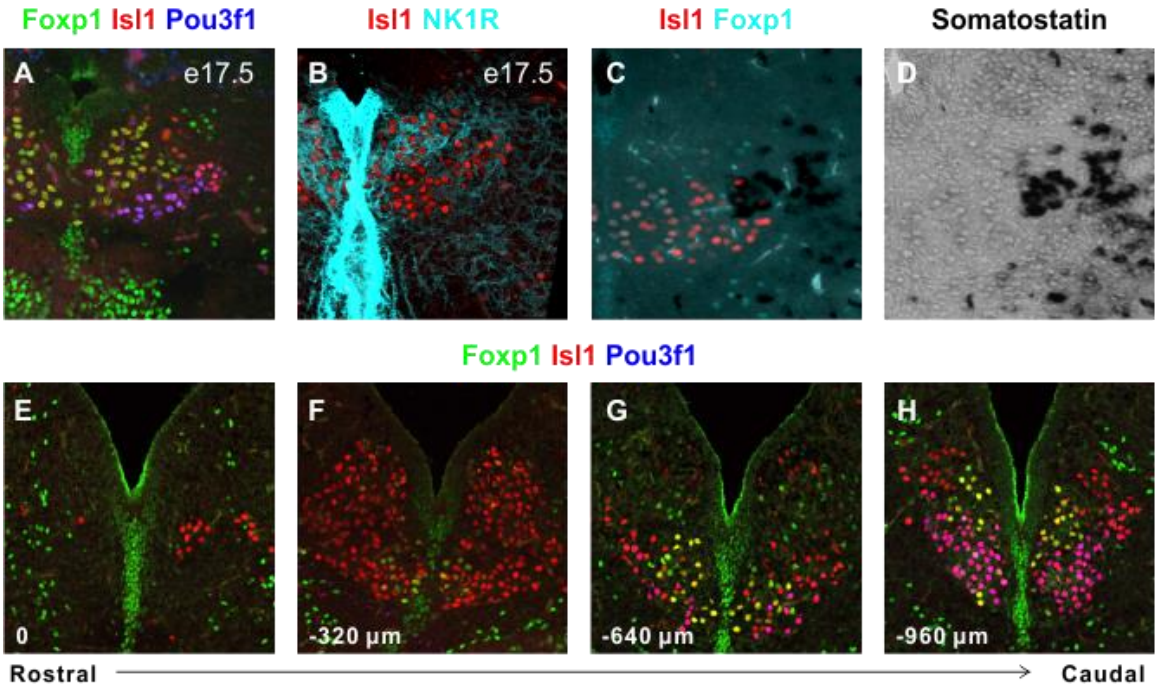

Figure 2-4. Motor pool organization of the hypoglossal motor nucleus

Foxp1 and Pou3f1 is expressed in largely non-overlapping pattern (A). Nk1R is expressed by dorsal hypoglossal MNs (B). SST is expressed by lateral-most cluster that putatively expresses high levels of Pou3f1 and Isl1 (C and D). Pou3f1 is expressed by ventrocaudal most MNs when assessed at different rostrocaudal levels (E-H).

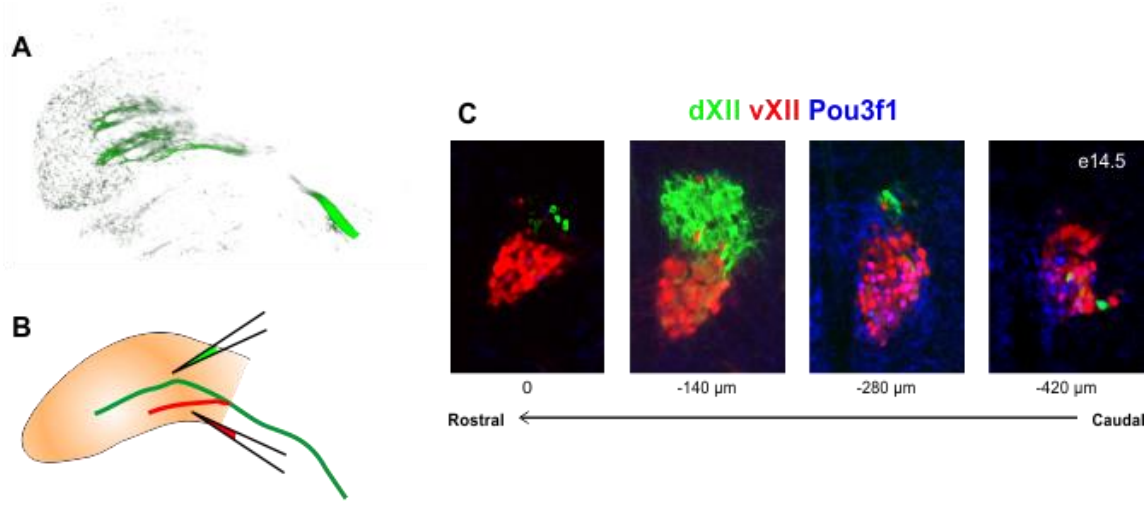

Figure 2-5. Pou3f1+ hypoglossal motor neurons project to genioglossus

Wholemount staining of Hb9GFP at e12.5 reveals medial and lateral (ventral and dorsal) branch of the hypoglossal nerve (A). Injection was done in the two nerve branches at e14.5 (B). Analysis of nXII MNs at different rostrocaudal levels reveal co-localization of ventral branch-projecting MNs with Pou3f1 at caudal medulla (C).

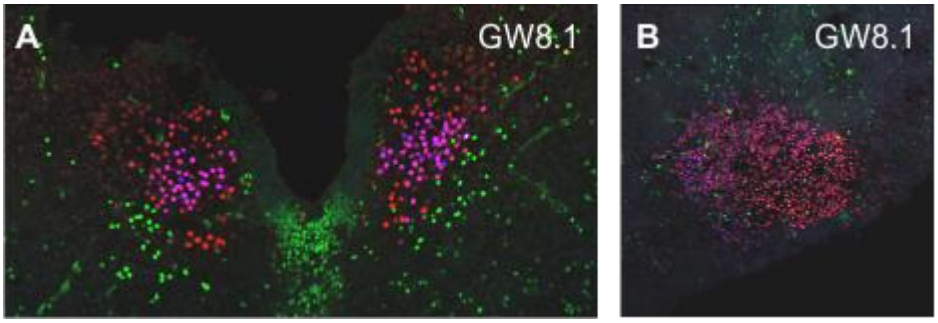

Figure 2-6. Expression of FOXP1 and POU3F1 in human hypoglossal development

GW8.1 human fetal hypoglossal nuclei express POU3F1 ventrally and different levels of Isl1 that allows the identification of distinct subnuclei (A). The expression pattern of POU3F1 in the facial nucleus is broader compared to the hypoglossal nucleus at GW8.1. However, different levels of ISL1 also allows the identification of distinct nuclei (B).

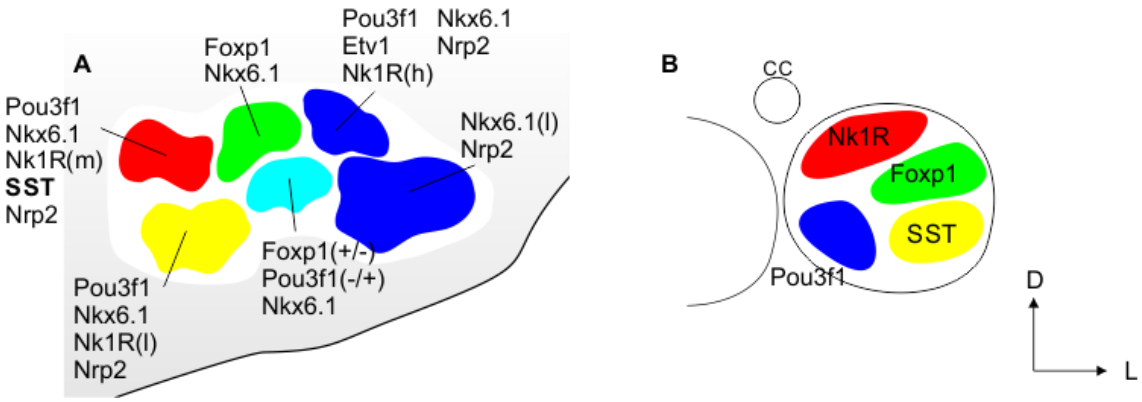

Figure 2-7. Summary of molecular organization of the developing hypoglossal and facial nuclei

The diversity of hypoglossal MNs can be determined by combinations of markers expressed by distinct subnuclei (A). The organization of the hypoglossal MNs is more simple compared to the facial nucleus, and different subnuclei are shown with putative innervation targets (B).

TABLES

Table 2-1. Sequences of primers used to generate anti-sense RNA probes

Gene	Forward	Revers e+ T3 promoter sequence
Neuropilin 2	gagaagccagcaagatccac	GAGattaaccctcactaaagggactggaaaccctggagattca
Somatostatin	gaggcaaggaagatgctgtc	GAGattaaccctcactaaagggagggccaggagttaaggaaga

Table 2-2. Summary of the molecular expression of the assessed markers in the hypoglossal nucleus

Gene	Dorsal	Intermediate	Lateral	Ventral
Foxp1	-	+	-	-
Pou3f1	-	-	-	+
Nk1R	+	-	-	-
SST	-	-	+	-
Nkx6.1	-	-	-	-
Etv1	-	-	-	-
Etv4	-	-	-	-
Raldh2	-	-	-	-
Nrp2	+	+	+	+

Table 2-3. Summary of the molecular expression of the assessed markers in the facial nucleus

Gene	DM	VM	DI	VI (medial/ lateral)	DL	L
Foxp1	-	-	+	+/-	-	-
Pou3f1	+	+	-	-/+	+	-
Nkx6.1	+	+	+	+	+	+(low)
Etv1	-	-	-	-	+	-
Etv4	-	-	-	-	-	-
Raldh2	-	-	-	-	-	-
Nk1R	+(med)	+(low)	-	-	+(high)	-
SST	+	-	-	-	-	-
Nrp2	+	+	-	-	+	

REFERENCES

Ashwell, K. W. (1982). The adult mouse facial nerve nucleus: morphology and musculotopic organization. *J Anat, 135*(Pt 3), 531-538.

Astick, M., Tubby, K., Mubarak, W. M., Guthrie, S., & Price, S. R. (2014). Central topography of cranial motor nuclei controlled by differential cadherin expression. *Curr Biol, 24*(21), 2541-2547. doi: 10.1016/j.cub.2014.08.067

Bailey, E. F., & Fregosi, R. F. (2004). Coordination of intrinsic and extrinsic tongue muscles during spontaneous breathing in the rat. *J Appl Physiol (1985), 96*(2), 440-449. doi: 10.1152/japplphysiol.00733.2003

Bermingham, J. R., Jr., Scherer, S. S., O'Connell, S., Arroyo, E., Kalla, K. A., Powell, F. L., & Rosenfeld, M. G. (1996). Tst-1/Oct-6/SCIP regulates a unique step in peripheral myelination and is required for normal respiration. *Genes Dev, 10*(14), 1751-1762.

Bieger, D., & Hopkins, D. A. (1987). Viscerotopic representation of the upper alimentary tract in the medulla oblongata in the rat: the nucleus ambiguus. *J Comp Neurol, 262*(4), 546-562. doi: 10.1002/cne.902620408

Cattaneo, L., & Pavesi, G. (2014). The facial motor system. *Neurosci Biobehav Rev, 38*, 135-159. doi: 10.1016/j.neubiorev.2013.11.002

Chen, H., Bagri, A., Zupicich, J. A., Zou, Y., Stoeckli, E., Pleasure, S. J., . . . Tessier-Lavigne, M. (2000). Neuropilin-2 regulates the development of selective cranial and sensory nerves and hippocampal mossy fiber projections. *Neuron, 25*(1), 43-56.

Dobbins, E. G., & Feldman, J. L. (1995). Differential innervation of protruder and retractor muscles of the tongue in rat. *J Comp Neurol, 357*(3), 376-394. doi: 10.1002/cne.903570305

Ensini, M., Tsuchida, T. N., Belting, H. G., & Jessell, T. M. (1998). The control of rostrocaudal pattern in the developing spinal cord: specification of motor neuron subtype identity is initiated by signals from paraxial mesoderm. *Development, 125*(6), 969-982.

Giger, R. J., Cloutier, J. F., Sahay, A., Prinjha, R. K., Levengood, D. V., Moore, S. E., . . . Geppert, M. (2000). Neuropilin-2 is required in vivo for selective axon guidance responses to secreted semaphorins. *Neuron, 25*(1), 29-41.

Guidato, S., Barrett, C., & Guthrie, S. (2003). Patterning of motor neurons by retinoic acid in the chick embryo hindbrain in vitro. *Mol Cell Neurosci, 23*(1), 81-95.

Guthrie, S. (2007). Patterning and axon guidance of cranial motor neurons. *Nat Rev Neurosci, 8*(11), 859-871. doi: 10.1038/nrn2254

Ho, R. H., Wu, W., & Elde, R. (1993). Pre-pro-somatostatin mRNA in the developing rat spinal cord with special reference to ventral horn motoneurons. *Neurosci Lett, 163*(2), 125-128.

Hwang, J. C., St John, W. M., & Bartlett, D., Jr. (1983). Respiratory-related hypoglossal nerve activity: influence of anesthetics. *J Appl Physiol Respir Environ Exerc Physiol, 55*(3), 785-792.

Jarrar, W., Dias, J. M., Ericson, J., Arnold, H. H., & Holz, A. (2015). Nkx2.2 and nkx2.9 are the key regulators to determine cell fate of branchial and visceral motor neurons in caudal hindbrain. *PLoS One, 10*(4), e0124408. doi: 10.1371/journal.pone.0124408

Ji, S. J., Zhuang, B., Falco, C., Schneider, A., Schuster-Gossler, K., Gossler, A., & Sockanathan, S. (2006). Mesodermal and neuronal retinoids regulate the induction and maintenance of limb innervating spinal motor neurons. *Dev Biol, 297*(1), 249-261. doi: 10.1016/j.ydbio.2006.05.015

Kleinfeld, D., Deschenes, M., Wang, F., & Moore, J. D. (2014). More than a rhythm of life: breathing as a binder of orofacial sensation. *Nat Neurosci, 17*(5), 647-651. doi: 10.1038/nn.3693

Lee, B. H., Lynn, R. B., Lee, H. S., Miselis, R. R., & Altschuler, S. M. (1992). Calcitonin gene-related peptide in nucleus ambiguus motoneurons in rat: viscerotopic organization. *J Comp Neurol, 320*(4), 531-543. doi: 10.1002/cne.903200410

Maden, M., Sonneveld, E., van der Saag, P. T., & Gale, E. (1998). The distribution of endogenous retinoic acid in the chick embryo: implications for developmental mechanisms. *Development, 125*(21), 4133-4144.

McClung, J. R., & Goldberg, S. J. (2000). Functional anatomy of the hypoglossal innervated muscles of the rat tongue: a model for elongation and protrusion of the mammalian tongue. *Anat Rec, 260*(4), 378-386.

Megirian, D., Hinrichsen, C. F., & Sherrey, J. H. (1985). Respiratory roles of genioglossus, sternothyroid, and sternohyoid muscles during sleep. *Exp Neurol, 90*(1), 118-128.

Moore, J. D., Deschenes, M., Furuta, T., Huber, D., Smear, M. C., Demers, M., & Kleinfeld, D. (2013). Hierarchy of orofacial rhythms revealed through whisking and breathing. *Nature, 497*(7448), 205-210. doi: 10.1038/nature12076

Moore, J. D., Kleinfeld, D., & Wang, F. (2014). How the brainstem controls orofacial behaviors comprised of rhythmic actions. *Trends Neurosci, 37*(7), 370-380. doi: 10.1016/j.tins.2014.05.001

Muller, F., & O'Rahilly, R. (2011). The initial appearance of the cranial nerves and related neuronal migration in staged human embryos. *Cells Tissues Organs, 193*(4), 215-238. doi: 10.1159/000320026

Onimaru, H., Kumagawa, Y., & Homma, I. (2006). Respiration-related rhythmic activity in the rostral medulla of newborn rats. *J Neurophysiol, 96*(1), 55-61. doi: 10.1152/jn.01175.2005

Rousso, D. L., Gaber, Z. B., Wellik, D., Morrisey, E. E., & Novitch, B. G. (2008). Coordinated actions of the forkhead protein Foxp1 and Hox proteins in the columnar organization of spinal motor neurons. *Neuron, 59*(2), 226-240. doi: 10.1016/j.neuron.2008.06.025

Saboisky, J. P., Butler, J. E., Fogel, R. B., Taylor, J. L., Trinder, J. A., White, D. P., & Gandevia, S. C. (2006). Tonic and phasic respiratory drives to human genioglossus motoneurons during breathing. *J Neurophysiol, 95*(4), 2213-2221. doi: 10.1152/jn.00940.2005

Sanes, J. R., & Yamagata, M. (2009). Many paths to synaptic specificity. *Annu Rev Cell Dev Biol, 25*, 161-195. doi: 10.1146/annurev.cellbio.24.110707.175402

Schwartz, J. P., Taniwaki, T., Messing, A., & Brenner, M. (1996). Somatostatin as a trophic factor. Analysis of transgenic mice overexpressing somatostatin in astrocytes. *Ann N Y Acad Sci, 780*, 29-35.

Seroogy, K. B., Bayliss, D. A., Szymeczek, C. L., Hokfelt, T., & Millhorn, D. E. (1991). Transient expression of somatostatin messenger RNA and peptide in the hypoglossal nucleus of the neonatal rat. *Brain Res Dev Brain Res, 60*(2), 241-252.

Stanek, E. t., Cheng, S., Takatoh, J., Han, B. X., & Wang, F. (2014). Monosynaptic premotor circuit tracing reveals neural substrates for oro-motor coordination. *Elife, 3*, e02511. doi: 10.7554/eLife.02511

Stifani, N. (2014). Motor neurons and the generation of spinal motor neuron diversity. *Frontiers in Cellular Neuroscience, 8*, 293. doi: 10.3389/fncel.2014.00293

ten Donkelaar, H., Lammens, M., Cruysberg, J. M., & Cremers, C. J. R. (2006). Development and Developmental Disorders of the Brain Stem *Clinical Neuroembryology* (pp. 269-308): Springer Berlin Heidelberg.

Wichterle, H., Lieberam, I., Porter, J. A., & Jessell, T. M. (2002). Directed differentiation of embryonic stem cells into motor neurons. *Cell, 110*(3), 385-397.

Yasuda, K., Nakayama, Y., Tanaka, M., Tanaka, M., Mori, R., & Furusawa, K. (2002). The distribution of respiration-related and swallowing-related motoneurons innervating the rat genioglossus muscle. *Somatosens Mot Res, 19*(1), 30-35. doi: 10.1080/08990220120113020

Yoshikawa, M., Hirabayashi, M., Ito, R., Ozaki, S., Aizawa, S., Masuda, T., . . . Shiga, T. (2015). Contribution of the Runx1 transcription factor to axonal pathfinding and muscle innervation by hypoglossal motoneurons. *Dev Neurobiol*. doi: 10.1002/dneu.22285

CHAPTER THREE – Respiratory conversion of limb-innervating brachial motor neurons in the absence of Foxp1

Breathing is an essential behavior found in all terrestrial species. Spinal and cranial respiratory motor neurons activate in a coordinated manner to achieve respiration modulated by microcircuits involving local interneurons as well as descending projections from the supraspinal regions. While physiological properties of respiratory motor neurons have been extensively characterized, the origins and the principles governing their circuit assembly are yet unclear. Here we show that the respiratory motor neurons are part of the respiratory motor column spanning the entire cervical spinal cord. Removal of *Foxp1* results in pan-cervical conversion of motor neurons resulting in concomitant expression of an array of molecular markers of endogenous respiratory motor neurons, exhibit respiratory motor output as well as transforming the topography of premotor fibers previously contacting brachial motor neurons. These converted respiratory-like motor neurons show molecular, anatomical and electrophysiological evidence that the assembly of respiratory motor circuit is uniquely and solely dependent on motor neuron identity.

INTRODUCTION

Breathing is achieved by sophisticated control of the muscles surrounding the rib cage thus expanding and contracting the lungs for proper gas exchange. The source of this life-sustaining respiratory rhythm arise from the pre-bötzinger complex of the brainstem as early as ~e15.5 (Dubreuil et al., 2009; Feldman, Del Negro, & Gray, 2013; Gray et al., 2010; Smith, Ellenberger, Ballanyi, Richter, & Feldman, 1991). The medullary respiratory premotor neurons are part of an extensive microcircuit of cardiorespiratory control in the ventrolateral region of the medulla (Spyer & Gourine, 2009). Thus, respiratory rhythm critically depends on the homeostatic parameters of the organism by modulating the MNs directly and indirectly. The medullary respiratory premotor neurons sends mono- and poly-synaptic innervation to the spinal respiratory motor neurons (MNs) (Dobbins & Feldman, 1994; Ellenberger & Feldman, 1990; Ellenberger, Feldman, & Goshgarian, 1990; Ellenberger, Vera, Haselton, Haselton, & Schneiderman, 1990; Gerrits, Vodde, & Holstege, 2000). The respiratory motor circuit becomes functional with the stable phrenic nerve activity emerging at e16.5 (Dubreuil et al., 2009; Gray et al., 2010). During development and even after birth, the respiratory MNs undergo extensive maturation process to forge the stable connectivity required to sustain life (Mantilla & Sieck, 2008; Sanes & Lichtman, 2001).

The MNs that control respiratory muscles reside throughout the spinal cord in the respiratory motor column (RMC; previously known as the hypaxial motor column) (Dasen & Jessell, 2009; Jessell, 2000). Several key features of these motor neurons warrant unified identification of these motor populations as a whole initially suggested by Rose et al (D. Rose, Larnicol, & Duron, 1984). First, the muscles of innervated by these MNs serve the similar function of changing the dimensions of the thoracic cavity. The diaphragm serves as the main

muscle of expanding the thoracic cavity during inspiration; however, ventilation can be assisted by cervical and thoracic accessory respiratory muscles including trapezius, cutaneous maximus, and intercostal muscles to exert pressure onto the rib cage (Holstege, van Neerven, & Evertse, 1987; Lane, 2011). Secondly, classic retrograde labeling experiments demonstrated the existence of monosynaptic connections to the spinal respiratory MNs exist from various parts within the cardiorespiratory control centers of the brainstem otherwise absent in non-RMC MN populations (Feldman, Loewy, & Speck, 1985; Holstege & Blok, 1989). Third, the somatic position of these MNs are placed in the ventrolateral-most corner between the medial motor column (MMC; or axial motor column) and limb-innervating lateral motor column (LMC). Despite these striking similarities the MN populations in the RMC, there is very little understanding of the general organization and developmental ontogeny of the RMC compared to the organization and control of LMC MNs. Finally, the neuronal maturation of respiratory MNs surpass the limb-innervating counterparts by postnatal stages suggesting that these MNs possess specific features of development that enhance maturation (Greer & Funk, 2005; D. Rose et al., 1984). Only recently, the role of transcription factors, developmental pathways, and principles of motor circuit assembly have begun with modern techniques to elucidate the molecular underpinnings of respiratory motor circuit development.

Several types of transcription factor families work in concert to consolidate MN identity during development (Jessell, 2000). The homeotic (Hox) code specifies MN position in the anterior-posterior axis of the spinal cord. Removal of HoxC9 resulted in transformation of thoracic segment into one that resembles caudal cervical (i.e. brachial) segmental organization (Jung et al., 2010). Within a given spinal segment, forkhead domain transcription factors such as *Foxp1* can confer limb-projecting identity when overexpressed at the expense of RMC territory

independent of the influence of Hox proteins (Dasen, De Camilli, Wang, Tucker, & Jessell, 2008; Rousso, Gaber, Wellik, Morrisey, & Novitch, 2008). Conversely, the removal of Foxp1 gene resulted in the expansion of putative RMC-like population with all features of the LMC becoming eroded (Rousso et al., 2008). Some have suggested that removal of LMC results in a "scrambled" MN identity lacking organization (Dasen et al., 2008; Dasen & Jessell, 2009). However, the exact organization and subsequent changes in the motor circuitry have not been fully characterized.

The anatomical layout of the respiratory motor circuitry became available with classic and viral tracing techniques by multiple groups (Billig, Foris, Enquist, Card, & Yates, 2000; Dobbins & Feldman, 1994; Qiu, Lane, Lee, Reier, & Fuller, 2010; Yates, Smail, Stocker, & Card, 1999). In the related segmental proprioceptive spinal circuitry, several aspects of motor circuit development have been identified. MN position have been shown to play a critical role in projection of premotor inputs (Surmeli, Akay, Ippolito, Tucker, & Jessell, 2011; Tripodi, Stepien, & Arber, 2011; Zlatic, Li, Strigini, Grueber, & Bate, 2009). In addition, molecular matching lock-and-key programs involving axon guidance molecules have been shown to play critical roles in synaptic specificity (Fukuhara et al., 2013; Pecho-Vrieseling, Sigrist, Yoshida, Jessell, & Arber, 2009; Sanes & Yamagata, 2009; Vrieseling & Arber, 2006). However, the requirement for precise matching between pre-RMC interneurons and RMC MNs have not yet been addressed. In this study, we sought to resolve the uncertainties posed above by molecular and physiological analyses to assess the development of the respiratory motor system. First, what are the molecular similarities of respiratory MNs? Secondly, what happens to the function and premotor afferent fibers when brachial MNs are converted to assume respiratory features? By

using *Foxp1* mutant system as a tool, we assessed the functional consequence of altering cell fates in the context of respiratory motor circuit assembly.

Our results provide the first insight into molecular and functional transformation of the brachial/caudal cervical LMC to RMC without the alteration of Hox code. We recommend the reclassification of respiratory-related MNs into a unified RMC. We found that the limb-innervating brachial MNs itself are organized into a medial-lateral pattern in $Foxp1^{\Delta MN}$ resembling the organization of true thoracic RMC. Furthermore, these respiratory-converted limb-innervating MNs in $Foxp1^{\Delta MN}$ fire show activity modulated by respiratory rhythm. We found that the cell fate transformation process altered the topography of segmental and bulbospinal premotor fibers, which parallels the changes in expression of candidate guidance cues.

MATERIALS AND METHODS

Animal preparation

The Office for the Protection of Research Subjects (University of California Animal Research Committee) approved all protocols. Foxp1 was selectively removed from motor neurons by crossing the Foxp1 floxed allele that flanks the fork-head domain of the protein encoded by exons 10, 11, 12, and 13 and Cre-recombinase knock-in in Olig2 locus (Dessaud et al., 2007; Zhang et al., 2010). This was the identical crossing scheme of the mouse utilized by Sürmeli and colleagues (Surmeli et al., 2011). Hb9::GFP reporter mice were maintained as previously described (Wichterle, Lieberam, Porter, & Jessell, 2002). We also used Foxp1 global mutant embryos for the microarray experiment (Rousso et al., 2008).

Preparation of RNA from e11.5 Foxp1$^{-/-}$ embryos

From timed mating, e11.5 Foxp1$^{+/-}$; Hb9::GFP and Foxp1$^{-/-}$; Hb9::GFP embryos were collected. The whole spinal cord was dissociated using papain. Motor neurons were isolated by fluorescent-activated cell sorting. RNA was extracted using RNAeasy micro kit (Qiagen). The RNA-processing was performed by Clinical Microarray Core at UCLA to be used in Affymetrix 430 2.0 GeneChips. The expression dataset was analyzed using dChip (Li & Wong, 2001).

Immunohistochemistry

The antibodies used in this study are of the following: guinea pig Foxp1 (Rousso et al., 2008), rabbit Pou3f1 (generous gift from Dies Meijer), goat Islet1 (R&D systems), goat HoxA5 (Santa Cruz), mouse 4D5 (Developmental Hybridoma Bank), and rat Bcl11b (Abcam). Immunohistochemistry procedures were performed as previously described (Rousso et al., 2008).

In situ hybridization

In situ hybridization was performed as previously described (Novitch, Chen, & Jessell, 2001; Novitch, Wichterle, Jessell, & Sockanathan, 2003; Rousso et al., 2008). The specific primers used for the generation of probes are as follows: Pappa (forward: aacggaagcattttgtccaac; reverse: ctttgccgaaagtggagaag), Ptn (forward: gggtgggtgctaagaacaaa; reverse: ctgactagctggctgccttt), and Pcdh10 (forward: acggaagcattttgtccaac; reverse: ctttgccgaaagtggagaag).

Embryonic retrograde labeling

The embryonic retrograde labeling procedure was performed as previously described (Rousso et al., 2008). Briefly, the embryos were collected at e14.5 or e16.5 in oxygenated (95% O_2/5% CO_2) DMEM/F12 media. The peripheral nerves visualized with Hb9::GFP were injected with tetramethylrhodamine dextran amine (RDA; Invitrogen), biotinylated dextran amine (BDA; Invitrogen), or horseradish peroxidase (Thermo Fisher Scientific). The injected embryos were cultured in bubbling media for 12 hours followed by fixation and subsequent tissue processing as previously described (Rousso et al., 2008).

"En bloc" brainstem-spinal cord preparation and recording

We used wild type and mutant neonatal C57BL/6 mice (P0) of either sex for experiments *in vitro*, and the experimenter was blinded to the genotype. The brainstem and spinal cord were dissected out as described previously (Mellen, Janczewski, Bocchiaro, & Feldman, 2003; M. F. Rose et al., 2009; Tupal et al., 2014). Briefly, following deep anesthesia with isoflurane, a

complete thoracotomy and coronal transection at the level of the bregma was performed, followed by dorsal laminectomy, and an intracollicular transection. The preparation was then placed ventral side up and the ventral surface of the brain was exposed and the cranial nerves cut. A ventral laminectomy revealed the ventral surface of the cord and ventral spinal nerves. Spinal nerves were visualized and then cut. The spinal cord was severed caudal to T6, and the pons was left attached. The preparation was dissected in artificial cerebrospinal fluid (ACSF) containing (in mM): 124 NaCl, 3 KCl, 1.5 $CaCl_2$, 1 $MgSO_4$, 25 $NaHCO_3$, 0.5 NaH_2PO_4, and 30 D-glucose, equilibrated with 95% O_2 and 5% CO_2 (27°C, pH=7.4).

En bloc preparations were perfused with 27°C ACSF at 4 ml/min in a 0.5 ml chamber mounted rostral side up in a fixed-stage DMLFS (Leica Microsystems, Buffalo Grove, IL, USA) microscope, and were allowed to equilibrate for 30 minutes. Respiratory activity reflecting suprathreshold action potential (AP) firing from populations of spinal motor neurons was simultaneously recorded from spinal nerves (C4, C6, C7, C8) using suction electrodes, amplified with a MultiClamp 700B (Molecular Devices, Sunnyvale, CA, USA) and a Model 1700 differential AC amplifier (A-M Systems, Sequim, WA, USA), filtered at 2–4 kHz, and digitized at 10 kHz. Activity was full-wave rectified and digitally integrated with a Paynter filter with a time constant of 20 ms.

Data analysis and statistics

Digitized data were analyzed off-line using custom procedures written for IgorPro (Wavemetrics, Portland, OR, USA) (Kam, Worrell, Janczewski, Cui, & Feldman, 2013). Semi-automated event detection was executed using custom procedures that used multiple criteria,

including slope and amplitude thresholds, to select events automatically, which were then confirmed visually by the experimenter.

Unlike intracellular recordings, suction electrode recordings lack a scale that allows comparisons across experiments, and the value of nerve discharge signals, i.e., measured voltage, varied significantly in absolute value between experiments. Therefore, for comparisons across experiments, the baseline was subtracted and the signal scaled to the maximum peak amplitude in the control condition for each experiment. The amplitude was then measured from the scaled signal. A peak-detection algorithm defined event amplitude as the difference between peak and baseline. The period was calculated as the time between the peaks of two consecutive events.

Data are represented as mean ± standard deviation (SD). Statistical significance was uniformly set at a minimum of $p<0.05$. For statistical comparisons of more than two groups, an ANOVA was first performed. In most cases, a two-way repeated measures ANOVA was used for comparisons of various parameters in different conditions and for making comparisons across different events. If the null hypothesis (equal means) was rejected, post-hoc paired t-tests were then used for pairwise comparisons of interest. Individual p-values are reported, but Holm-Bonferroni analysis for multiple comparisons was conducted to correct for interactions between the multiple groups. For one-way and two-way ANOVAs, post-hoc significance for pairwise comparisons was analyzed using Tukey-Kramer analysis.

RESULTS

Organization of the respiratory motor column in the rostral spinal cord

In order to obtain a better understanding of the RMC organization, we first mapped the location of respiratory MNs defined by the absence of *Foxp1* and *Lhx3* expression, which labels the LMC and MMC, respectively. These respiratory MNs are present throughout the entire cervical spinal cord, and these MN population receive premotor inputs and project out to the respiratory muscles (Feldman et al., 1985; Lane, 2011). Rostral to C3 level, the respiratory MNs innervate the cervical neck musculature. Beginning with C3 level of the cervical spinal cord, phrenic motor neurons (RMCph), rhomboids/trapezius (RMCrh) MNs begin to appear **(Fig 3-1A-C)** (Rousso et al., 2008). By C6 level, RMCph and RMCrh had disappeared and the cutaneous maximus motor neurons (RMCcm) begins to appear that extends down to the level of the thoracic spinal cord **(Fig 3-1D-F)**. RMCph, RMCrh, and RMCcm all share similar somatic locations sandwiched between the LMC and the MMC in the ventrolateral-most corner of the ventral horn **(Fig 3-1K)**. RMCcm has been shown to receive monosynaptic projection from the medullary respiratory premotor column (Feldman et al., 1985). RMCcm expresses the marker Ets variant 4 transcription factor (*Etv4*), and express very low levels of Foxp1 compared to LMCm (Foxp1 intensity is 22.24 fold less in RMCcm vs. LMCm; $p<0.0001$) **(Fig 3-1G, 1I)**. The low-levels of Foxp1 are visible in RMCcm as early as e11.5 (data not shown). However, the *Etv4* expression is absent in *Foxp1* mutant mice suggesting that establishment of RMCcm motor pool may be a *Foxp*-dependent process (Dasen et al., 2008; Rousso et al., 2008). The reclassification of the respiratory-related motor neurons into a single column would provide a better understanding of their role in respiratory motor circuitry development.

Removal of Foxp1 results in generation of excess number of RMC-like MNs

Previous reports involving *Foxp1* global knockout mice have shown that the number of LMC motor neurons are reduced and alternate LMC markers such as *Raldh2* and *Nkx* limb motor pool markers are entirely absent (Rousso et al., 2008; Surmeli et al., 2011). To assess the ultimate cell fate of the Foxp1-removed LMC motor neurons at forelimb levels, we assessed any changes to the RMC size and their molecular profile in the *Foxp1* mutant spinal cord at early and late stages of development. In agreement with the previous reports, the RMC population was enlarged in the mid-cervical spinal cord of $Foxp1^{\Delta MN}$ **(Fig 3-2A, 2D)**. We then looked at the phrenic motor neuron marker Pou3f1 at this level, in which have been demonstrated as exclusively HoxA5+ (Machado et al., 2014). Of the expanded RMC, we confirmed that ~2.2-fold more Pou3f1+/HoxA5+ MNs exist in $Foxp1^{\Delta MN}$ at e12.5 *($p<0.0001$)* **(Fig 3-2B, 2E, 2G)**. However, to our surprise, this number dramatically corrects by e16.5, reducing the number to levels comparable to control (p=0.1836) **(Fig 3-2C, 2F, 2G)**. In addition, when *bona fide* phrenic motor neurons are retrograde labeled from the phrenic nerve, the number of diaphragm-projecting motor neurons are initially born ~1.8-fold greater but by e14.5 *($p=0.0011$)*, this number corrects to the number of the control spinal cord **(Fig 3-2H)**. The corrected number of phrenic motor neurons persists until postnatal stages ~P17 *($p=0.5593$)* **(Fig 3-2H)**.

While we predicted that the final pattern of diaphragm innervation would be preserved in the absence of *Foxp1*, we were curious what impact the initial burst of RMC-like MNs might have on initial diaphragm innervation. Previous examination of the phrenic nerve at e12.5 reported thickened phrenic nerve bundles (Rousso et al., 2008). However, the projection pattern following this time point has never been assessed. The diaphragm makes its initial contact with the primordial diaphragm ~e11.5 and the primary diaphragm projects the sternum by

~e15.5(Mantilla & Sieck, 2008). Thus, we did not expect that the length of the primary branch of the phrenic nerve would be different between *Foxp1*$^{\Delta MN}$ and control **(Fig 3-2I-O)** (*p=0.3827* (e14.5), *p=0.4246* (e16.5), Student's *t*-test). However, the diaphragm of *Foxp1*$^{\Delta MN}$ seemed much branchy compared to control. Indeed, we found that the secondary phrenic branches in *Foxp1*$^{\Delta MN}$ were significantly longer than that of the control **(Fig 3-2P)** (59.75µm longer in *Foxp1*$^{\Delta MN}$ than control; *p=0.0196*, Student's *t*-test). This difference disappeared by e16.5 (*p=0.1958*, Student's *t*-test) showing that the branchy appearance of early phrenic primary branches results from early growth spurt due to expanded RMC-like population.

At caudal cervical levels where motor neurons are predominantly HoxC8+, a Pou3f1+ LMC motor pool exists and innervates distal forelimb/hand muscles **(Fig 3-3A)**. This population continues to exist into later in development- e16.5 **(Fig 3-3B)**. We were curious whether this population would disappear in *Foxp1*$^{\Delta MN}$. In *Foxp1*$^{\Delta MN}$, the Pou3f1+ motor pool also exists, but its position is shifted ventrally compared to control **(Fig 3-3E, 3F)**. Etv4 is not detected at these levels of *Foxp1*$^{\Delta MN}$, which is consistent with previous reports (data not shown) (Rousso et al., 2008). In addition, large portions of MNs at caudal cervical levels begin to wither by e14.5 in *Foxp1*$^{\Delta MN}$ **(Fig 3-3D)**. The MNs at these levels have diminished capabilities projecting to the cutaneous maximus muscle at e14.5, thus these MNs are projecting to other muscle groups of the limbs **(Fig 3-3G)**. It may be possible that similar to saturated phrenic projecting RMC-like MNs undergoes rapid pruning, other limb nerves may be experiencing similar environmental pressure as well. We were curious to what and why are these MN projecting to the aberrant muscle targets.

Proximal forelimb muscle innervation requires Foxp1

Proper muscle innervation requires responsiveness of MNs to guidance cues available as they project out to the periphery. We were curious what the impact of respiratory conversion of *Foxp1*$^{\Delta MN}$ brachial MNs might be in later development. Indeed, an earlier report showed that dorsal limb projections are compromised, whereas ventral limb innervation was preserved (Rousso et al., 2008). However, the exact muscles affected as well as whether these innervation are maintained until birth have not been examined. Thus, we looked at three locations of the forelimbs- the upper shoulder, distal extensors, and distal flexors at e14.5 **(Fig 3-3H)**. When looked at upper shoulder muscles- infrascapularis, spinodeltoid, and acromiodeltoid muscle innervation, the *Foxp1*$^{\Delta MN}$ showed below detectable levels of innervation compared to control **(Fig 3-3I)**. However, the distal extensors that innervate the dorsal limb (radial nerve) were preserved in *Foxp1*$^{\Delta MN}$ as with median and ulnar nerves that innervate distal flexors **(Fig 3-3I)**. While the nerve projection was intact, the nerve width was thinner in *Foxp1*$^{\Delta MN}$ compared to control **(Fig 3-3K)**. Radial nerve was 23.6% thinner ($p=0.030$, Student's *t*-test). Median nerve was 25.1% thinner ($p=0.0069$, Student's *t*-test), and ulnar nerve was 43.1% reduced compared to control ($p=0.042$, Student's *t*-test). The general reduction of nerve width is consistent with massive cell death at caudal cervical level of the spinal cord already seen by e14.5 **(Fig 3-1M)**.

Muscle innervation and maintenance of the innervation underlie distinct molecular requirement. Indeed, transplantation of avian thoracic spinal cord into the brachial segments resulted in proper initial innervation with eventual denervation (Butler, Cauwenbergs, & Cosmos, 1986). Thus, we sought to validate that the innervation and stable end-plate exists at birth. We analyzed Neuronal Class III β-tubulin (Tuj1) and nicotinic acetylcholine receptors revealed with α-bungarotoxin (alpha-BTX) at postnatal stages. In control and *Foxp1*$^{\Delta MN}$, the

alpha-BTX are scattered throughout the bicep, triceps, distal extensors and distal flexor muscles **(Fig 3-3J)**. When the surface area of the NMJ was calculated, it was found that the surface area of bicep end-plate is 21.0% smaller than control ($p<0.043$, Student's *t*-test). However, the same analyses for triceps muscle was found to be not significant ($p<0.087$, Student's *t*-test). The projection analyses show that RMC-like MNs at caudal cervical levels can innervate and maintain structurally sound neuromuscular junction with various muscles in the distal limbs.

RMC-like MNs in Foxp1$^{\Delta MN}$ show molecular characteristics of RMC MNs

In order to obtain a better understanding of increased size of RMC-like population, we performed a microarray experiment comparing the transcriptome of MNs of *Foxp1*-mutant embryo and control at e11.5. The full list of differential gene expression can be found in **Table 3-s1**. Among the genes we found to be upregulated in Foxp1 mutants, we were most interested in the four genes that showed robust expression in the RMCph population. These four genes include *Developmentally-Regulated Endothelial Cell Locus 1 Protein (Del1), pleitrophin (Ptn), pregnancy associated plasma protein A (Pappa), protocadherin 10 (Pcdh10)* **(Fig 3-s1A)**. These markers have also been reported by other groups as well **(Fig 3-s1B-s1F)** (Machado et al., 2014).

With novel RMC markers at hand, we wanted to probe the molecular profile of the newly converted RMC-like MNs at caudal cervical spinal cord that are under the HoxC8 context. In control, subpopulations of LMC and RMCcm show expressions of these markers. More specifically, *Ptn* expression is localized to LMCm and RMCcm populations **(Fig 3-s1H).** *Pcdh10* expression is quite broad in the LMC **(Fig 3-s1K)**. *Pappa* is expressed in LMCl **(Fig 3-s1I)**. *Del1* exclusively demarcates *RMCcm* populations as well **(Fig 3-s1J)**. In *Foxp1$^{\Delta MN}$*, all of these markers are robustly expressed in the RMC-like population located ventromedially **(Fig 3-s1M-**

1R, s1X, s1Y). The expression of these markers are located in RMC-like, not RMCph-like cells, as co-expressed by HoxC8 **(Fig 3-s1T-s1W)**. The more lateral population of *Foxp1*$^{\Delta MN}$ designated as LMC* show milder expression of these markers, illustrating that the transformation would be incomplete in these populations possibly due to the influence of retinoic acid from paraxial mesoderm. Our results show that the converted RMC-like population in *Foxp1*$^{\Delta MN}$ indeed recapitulates many aspects of the developmental processes of respiratory MNs in a Hox level where normally Pou3f1+ respiratory MNs do not exist.

Medial-lateral organization of RMC-like motor neurons in Foxp1$^{\Delta MN}$

Because of the proper innervation of some muscle groups in *Foxp1*$^{\Delta MN}$, we were curious whether the muscle projection of MNs might be correlated with the somatic position. Furthermore, the changes in somatic position resulting from respiratory conversion could impact on organization of bona fide RMCph MNs. Thus, we retrogradely labeled phrenic MNs and different nerves present at e12.5 **(Fig 3-4A, 4F)**. First, we injected BDA into the ventral limb (presumably the median nerve) and RDA into the phrenic nerve **(Fig 3-4A)**. The analyses have been done at rostral brachial levels where RMCph MNs are normally present. In control, flexor muscles are innervated by LMCm MNs present at the dorsal-most extreme **(Fig 3-4D)**. In *Foxp1*$^{\Delta MN}$, however, the positions of flexor innervating MNs are positioned far ventrally and intermingled with the phrenic motor neuron population **(Fig 3-4I)**. In contrast to distal flexors, distal extensors are normally innervated by LMCl MNs. We were then curious about the somatic location of extensor-innervating motor neurons in control and *Foxp1*$^{\Delta MN}$. This location was found by injecting BDA into the dorsal limb (presumably the radial nerve) and RDA into the phrenic nerve. In control, extensor muscle innervating motor neurons were positioned in the

laterally where LMCl MNs are normally found **(Fig 3-4H)**. Interestingly in *Foxp1*$^{\Delta MN}$, the radial MNs continue to exist in the lateral location as in its own defined cluster, and mostly away from the phrenic-like motor pool **(Fig 3-4I)**.

Medial-lateral organization of respiratory motor pools in the thoracic spinal cord

After discovering the medial-lateral organization of the motor pool, we looked at the respiratory motor neurons at the thoracic level where normally there are respiratory motor neurons presumably inspiratory and expiratory in function by anatomical and functional studies (Merrill & Lipski, 1987; Road, Ford, & Kirkwood, 2013). Thus, we retrogradely labeled two nerve branches that emerge from the thoracic intercostal nerve guided by Hb9::GFP reporter. One intercostal branch had a more ventral trajectory (indicated as vIC) than the other (dIC) **(Fig 3-4K)**. To our surprise, the MNs that innervate the dorsal branch were positioned more medially compared to the MNs that innervate the ventral branch **(Fig 3-4L, 4M, and 4N)**. The dorsal branch of the intercostal muscle innervates the external intercostal muscle and thus it is mainly inspiratory in function. The medial-lateral organization was present throughout the spinal cord **(Fig 3-4P, 4O)**. This respiratory motor pool organization shares striking resemblance with what we see in converted respiratory brachial MNs of *Foxp1*$^{\Delta MN}$. Furthermore, when examining the thoracic spinal cord of control embryos, we found that the thoracic intercostal MNs could be defined into multiple motor pools by the expression of different markers identified in our microarray analysis **(Fig 3-2A-F)**. Most salient organization was the medio-lateral organization of the RMC motor pools revealed by Pou3f1, *Del1* and Bcl11b expression patterns **(Fig 3-s2G)**. Other markers, such as Etv1 and *Ptn* also labeled subsets of the RMC MNs, but the somatic positions of these MNs appeared more dorsally than medially **(Fig 3-s2H)**. In addition, Unc5C

and Nrp2 expression altered with the removal of Foxp1 as well. In phrenic MNs, low levels of Unc5C are present in control *Foxp1*$^{\Delta MN}$ **(Fig 3-s3A-D, 3M)**. At caudal cervical regions, Unc5C and Nrp2 are present in Pou3f1+ LMCm MNs **(Fig 3-s3E-F, 3I-J)**. However, in *Foxp1*$^{\Delta MN}$, Unc5C and Nrp2 both decreased in expression levels in medially-positioned Pou3f1+ FCU-projecting MNs **(Fig 3-s3G-H, K-L, 3M)**. However, the lateral Pou3f1- RMC-like population had significantly higher levels of Unc5C than LMCm MNs in control **(Fig 3-s3M)**. Furthermore, the absence of Nrp2 in medial RMC-like MNs parallels the absence of Nrp2 in medial RMC MNs in the thoracic spinal cord **(Fig 3-s3O-P)**.

Extension of the respiratory drive to brachial limb-innervating motor neurons in Foxp1$^{\Delta MN}$

We hypothesized that the respiratory conversion of MNs would initiate the transformation of motor circuitry harboring brachial MNs and ultimately instituting different motor programs for these MNs in *Foxp1*$^{\Delta MN}$. In order to measure the final activity of motor output, we turned to the *en bloc* brainstem-spinal cord reduced preparation of the neonatal pup **(Fig 3-5A)**. This was determined as the ideal approach because it is a reduced preparation where the minimum components of the respiratory circuitry were preserved but other inputs such as proprioceptive afferents (i.e. dorsal root) and cortical influences were severed away. In control preparations, the C4 ventral root activity had very robust activity reflecting phrenic output **(Fig 3-5B)**. This signal was in-phase (less than $\pi/2$) with the coincident bursts at C8 level, which reflects the inspiratory intercostal activity. In contrast, at C6 and C7 levels only modest amplitude of activity could be seen **(Fig 3-5E)**.

We then assessed the cervical ventral root activity in neonatal *Foxp1*$^{\Delta MN}$ pups using the *en bloc* preparation. As expected, the C4 and C8 ventral roots exhibited activity synchronous to

one another. However, striking similarities in amplitude were found in C6/7 ventral roots compared to C4 of *Foxp1*$^{\Delta MN}$ **(Fig 3-5C)**. The normalized amplitude of C6/7 ventral roots were not significantly different from that of C4 levels **(Fig 3-5F)**. Furthermore, the respiratory-like activity at C6 and C7 ventral roots of *Foxp1*$^{\Delta MN}$ was in-phase (less than $\pi/2$) compared to C4 **(Fig 3-5G)**. From these results, we conclude that respiratory conversion of brachial MNs are truly functional respiratory MNs firing in synchrony with respiratory rhythm.

Reorganization of premotor fibers projecting to respiratory-converted motor neurons

The striking electrophysiological findings led us to assess the premotor/motor interface at the caudal cervical levels. We utilized two markers of premotor fibers- parvalbumin (PV) and enkephalin (Enk) for this approach. PV has been used extensively to label the proprioceptive sensory afferents that make contact with homonymous alpha-motor neurons (Fukuhara et al., 2013; Pecho-Vrieseling et al., 2009). We visualized forearm flexor (flexi carpi ulnaris; FCU)-projecting MNs using beta-subunit of cholera toxin (Ctb) **(Fig 3-6A, 6F)**. The proprioceptive afferents visualized by PV revealed a dramatic shift in the trajectory of these afferents to the deep down to the ventral where FCU MNs are present in *Foxp1*$^{\Delta MN}$ (angle from midline is 57.12 in control vs. 38.75 in *Foxp1*$^{\Delta MN}$; *p=0.0284, Student's t test*) **(Fig 3-6B, 6D, 6E, 6G, 6I)**. In *Foxp1*$^{\Delta MN}$, the PV+ fibers reach the FCU MNs, but forms fewer synaptic contacts measured by co-localization of vGlut1 and PV onto the Ctb+ surface (9.167 in control vs. 3.750 in *Foxp1*$^{\Delta MN}$; *p=0.0007, Student's t test*) **(Fig 3-6C, 6H)**.

We sought to analyze the bulbospinal fibers that project to the brachial levels of the spinal cord. Enk+ fibers have been found in respiratory-related bulbospinal fibers to phrenic MNs as well as presympathetic fibers that project to thoracic preganglionic MNs originating

from the ventral respiratory group (VRG) and rostral ventrolateral medulla (RVLM), respectively **(Fig 3-6K-6N)** (Stornetta, 2009; Stornetta, Sevigny, & Guyenet, 2003). In the control, we looked for Enk+ fibers and found in the cutaneous maximus. In the *Foxp1*$^{\Delta MN,}$ the dense collection of Enk+ fibers are largely disappeared despite the presence of MNs **(Fig 3-6P, 6T)**. When counting the number of synaptic contacts that onto the FCU MNs, we found that there is slightly more Enk+ vGlut2+ contacts in *Foxp1*$^{\Delta MN}$ (4.000 in control vs. 9.250 in *Foxp1*$^{\Delta MN}$) **(Fig 3-6Q, 6R, 6U)**. Interestingly, when we looked at the expression of PV and Enk by combining two serial section images, we discovered that the presence of two markers show mutually exclusive pattern that is absent in *Foxp1*$^{\Delta MN}$). Furthermore, at least one member of the Semaphorin family, Sema7A, seems to be present in LMC but lower in RMCcm **(Fig 3-s4K-4M)**. In *Foxp1*$^{\Delta MN}$, the expression is also altered where the expression of Sema7a is the lowest in RMCm* that putatively innervate ventral limbs and higher in RMCl* that innervates the dorsal musculature (Supplemental figure 4N-4P). Thus, the rearrangement of attractant molecules such as semaphorins may underlie recruitment of premotor fibers.

DISCUSSION

Unified classification of the respiratory motor column

In this study, we put forth the idea that cervical hypaxial motor neurons comprise a unified RMC throughout the cervical and thoracic spinal cord. While most RMC MNs never express Foxp1 and their identity is preserved in *Foxp1*$^{\Delta MN}$, some of RMC MNs, including RMCcm, may require a *Foxp1*-dependent step as Etv4 expression and CM-projection disappear in *Foxp1*$^{\Delta MN}$. Transient expression of Foxp-proteins have been reported during normal MN development process, and a similar process may underlie maturation of RMCcm (Rousso et al., 2012). Essentially the removal of *Foxp1* results in generation of *Foxp1*-independent RMC MNs in the brachial/caudal cervical spinal cord.

Respiratory conversion of Foxp1-dependent MNs in the brachial spinal cord

We explored the underlying circuit organization of the cervical spinal cord by removing *Foxp1*. Previously, *Foxp1* mutant motor phenotypes have been attributed as "scrambling" of MN identity by stripping away the LMC identity from these MNs (Surmeli et al., 2011). Consistent with earlier findings, we have found that developmental programs for proper limb muscle control lack in *Foxp1*$^{\Delta MN}$. However, our findings suggest that the cervical MNs with eroded LMC identity have gone into a partial commitment to RMC identity in the absence of *Foxp1*. Furthermore, our results show a medial-lateral partitioning of the cervical MNs in developing *Foxp1*$^{\Delta MN}$, where flexor projecting MNs make up part of the phrenic nucleus or mimic its organization, where extensor projecting MNs segregate into their characteristic position similar to control conditions. The underlying organization of the limb-innervating RMC-like MNs resemble the organization of the thoracic spinal cord where inspiratory MNs innervating

expiratory intercostal muscles are positioned medially and expiratory MNs innervating internal intercostal muscles are positioned more laterally. We speculate that the expiratory MNs may share origins with the extensor-innervating *Foxp1*$^{\Delta MN}$ MNs as the two muscles groups share the somatic position and function, such as maintenance of posture.

We have found that *Pou3f1* expression correlates with expression of other RMC-markers such as Ptn and Pappa in thoracic region of control (data not shown). Here we showed that when *Foxp1* is removed, the ectopic *Pou3f1*+ RMC-like MNs also express many markers associated with *Pou3f1*. Thus, previously reported phrenic markers are not unique to phrenic identity but they may serve more a universal purpose of consolidating RMC motor pool identity and potentially other neuronal properties relevant for rhythmic control.

RMC-like MNs innervate distal arm and forearm muscles

Previous reports showed that *Foxp1* overexpression in an embryonic stem cell-derived motor neuron allows for directed differentiation into MNs of LMC phenotype (Adams, Rousso, Umbach, & Novitch, 2015). In this case, *Foxp1*-expressing motor axons choose to take limb nerves instead of nerves that innervate the axial muscles and form structurally intact neuromuscular junctions. In our study, we found that the RMC-like MNs have the ability to project out into the brachial plexus and form structurally stable neuromuscular junctions at the limb muscles. This is in contrast with classic transplantation experiments using the avian model system where the brachial segments of spinal cord were replaced with thoracic segments (Butler et al., 1986). Bona fide thoracic motor neurons could project out to the specific limb muscles; however, the muscles were ultimately denervated during later stages of development(Butler et al., 1986). The compatibilities of RMC-like MNs and distal limb muscles show that the RMC-

like MNs are different from thoracic RMC MNs. At mid-cervical levels, HoxA5+ Pou3f1+ MNs primarily projected out into the diaphragm, away from their normal targets that are the proximal limb muscles of the upper shoulder. The diaphragm itself is made up of multiple muscles patterned during development, although the developmental process is yet unknown(Merrell & Kardon, 2013). We predict that shared molecular features must exist between distal limb muscles and the parts of the diaphragm and respective LMC and RMC motor pools that innervate these muscles. Supporting this idea, when HoxC9 is removed the Pou3f1+ LMC motor pool extends caudally into the thoracic segments of the spinal cord (Jung et al., 2010). Surprisingly, The Pou3f1+ LMC MNs project and innervate the intercostal muscles.

Respiratory drive transference to ectopic RMC motor neurons in Foxp1$^{\Delta MN}$

In *Foxp1$^{\Delta MN}$*, C6 and C7 spinal ventral roots that normally do not show significant respiratory activity show robust signal. From our results, we interpret that the descending cardiorespiratory premotor network has changed to accommodate the altered motor neuron landscape **(Fig 3-7A)**. Assessing two premotor afferent fiber types, that are PV+ and Enk+, we see that the topography of proprioceptive and cardiorespiratory premotor fibers and their synaptic contacts have been altered. This change could be the denervation of the monosynaptic connection between medullary cardiorespiratory interneurons and RMCcm population, which have been described previously (Feldman et al., 1985; Gerrits et al., 2000). The medullary respiratory interneurons in the VRG form primarily monosynaptic connections to the phrenic motor neurons in the mouse that are vGlut2^{+}Enk^{+} (Stornetta, 2009; Stornetta, Schreihofer, Pelaez, Sevigny, & Guyenet, 2001; Stornetta et al., 2003). The remaining Enk+ premotor afferent are likely the respiratory premotor fibers in *Foxp1$^{\Delta MN}$*; however, alternate indirect

transference of respiratory drive could underlie this phenomena **(Fig 3-7C)**. Future studies assessing whether this change in premotor circuit involves mono- or polysynaptic respiratory inputs into these motor neurons might allow us to know the further requirement for application to respiratory rehabilitation and potential regenerative therapy. It is interesting to note that in some cases of brachial plexopathy, regenerating phrenic and intercostal nerves have been reported to aberrantly innervate limb muscles **(Fig 3-7B)** (Carlstedt, Anand, Htut, Misra, & Svensson, 2004; Malessy, van Dijk, & Thomeer, 1993; Swift, 1994). In the cat, the phrenic motor neurons can follow a behavior that can be voluntarily controlled when cross-innervated with a limb nerve (Fujito, Kawasaki, & Aoki, 1989). As breathing is one of life sustaining muscular activities, an enormous room for plasticity and rearrangement may be possible as well. Indeed, hemisection at the rostral cervical spinal cord (e.g. C2) results in respiratory drive crossing the midline to reach the phrenic MNs in the contralateral side – this is known as the crossed phrenic phenomenon (CPP). Similar molecular mechanisms might underlie CPP and respiratory conversion (see Chapter 5 for further discussion on the relevance of CPP and respiratory conversion). Combining our results and previous reports, we predict that the involuntary breathing circuitry may transfer respiratory drive to the ectopic phrenic MNs but not ones that are responsible for volitional movement.

Potential roles of guidance cues in respiratory motor circuit development

Due to the critical nature of respiratory motor circuit assembly, it is likely that redundant mechanisms shape functional respiratory circuitry. One interesting feature of brachial MNs in the control is that the LMC MNs receive PV+ premotor fibers and RMCcm receive Enk+ premotor fibers. This mutually exclusive premotor trajectory matches the differential expression of

Sema3E expression and Sema7A expression **(Fig 3-s3I)**. Removal of Sema3E results in an invasion of Sema3E into RMCcm territory, suggesting that Sema3E is important for repelling PV+ afferent fibers. However, it is not yet known what roles these Semaphorin molecules have on cardiorespiratory Enk+ fibers in the RMCcm territory. It would be interesting to assess the Enk+ fibers when Sema3E is overexpressed in LMC and Sema7A is removed in the LMC. One important aspect that we have not yet explored is the difference in MN-intrinsic properties between LMC, RMC proper, and RMC-like MNs. Differential expression of ion channels and types of neurotransmitter expression could confer different properties of MNs and alter their firing patterns, even in the absence of altered premotor network.

In conclusion, this study has shown that removal of Foxp1 converts Foxp1-dependent LMC and RMC MNs into Foxp1-independent inspiratory RMC MNs. The respiratory converted brachial MNs can innervate the limbs and fire with inspiration. The altered MN landscape results in altered topography of premotor fibers. The mutually exclusive fiber presence matches with candidate guidance cues that may underlie organization of premotor afferents. Future studies delineating the molecular requirement of respiratory plasticity and circuit assembly will light on the potentials of respiratory plasticity and rehabilitation for application in cases of MN disease and injury.

FIGURES

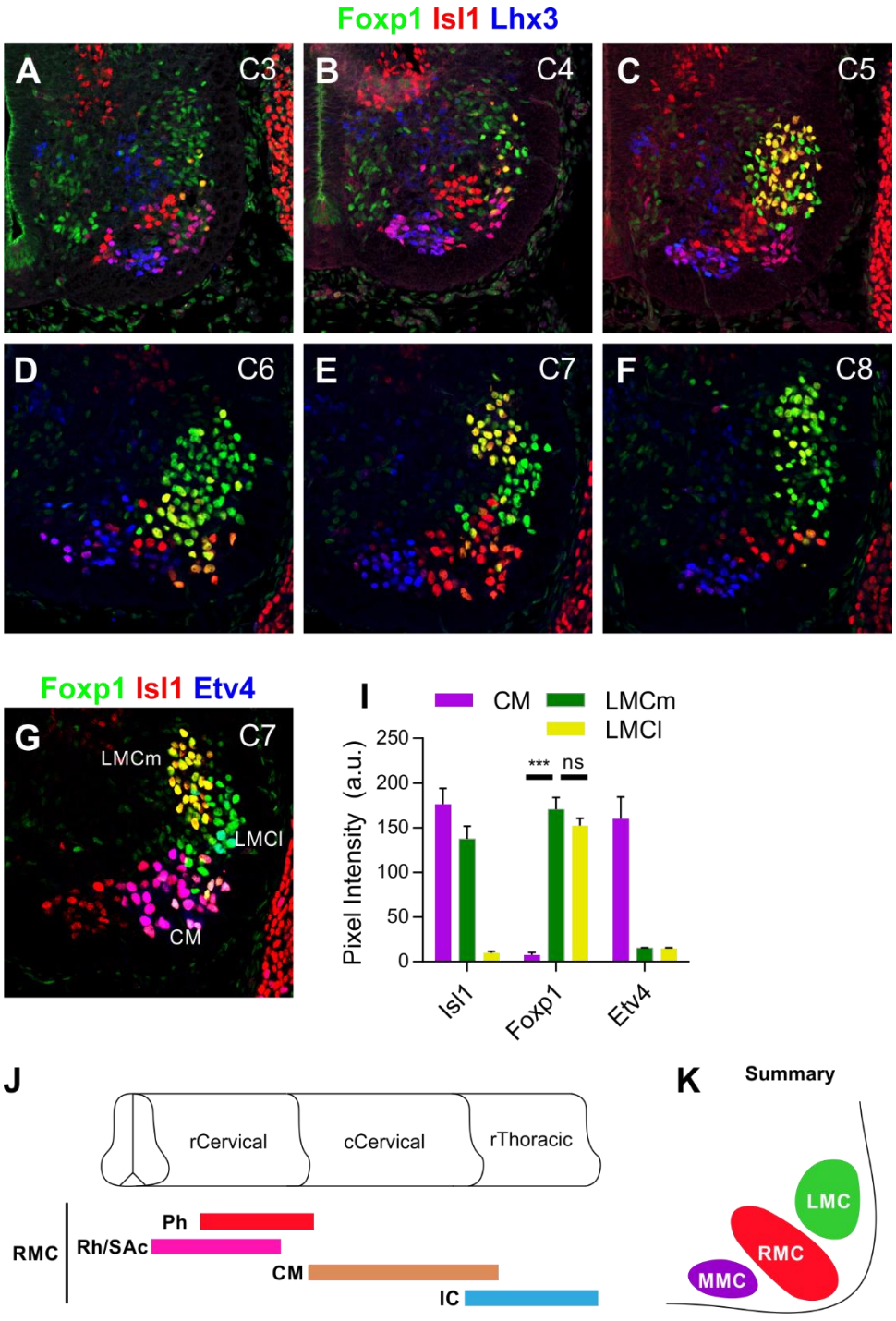

Figure 3-1. Respiratory motor column organization in the developing spinal cord

(A-F) Expression of Foxp1, Isl1, and Lhx3 reveals the location of respiratory MNs (also known as hypaxial MNs) in the cervical spinal cord of e12.5 mouse embryo. Cutaneous maximus motor

pool expresses Etv4 (in blue) but very low levels of Foxp1 (in green) in the C7 spinal cord of e12.5 mouse embryo (G, I). Unified classification of respiratory MNs as the respiratory motor column (RMC) comprises of MNs that have the ability to assist in breathing activity, which includes the rhomboids/spinal accessory MNs, phrenic MNs, cutaneous maximus MNs, and thoracic intercostal MNs that continues into the more caudal segments of the spinal cord (J).

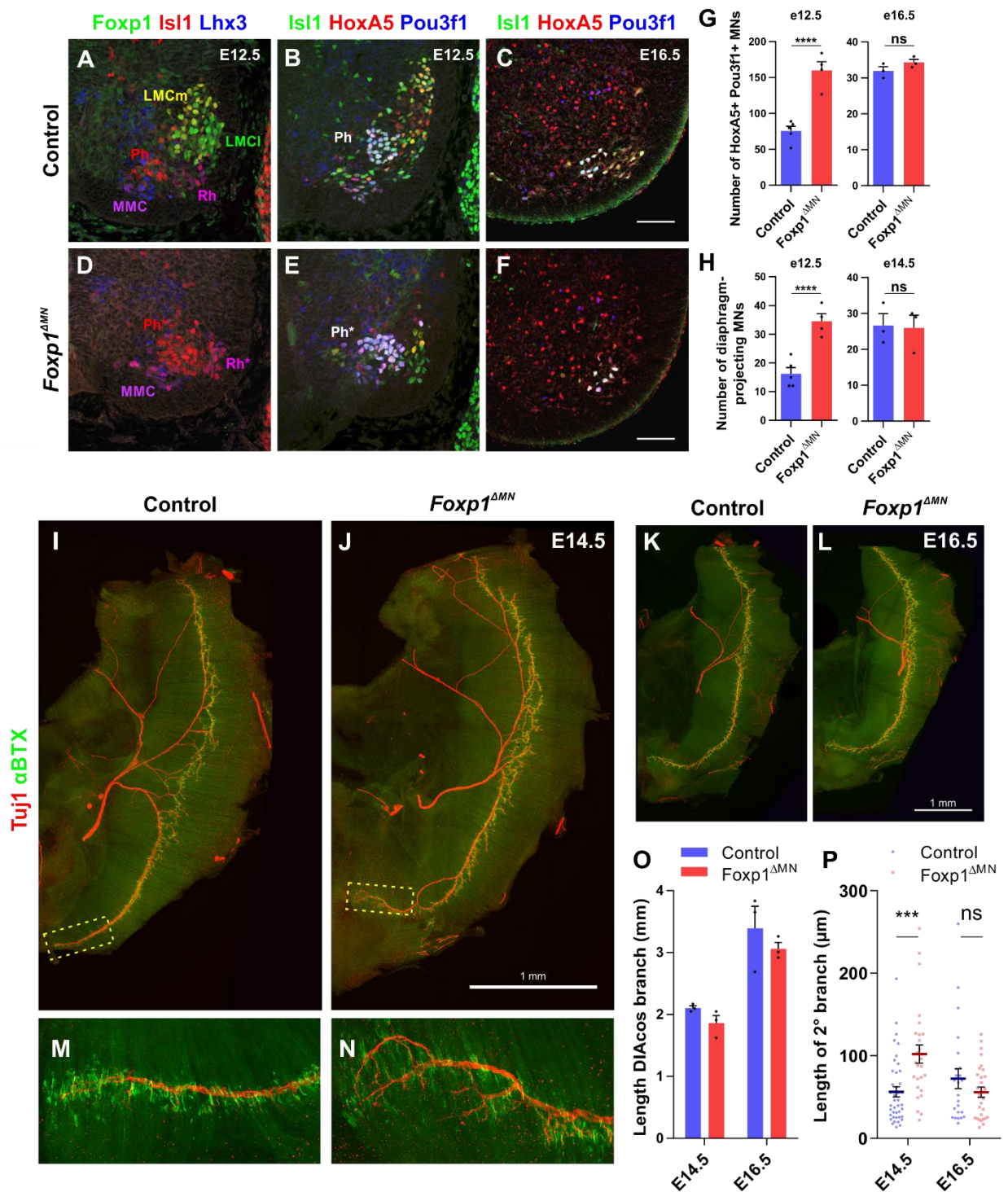
Foxp1 Isl1 Lhx3
Isl1 HoxA5 Pou3f1
Isl1 HoxA5 Pou3f1
Control
Foxp1ΔMN
A
E12.5
LMCm
LMCl
Ph
Rh
MMC
B
E12.5
Ph
C
E16.5
D
Ph*
Rh*
MMC
E
Ph*
F
G
e12.5
e16.5
****
ns
Number of HoxA5+ Pou3f1+ MNs
Control
Foxp1ΔMN
H
e12.5
e14.5
****
ns
Number of diaphragm-projecting MNs
Control
Foxp1ΔMN
Control
Foxp1ΔMN
I
J
E14.5
1 mm
K
L
E16.5
1 mm
Tuj1 αBTX
M
N
O
Control
Foxp1ΔMN
Length DIAcos branch (mm)
E14.5
E16.5
P
Control
Foxp1ΔMN
***
ns
Length of 2° branch (μm)
E14.5
E16.5

Figure 3-2. Removal of Foxp1 results in generation of excess number of RMC-like MNs in mid-cervical spinal cord

The RMC MNs in rostral cervical spinal cord can be identified by the lack of expression of Foxp1 and Lhx3 at e12.5 as mentioned previously (A). The phrenic MNs can be identified by their Hox level, HoxA5, as well as the transcription factor, Pou3f1 (B, C). In *Foxp1*$^{\Delta MN}$, phrenic motor population is enlarged at e12.5 (D, E), which is corrected by E16.5 (F). The number of MNs that co-express HoxA5 and Pou3f1 in the cervical spinal cord at e12.5 and E16.5 (G). The number of MNs that project to the diaphragm revealed by retrograde labeling (H). Wholemount immunohistochemistry of diaphragm of control (I) and *Foxp1*$^{\Delta MN}$ (J) at e14.5 with beta-tubulin III and alpha-bungarotoxin in control and *Foxp1*$^{\Delta MN}$, with the distal-most branch zoomed in for control (M) and *Foxp1*$^{\Delta MN}$ (N). Wholemount immunohistochemistry of diaphragm of control (K) and *Foxp1*$^{\Delta MN}$ (L) at E16.5. Quantification of the length of the costal branch of the diaphragm at e14.5 and E16.5 (O). Length of secondary branch off the costal branch of the diaphragm at e14.5 and E16.5 (P).

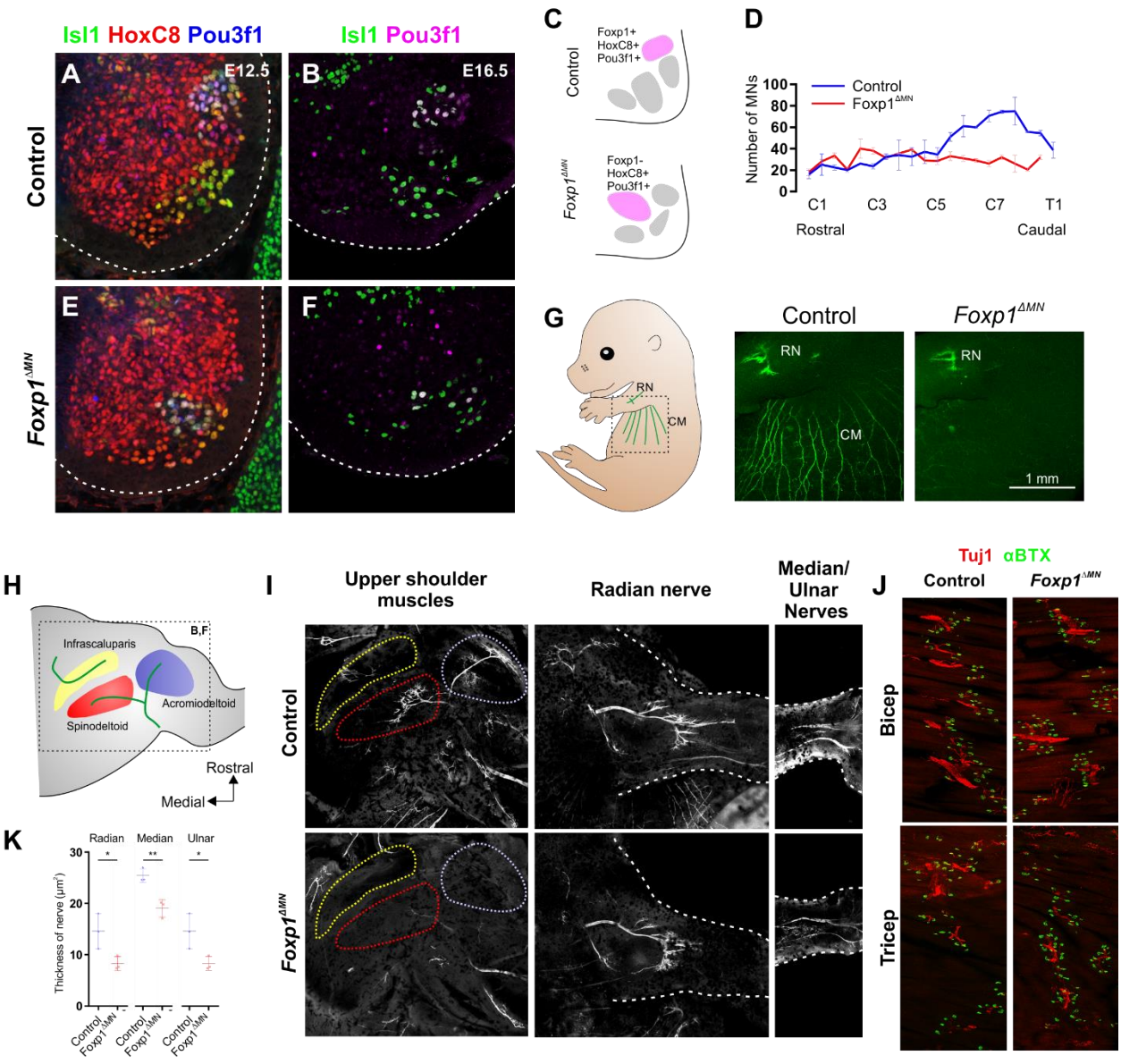

Figure 3-3. Removal of Foxp1 results in excess number of RMC-like MNs at the caudal cervical spinal cord

FCU-projecting MNs express Pou3f1 caudal cervical spinal cord in control at e12.5 (A) and E16.5 (B). Pou3f1+ RMC-like MNs are present in *Foxp1*$^{\Delta MN}$ at e12.5 (E) and E16.5 (F). Summary of location of the HoxC8+ Pou3f1+ populations in control and *Foxp1*$^{\Delta MN}$ (C). Number of MNs from rostral to caudal cervical spinal cord at e14.5 in control and *Foxp1*$^{\Delta MN}$ (D). Projection patterns of cutaneous maximus nerves in control and *Foxp1*$^{\Delta MN}$ (G). Organization of

upper shoulder muscles in the mouse (H). Gross upper shoulder muscle innervation, radial nerve, and median nerve patterns in control and *Foxp1*$^{\Delta MN}$ at e14.5 (I). Endplate in arm muscles revealed by alpha-bungarotoxin labeling in control and *Foxp1*$^{\Delta MN}$ (J).

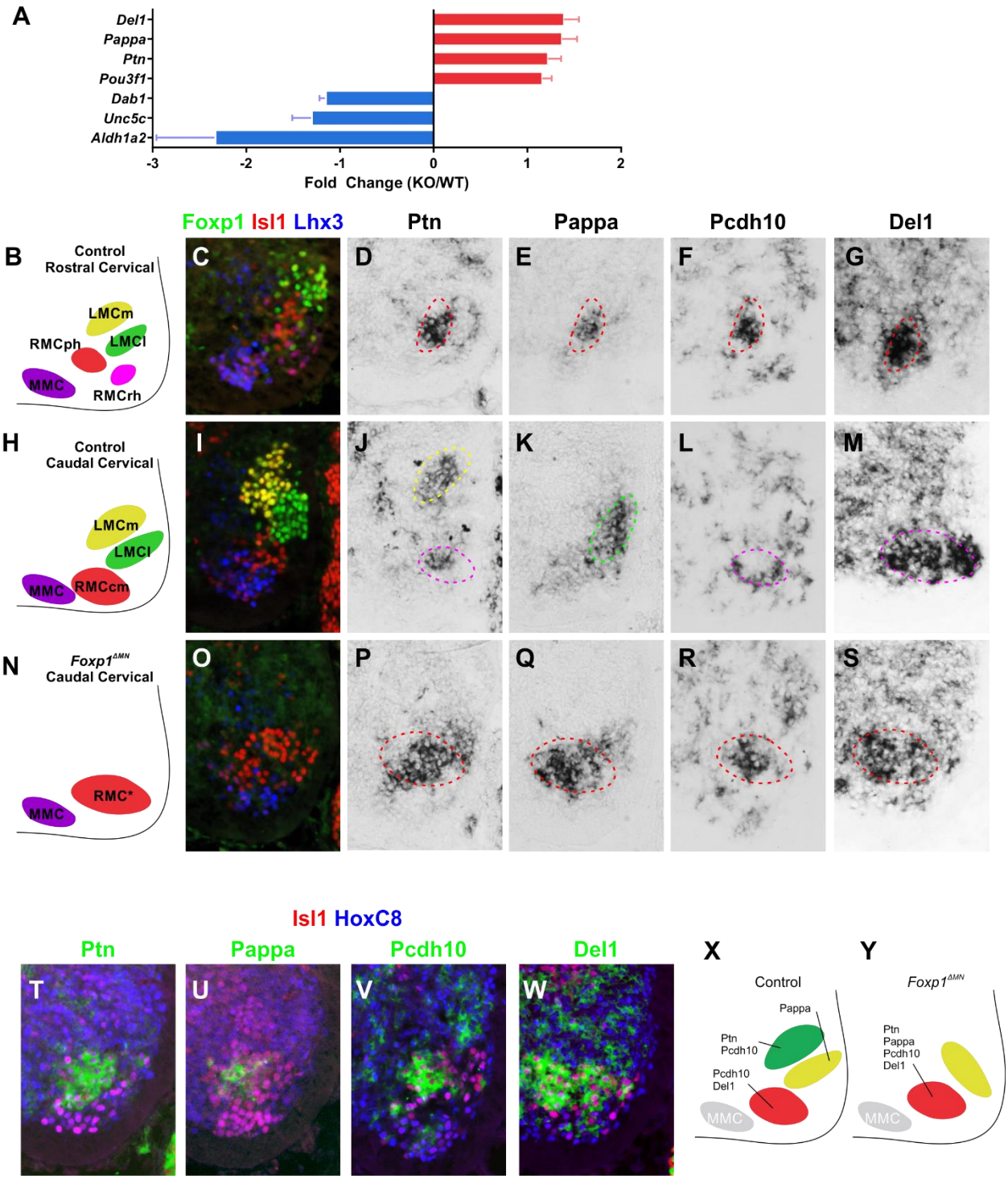
A
Del1
Pappa
Ptn
Pou3f1
Dab1
Unc5c
Aldh1a2
-3
-2
-1
0
1
2
Fold Change (KO/WT)
Foxp1 Isl1 Lhx3
Ptn
Pappa
Pcdh10
Del1
B
Control
Rostral Cervical
LMCm
LMCl
RMCph
MMC
RMCrh
C
D
E
F
G
H
Control
Caudal Cervical
LMCm
LMCl
MMC
RMCcm
I
J
K
L
M
N
Foxp1ΔMN
Caudal Cervical
RMC*
MMC
O
P
Q
R
S
Isl1 HoxC8
Ptn
Pappa
Pcdh10
Del1
T
U
V
W
X
Control
Pappa
Ptn
Pcdh10
Pcdh10
Del1
MMC
Y
Foxp1ΔMN
Ptn
Pappa
Pcdh10
Del1
MMC

Figure 3-s1. RMC-like MNs in caudal cervical levels of *Foxp1*$^{\Delta MN}$ express the combinations of RMC markers previously identified in RMC MN populations

(A) Genes up-regulated (in red) and down-regulated (in blue) in Foxp1$^{-/-}$. (B) Motor column organization of the mid-cervical spinal cord in control also revealed by immunohistochemical analysis with Foxp1, Isl1, and Lhx3 (C). The phrenic MNs at e12.5 express Ptn (D), Pappa (E), Pcdh10 (F), and Del1 (G). (H) Motor column organization of the caudal cervical spinal cord in control also revealed by immunohistochemical analysis with Foxp1, Isl1, and Lhx3 (I). (J) Ptn is expressed by LMCm and RMCcm. (K) Pappa is expressed by LMCl. (L) Pcdh10 is expressed diffusely in the ventral horn. (M) Del1 is expressed strongly in the CM population. (N) Motor column organization of the caudal cervical spinal cord in *Foxp1*$^{\Delta MN}$, also revealed by immunohistochemical analysis of Foxp1, Isl1, and Lhx3 (O). (P-S) Expression of Ptn, Pappa, Pcdh10, and Del1 are all present in the medial RMC-like MNs in the HoxC8 context (T-W). (X, Y) Summary of RMC markers in caudal cervical spinal cord of control and *Foxp1*$^{\Delta MN}$.

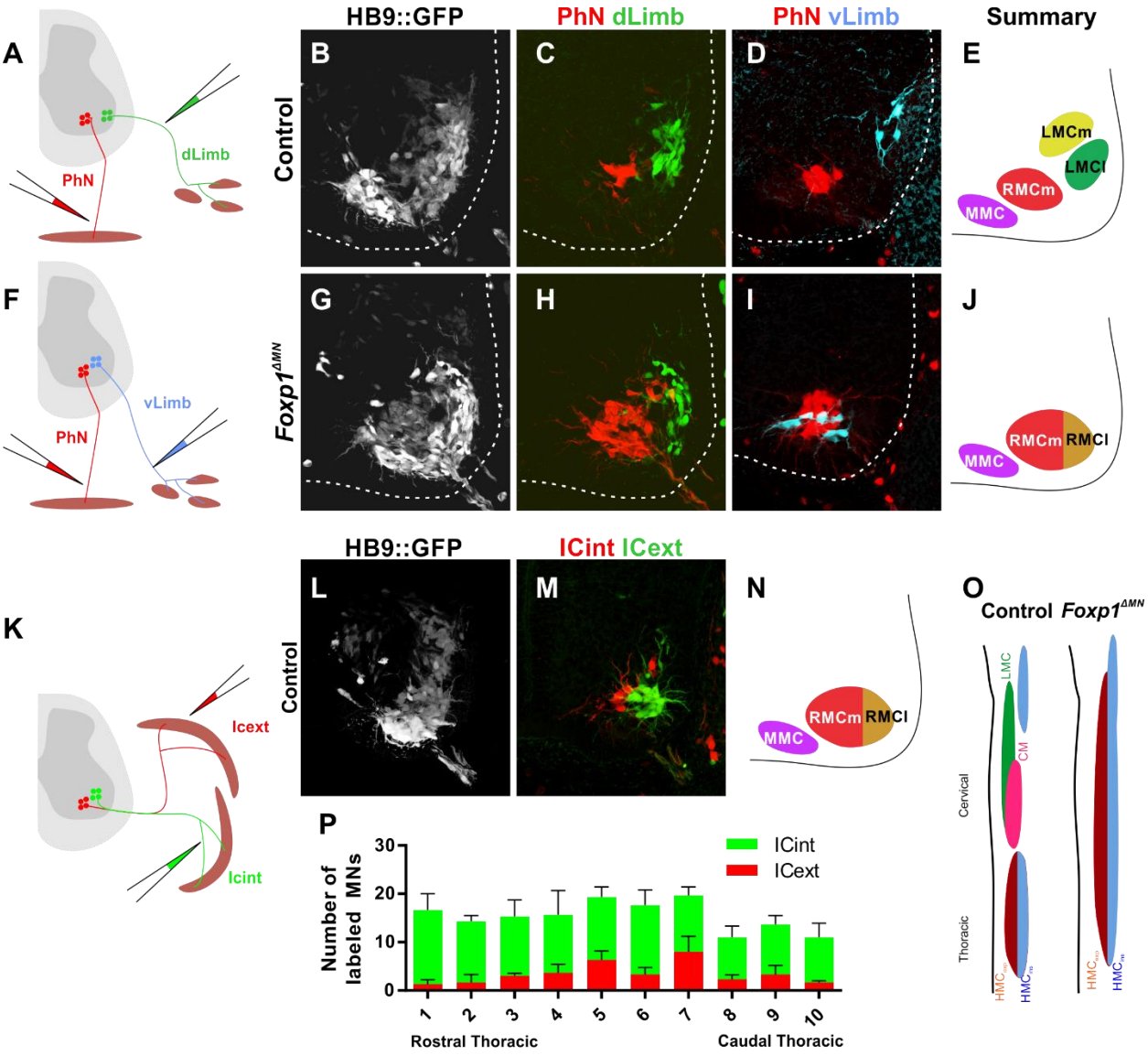

Figure 3-4. Inherent medial-lateral organization of RMC-like MNs in Foxp1ΔMN

Schematic diaphragm of phrenic/dorsal limb (A) and phrenic/ventral limb (F) injection experiments. Hb9::GFP expression of control (B) and *Foxp1*$^{\Delta MN}$ (G). Retrogradely labeled phrenic MNs (in red) and dorsal limb-projecting MNs (in green) in control (C) and *Foxp1*$^{\Delta MN}$ (H). Retrogradely labeled phrenic MNs (in red) and ventral limb-projecting MNs (in green) in control (D) and *Foxp1*$^{\Delta MN}$ (I). Summary of dorsal- vs. ventral-projecting MNs in control (E) and *Foxp1*$^{\Delta MN}$ (J). (K) Schematic diaphragm of intercostal branch injection in the ribcage of control

mouse embryo at e12.5. (L) Hb9GFP expression of thoracic spinal cord of control mouse embryo at e12.5. (M) Retrogradely labeled internal intercostal projecting MNs (in red) and external intercostal projecting MNs (in green). (N) Summary of thoracic RMC organization in the control at e12.5. (P) Rostro-caudal organization of ICint and ICext in the thoracic spinal cord of control mouse embryo. (O) Summary of RMC extension from thoracic spinal cord to caudal cervical spinal cord.

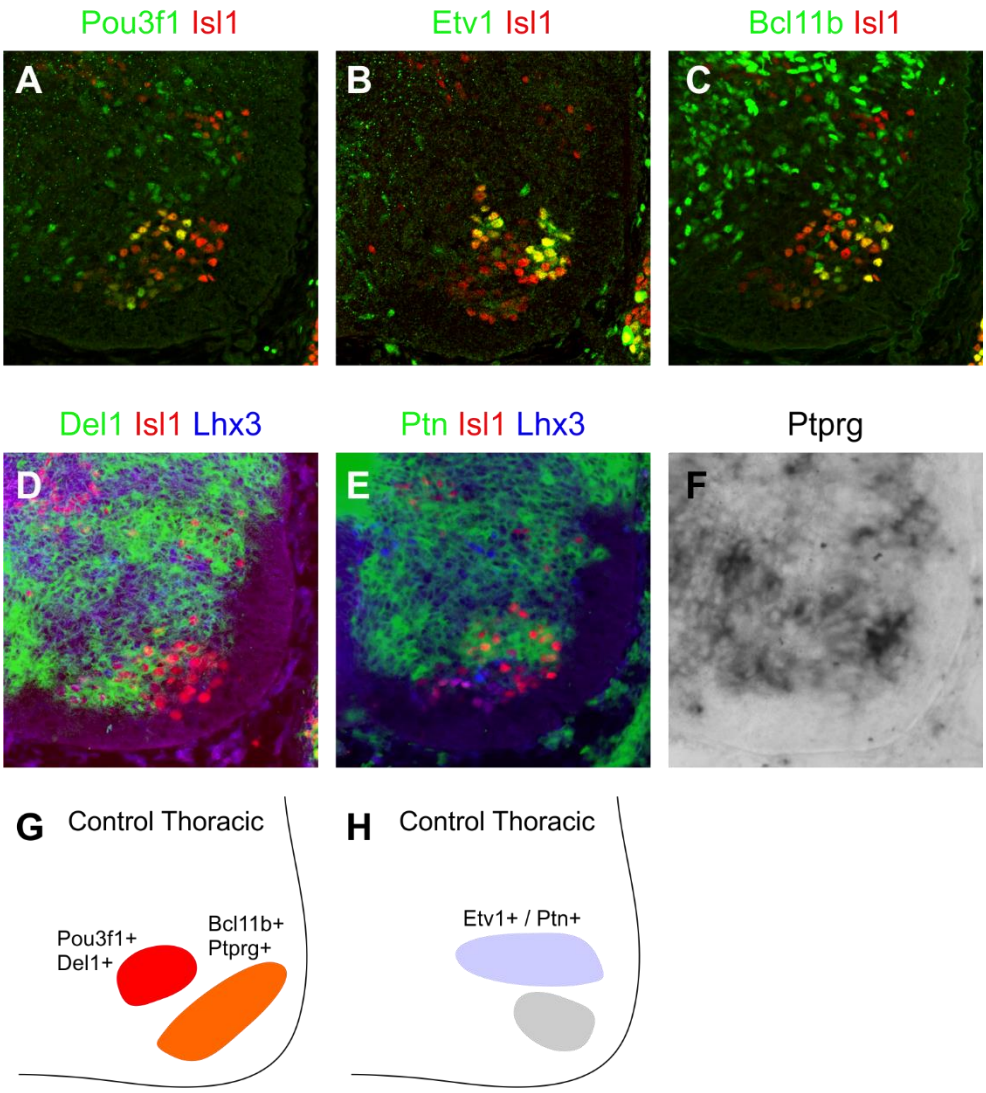

Figure 3-s2. Comparable molecular organization between phrenic and thoracic RMC MNs

(A) Expression of Pou3f1 in the thoracic spinal cord of e12.5 mouse embryo. (B) Expression of Etv1 in the thoracic spinal cord of e12.5 mouse embryo. (C). Expression of Bcl11b in the thoracic spinal cord of e12.5 mouse embryo. (D) Localization of *Del1* transcript in the thoracic spinal cord of e12.5 mouse embryo. (E) Localization of Ptn transcript in the thoracic spinal cord of e12.5 mouse embryo. (F) Localization of Ptprg transcript in the thoracic spinal cord of e12.5 mouse embryo. (G-H) Summary of expression patterns of novel thoracic RMC markers.

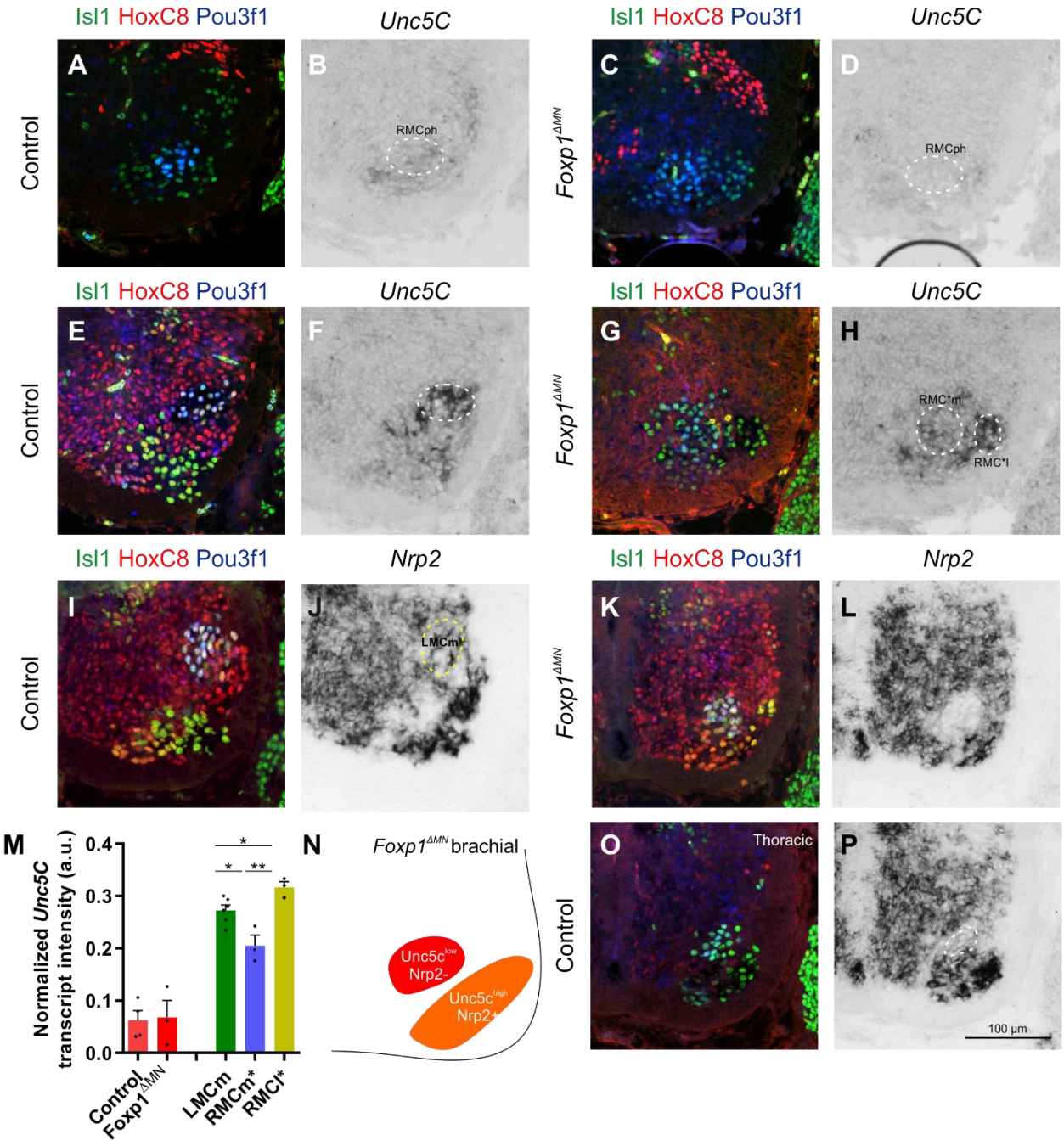

Figure 3-s3. Expression of netrin-1 receptor Unc5C in the caudal cervical spinal cord of control and Foxp1ΔMN mouse embryo

Expression of Isl1, HoxC8 and Pou3f1 in the mid-cervical spinal cord of the mid-cervical levels of control (A) and *Foxp1*$^{\Delta MN}$ (C) e12.5 mouse embryo. Localization of Unc5C in phrenic MNs of

the mid-cervical levels of control (B) and *Foxp1*$^{\Delta MN}$ (D) e12.5 mouse embryo. Expression of Isl1, HoxC8 and Pou3f1 in the mid-cervical spinal cord of the caudal cervical levels of control (E, I) and Foxp1$^{\Delta MN}$ (G, K) e12.5 mouse embryo. Localization of *Unc5C* transcript in FCU-projecting MNs of the caudal cervical levels of control (F) and *Foxp1*$^{\Delta MN}$ (H) e12.5 mouse embryo. (M) Quantification of the intensity levels of Unc5C transcript intensity in control and *Foxp1*$^{\Delta MN}$. Localization of *Nrp2* transcript in FCU-projecting MNs of the caudal cervical levels of control (J) and *Foxp1*$^{\Delta MN}$ (L) e12.5 mouse embryo. Localization of *Nrp2* transcript in RMC MNs of the thoracic levels of control (O) of e12.5 mouse embryo. (N) Summary of Unc5C and Nrp2 expression in the caudal cervical levels of *Foxp1*$^{\Delta MN}$.

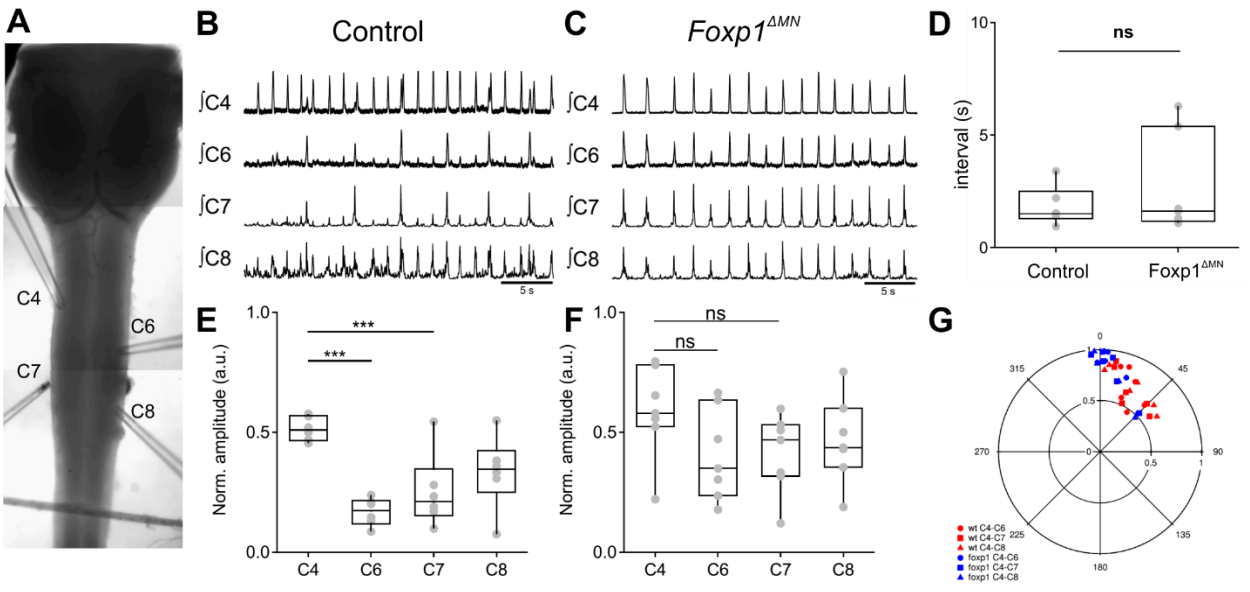

Figure 3-5. En bloc brainstem-spinal cord recording preparation of P0 Foxp1$^{\Delta MN}$ neonatal mouse embryo

(A) Experimental set up of ventral root recording using glass capillary electrodes. Raw integrated trace of ventral root activities of C4, C6, C7, and C8 of control (B) and Foxp1$^{\Delta MN}$ (C) preparations. (D) Intervals lengths between bursts in control and *Foxp1$^{\Delta MN}$*. Normalized amplitude of integrated trace of ventral roots in control (E) and *Foxp1$^{\Delta MN}$* (F). (G) Radial plot summarizing the phase differences between ventral root activities in control and Foxp1$^{\Delta MN}$.

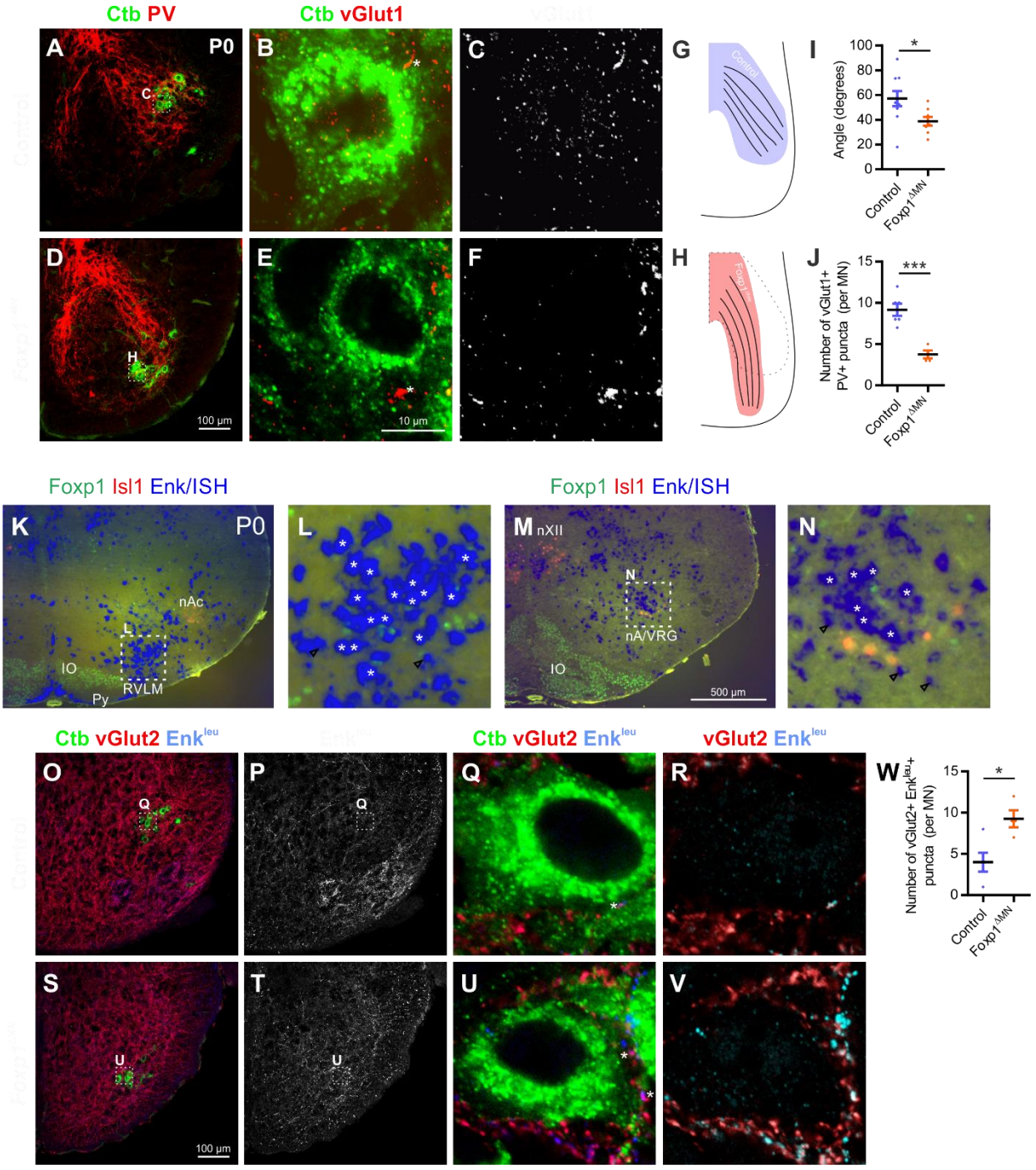

Figure 3-6. Altered proprioceptive and cardiorespiratory afferents upon removal upon respiratory transformation of caudal cervical MNs

Retrogradely labeled FCU MNs (in green) with proprioceptive afferents labeled by parvalbumin immunohistochemistry in control (A) and Foxp1$^{\Delta MN}$ (D). Localization of vGlut1 contacting Ctb+

soma in control (B) and Foxp1$^{\Delta MN}$ (E); vGlut1-only signal is shown for control (C) and Foxp1$^{\Delta MN}$ (F). (G and H) Diagram illustrating the angle of proprioceptive fibers from midline (quantified in I). (J) The number of vGlut1+ PV+ contacts onto the Ctb+ MNs in control and Foxp1$^{\Delta MN}$. (K-N) Location of Preproenkephalin gene expression in the brainstem of wild type P0 brainstem. Retrogradely labeled FCU MNs (in green) with cardiorespiratory afferents labeled by leu-enkephalin immunohistochemistry in control (O) and Foxp1$^{\Delta MN}$ (S). Leu-enkephalin-only signal is shown for control (P) and *Foxp1*$^{\Delta MN}$ (T). Localization of vGlut1 contacting Ctb+ soma in control (Q) and Foxp1$^{\Delta MN}$ (U). Co-localizing signal for vGlut2 and leu-enkephalin signal is shown for control (R) and Foxp1$^{\Delta MN}$ (V). (W) The number of vGlut2+ leu-enk+ contacts onto the Ctb+ MNs in control and Foxp1$^{\Delta MN}$.

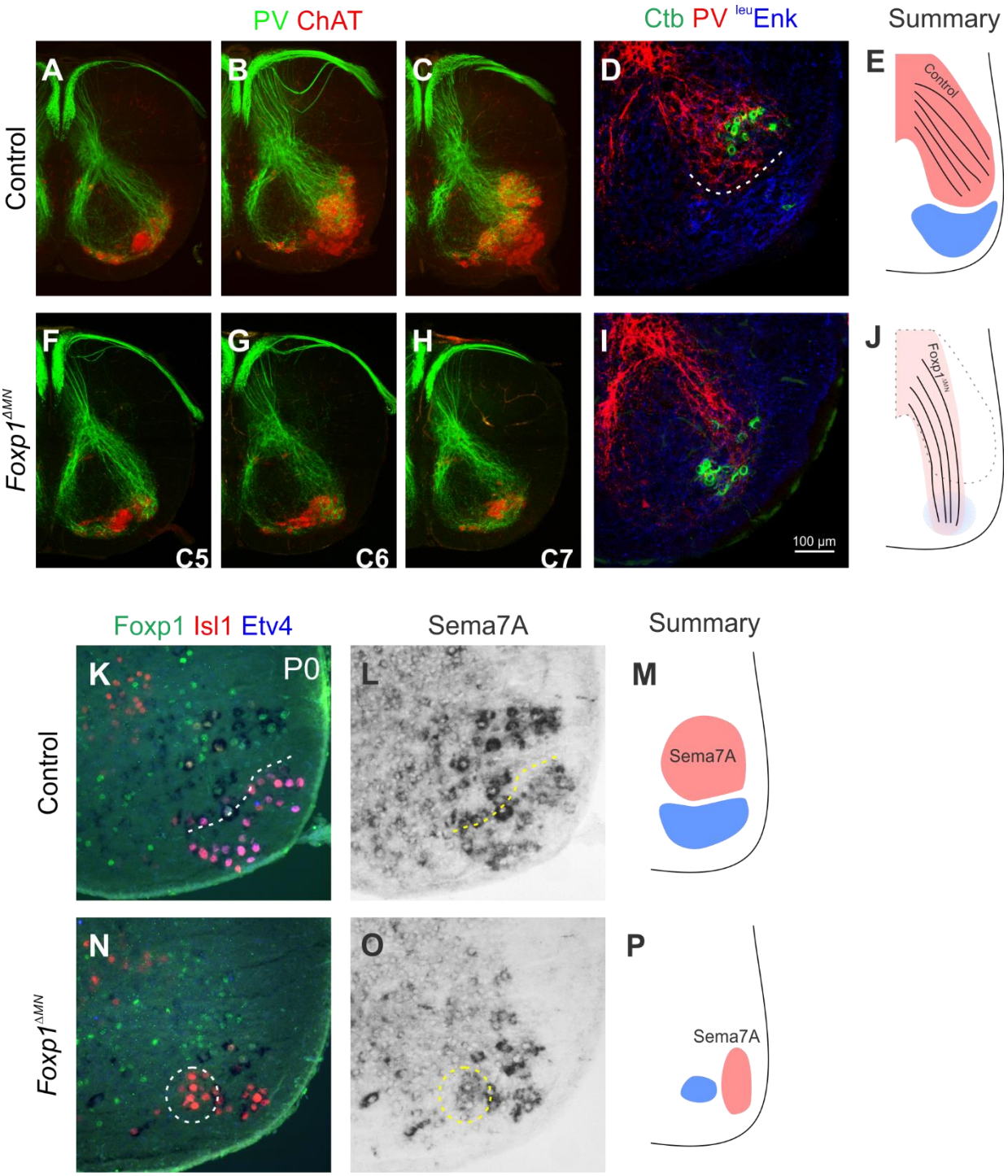

Figure 3-s4. Sema7A expression co-localizes with caudal cervical Etv4- LMC MNs

Thick-section proprioceptive afferent coverage on MNs of control (A-C) and *Foxp1*$^{\Delta MN}$ (F-H). Overlay of PV+ proprioceptive afferents (in red) and FCU MNs (in green), and leu-enkephalin+

fibers of adjacent section of control (D) and *Foxp1*$^{\Delta MN}$ (I) summarized in E and J. The expression of Foxp1, Isl1 and Etv4 in caudal cervical level of control (K) and *Foxp1*$^{\Delta MN}$ (N) P0 neonatal spinal cord. Sema7A transcript in caudal cervical level of control (L) and *Foxp1*$^{\Delta MN}$ (O) P0 neonatal spinal cord summarized in M and P.

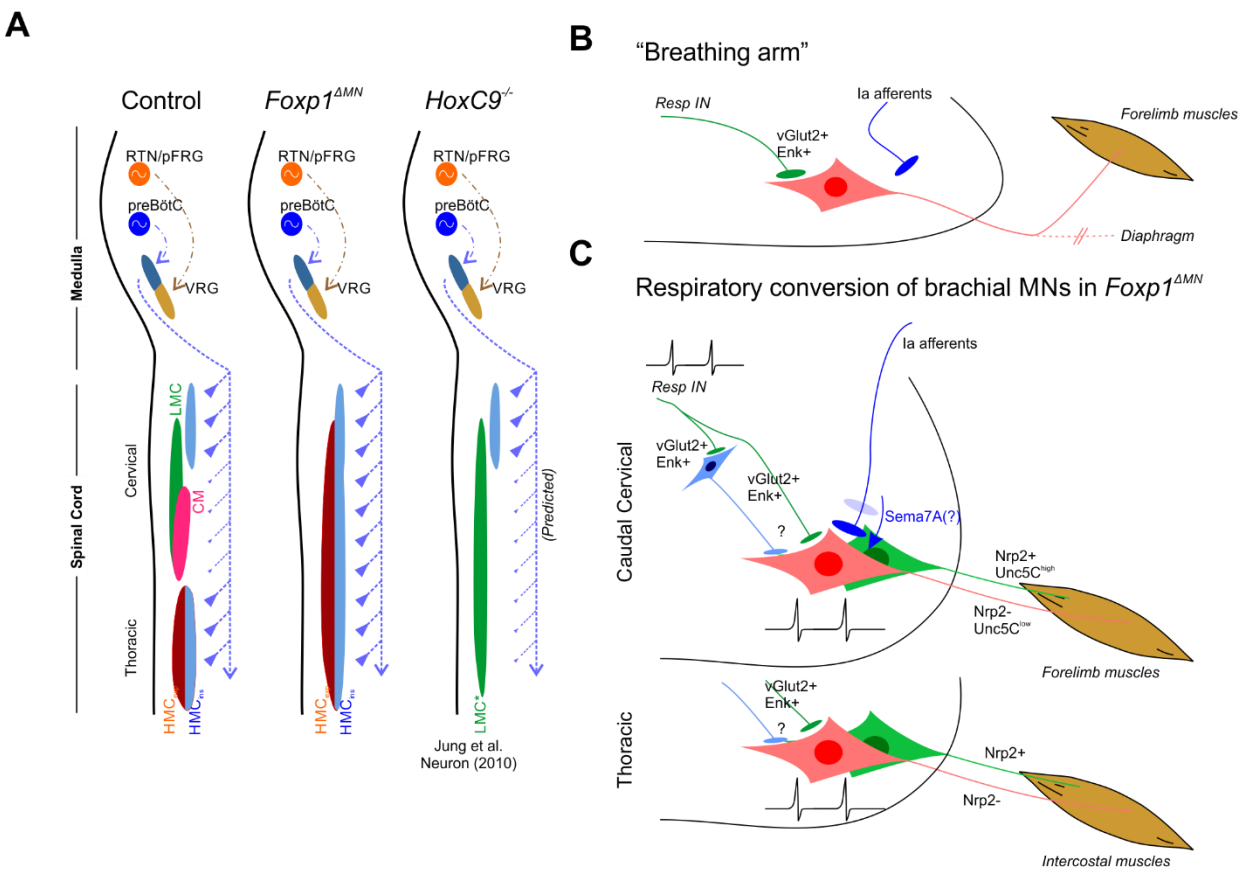

Figure 3-7. Models for respiratory transference to limb-innervating RMC-like motor neurons in *Foxp1$^{\Delta MN}$*

(A) Summary of molecular and physiological characterization of *Foxp1$^{\Delta MN}$* phenotype. (B) Illustration of the altered circuit in "breathing arm" phenomena. (C) Summary of respiratory conversion of caudal cervical MNs in *Foxp1$^{\Delta MN}$* compared with organization of thoracic MNs.

Table 3-s1. Genes upregulated in Foxp1 mutant motor neurons at e11.5

probe set	gene	Accession	Entrez Gene	Description	$Mean_B$	$Mean_E$	FC	t stat.	p value
1442742_at	Atp2c1: ATPase, Ca++-sequestering	BE994454	235574	Mm.37258.1	32.82	64.97	1.98	2.671	0.048961
1428692_at	Hddc3: HD domain containing 3	AW259452	68695	Mm.21171.1	649.53	1217.5	1.87	4.064	0.00883
1449060_at	Kif2c: kinesin family member 2C	NM_134471	73804	Mm.27828.1	276.64	430.02	1.55	2.796	0.048981
1433682_at	Arhgef17: Rho guanine nucleotide exchange factor (GEF) 17	BE287052	207212	Mm.29954.1	547.24	789.69	1.44	4.31	0.006293
1451919_a_at	Mpl: myeloproliferative leukemia virus oncogene	AF360122	17480	Mm.4864.2	294.47	422.34	1.43	3.175	0.031302
1448823_at	Cxcl12: chemokine (C-X-C motif) ligand 12	BC006640	20315	Mm.465.2	108.07	153.44	1.42	3	0.030112
1437368_at	Gtf2h4: general transcription factor II H, polypeptide 4	BE457600	14885	Mm.10182.4	227.95	323.61	1.42	2.627	0.040033
1439906_at	Mm.23555.1	BB184086		Mm.23555.1	170.33	239.65	1.41	3.265	0.035277
1423725_at	Pls3: plastin 3 (T-isoform)	BC005459	102866	Mm.28777.1	317.66	449.21	1.41	2.682	0.036438
1420913_at	Slco2a1: solute carrier organic anion transporter family, member 2a1	NM_033314	24059	Mm.23996.1	229.29	319.38	1.39	4.207	0.013091
1435283_s_at	Fam189a2: family with sequence similarity 189, member A2	BE647179	381217	Mm.25363.1	285.89	396.13	1.39	3.395	0.026865
1426004_a_at	Tgm2: transglutaminase 2, C polypeptide	AF114266	21817	Mm.18843.3	450.74	625.44	1.39	2.494	0.047834
1433739_at	Nol10: nucleolar protein 10	BG071110	217431	Mm.27536.1	557.27	774.6	1.39	2.903	0.033823
1425622_at	Edil3: EGF-like repeats and discoidin I-like domains 3	AF031524	13612	Mm.41716.1	675.62	941.55	1.39	4.631	0.010579
1418540_a_at	Ptpre: protein tyrosine phosphatase, receptor type, E	U35368	19267	Mm.945.1	126.49	173.96	1.38	3.061	0.0227
1421145_at	Slc26a2: solute carrier family 26 (sulfate transporter), member 2	NM_007885	13521	Mm.24803.1	142.87	197.86	1.38	2.479	0.048683
1432420_a_at	2310002L09Rik: RIKEN cDNA 2310002L09 gene	AK009097	71886	Mm.158769.2	131.03	179.95	1.37	3.71	0.01023
1438266_at	LOC100503741: hypothetical LOC100503741	BB764453	1.01E+08	Mm.30858.1	221.55	302.85	1.37	3.647	0.015965
1427633_a_at	Pappa: pregnancy-associated plasma protein A	AF439513	18491	Mm.103481.2	227.9	311.26	1.37	3.051	0.041837
1443734_at	D5Wsu148e: DNA segment, Chr 5, Wayne State University 148, expressed	BE335271	28024	Mm.100532.1	229.72	313.19	1.36	3.403	0.020034
1430036_at	2310015B20Rik: RIKEN cDNA 2310015B20 gene	AK009351	69563	Mm.64672.1	256.87	348.08	1.36	3.301	0.039103
1438709_at	Wipi1: WD repeat domain, phosphoinositide interacting 1	BB044002	52639	Mm.221045.1	264.93	360.69	1.36	3.31	0.016245
1459813_at	1700012D01Rik: RIKEN cDNA 1700012D01 gene	AV040390	72243	Mm.65511.1	92.47	125.03	1.35	2.602	0.044956
1446343_at	Mm.26351.1	BG068486		Mm.26351.1	182.17	246.41	1.35	2.955	0.025532
1427854_x_at	Gm9817: predicted gene 9817	AF047377	1E+08	Mm.13849.5	261.72	353.78	1.35	3.198	0.020155
1459483_at	Mm.209303.1	BB461295		Mm.209303.1	311.37	420.58	1.35	3.456	0.016015
1429342_s_at	2310021H06Rik: RIKEN cDNA 2310021H06 gene	AK009441	67135	Mm.140317.1	337.44	455.55	1.35	3.34	0.028019
1425035_s_at	Dnmt3l: DNA (cytosine-5-)-methyltransferase 3-like	AF220524	54427	Mm.13433.1	220.45	296	1.34	2.545	0.049821
1455203_at	A930003A15Rik: RIKEN cDNA A930003A15 gene	BB522820	68162	Mm.35159.1	223.72	300.55	1.34	2.76	0.03287
1442538_at	Mm.148914.1	AW742720		Mm.148914.1	226.57	303.93	1.34	2.933	0.041106
1442828_at	Ifi204: Interferon activated gene 204	BB200491	15951	Mm.209962.1	450.74	603.11	1.34	3.252	0.020918
1437854_at	Mm.217322.1	BM239897		Mm.217322.1	154.72	206.21	1.33	2.694	0.04376
1425548_a_at	Lst1: leukocyte specific transcript 1	U72644	16988	Mm.19379.1	323.73	428.96	1.33	3.049	0.022711
1426144_x_at	Trdn: triadin	AF223417	76757	Mm.55320.3	135.73	179.67	1.32	2.899	0.029156
1418600_at	Klf1: Kruppel-like factor 1 (erythroid)	NM_010635	16596	Mm.4847.1	182.19	241.3	1.32	2.726	0.034397
1429702_at	2900072G11Rik: RIKEN cDNA 2900072G11 gene	AV154947	73005	Mm.138210.1	185.32	244.24	1.32	2.709	0.048161
1424083_at	Rod1: ROD1 regulator of differentiation 1 (S. pombe)	BB519382	230257	Mm.220991.1	957.55	1261.63	1.32	4.571	0.004371
1437231_at	Slitrk6: SLIT and NTRK-like family, member 6	AV246497	239250	Mm.49728.1	103.4	135.67	1.31	2.758	0.048161
1427840_at	Mm.220131.1	J02644		Mm.220131.1	140.98	185.14	1.31	3.002	0.038201
1418995_at	Neurod2: neurogenic differentiation 2	NM_010895	18013	Mm.4814.1	217.46	284.19	1.31	2.66	0.041483
1441622_at	Gm5485: predicted gene 5485	AV374024	433023	Mm.213009.1	241.43	315.83	1.31	2.663	0.03743
1432592_at	Pappa: pregnancy-associated plasma protein A	BB635017	18491	Mm.158706.1	554.28	723.44	1.31	2.824	0.030707
1447825_x_at	Pcdh8: protocadherin 8	BB076893	18530	Mm.117885.1	1671.12	2181.27	1.31	2.704	0.035428
1437899_at	Lyg2: lysozyme G-like 2	AV234966	332427	Mm.34185.1	109.8	143	1.3	3.351	0.018013
1453809_at	Lypd5: Ly6/Plaur domain containing 5	AK008654	76942	Mm.32861.1	119.26	154.83	1.3	3.632	0.018526
1422252_a_at	Cdc25c: cell division cycle 25 homolog C (S. pombe)	NM_009860	12532	Mm.16857.1	185.77	241.86	1.3	4.714	0.003296
1426176_a_at	Prok2: prokineticin 2	AF182065	50501	Mm.87365.3	190.8	247.64	1.3	3.847	0.009266
1459792_at	Mm.44845.1	AI844315		Mm.44845.1	456.68	592.77	1.3	3.246	0.025962
1452514_a_at	Kit: kit oncogene	X65997	16590	Mm.4394.2	146.44	188.69	1.29	3.828	0.009448

1451790_a_at	Tfpi: tissue factor pathway inhibitor	AF004833	21788	Mm.3601.1	162.49	209.96	1.29	2.808	0.041052
1442515_at	Mm.17713.1	BG084330		Mm.17713.1	228.38	293.98	1.29	3.521	0.013497
1448554_s_at	Myh6 /// Myh7: myosin, heavy polypeptide 6, cardiac muscle, alpha /// myosin, heavy polypeptide 7, cardiac muscle, beta	NM_080728	140781 /// 17888	Mm.155714.1	229.53	295.18	1.29	2.746	0.03653
1431302_a_at	Nudt7: nudix (nucleoside diphosphate linked moiety X)-type motif 7	AK011172	67528	Mm.27889.3	231.67	299.09	1.29	3.813	0.010954
1453769_at	Ckap2l: cytoskeleton associated protein 2-like	BI466124	70466	Mm.45785.1	244.75	315.53	1.29	2.927	0.03864
1419148_at	Avil: advillin	AF059486	11567	Mm.10739.1	247.52	319.75	1.29	2.669	0.040832
1425762_a_at	Rxra: retinoid X receptor alpha	U77683	20181	Mm.3470.2	316.58	409.26	1.29	4.906	0.002736
1434905_at	Ndufa4l2: NADH dehydrogenase (ubiquinone) 1 alpha subcomplex, 4-like 2	BB610230	407790	Mm.45843.1	321.27	415.33	1.29	2.711	0.047871
1455881_at	Ier5l: immediate early response 5-like	BB078200	72500	Mm.117963.1	328.8	423	1.29	2.611	0.047161
1456510_x_at	Higd1c /// Mettl7a2: HIG1 domain family, member 1C /// methyltransferase like 7A2	BB703414	380975 /// 393082	Mm.220975.3	331.33	428.24	1.29	3.13	0.02043
1439472_at	Gcn1l1: GCN1 general control of amino-acid synthesis 1-like 1 (yeast)	BB837280	231659	Mm.214050.1	333.72	431.63	1.29	2.882	0.040027
1453386_at	Tusc1: tumor suppressor candidate 1	AK008612	69136	Mm.171558.1	1732.49	2228.11	1.29	2.906	0.041599
1447339_at	Mm.197386.1	BE946220		Mm.197386.1	111.52	142.69	1.28	2.554	0.047025
1430269_at	Mybphl: myosin binding protein H-like	AK004148	68753	Mm.75201.1	118.03	150.89	1.28	2.863	0.028674
1442545_at	Mm.151528.1	BE984743		Mm.151528.1	149.16	191.63	1.28	4.053	0.0067
1422931_at	Fosl2: fos-like antigen 2	NM_008037	14284	Mm.23704.1	163.6	209.79	1.28	3.498	0.017042
1417910_at	Ccna2: cyclin A2	X75483	12428	Mm.4189.1	213.74	272.9	1.28	2.471	0.048399
1418595_at	Plin4: perilipin 4	NM_020568	57435	Mm.12966.1	217.78	278.19	1.28	3.164	0.022292
1449371_at	Hars2: histidyl-tRNA synthetase 2, mitochondrial (putative)	NM_080636	70791	Mm.46741.1	302.04	387.26	1.28	3.929	0.011188
1416041_at	Sgk1: serum/glucocorticoid regulated kinase 1	NM_011361	20393	Mm.28405.1	597.7	765.71	1.28	3.294	0.033728
1425192_at	Klhl25: kelch-like 25 (Drosophila)	BC027373	207952	Mm.206223.1	666.19	853.36	1.28	3.391	0.015121
1417051_at	Pcdh8: protocadherin 8	NM_021543	18530	Mm.103811.1	680.09	867.15	1.28	2.821	0.033225
1424015_at	Dennd5a: DENN/MADD domain containing 5A	BC022119	19347	Mm.21904.1	1423.06	1823.22	1.28	3.196	0.022092
1423484_at	Bicc1: bicaudal C homolog 1 (Drosophila)	BM217996	83675	Mm.46051.1	158.56	201.19	1.27	3.025	0.034537
1448818_at	Wnt5a: wingless-related MMTV integration site 5A	BC018425	22418	Mm.32207.1	163.79	208.8	1.27	3.136	0.02781
1453714_a_at	Shroom3: shroom family member 3	BB504666	27428	Mm.46014.3	220.7	279.69	1.27	3.234	0.0266
1419044_at	Cntnap4: contactin associated protein-like 4	NM_130457	170571	Mm.117915.1	250.45	318.57	1.27	2.984	0.024531
1434642_at	Hsd17b11: hydroxysteroid (17-beta) dehydrogenase 11	BB546344	114664	Mm.1187.2	425.72	540.37	1.27	4.25	0.007405
1443824_s_at	Car7: carbonic anhydrase 7	BB193643	12354	Mm.129265.1	133.18	167.69	1.26	2.906	0.032493
1444438_at	Cib3: calcium and integrin binding family member 3	BB667454	234421	Mm.211247.1	167.36	211.57	1.26	3.325	0.016543
1456866_x_at	1700027D21Rik: RIKEN cDNA 1700027D21 gene	AV047101	76573	Mm.45613.1	184.31	231.67	1.26	2.57	0.042982
1429567_at	Rassf10: Ras association (RalGDS/AF-6) domain family (N-terminal) member 10	BB832200	78748	Mm.62480.1	199.81	252.19	1.26	2.806	0.031254
1421719_at	Vmn2r26: vomeronasal 2, receptor 26	NM_019917	56552	Mm.23795.1	200.85	252.98	1.26	3.223	0.024255
1449449_at	Ptges: prostaglandin E synthase	NM_022415	64292	Mm.28768.1	225.67	283.38	1.26	3.055	0.022385
1431171_at	D730001G18Rik: RIKEN cDNA D730001G18 gene	BF535767	78725	Mm.171357.1	226.46	285.9	1.26	2.872	0.029765
1428815_at	Gstt4: glutathione S-transferase, theta 4	BF319534	75886	Mm.33626.1	233.07	294.01	1.26	2.683	0.037534
1455167_at	Cox8c: cytochrome c oxidase, subunit VIIIc	AA144594	75483	Mm.660.1	250.54	315.79	1.26	3.031	0.023341
1445431_at	Mm.133474.1	BB371883		Mm.133474.1	252.38	316.76	1.26	2.491	0.049507
1431335_a_at	Wfdc1: WAP four-disulfide core domain 1	AK018575	67866	Mm.87599.2	305.39	385.24	1.26	3.296	0.02108
1456394_at	Rint1: RAD50 interactor 1	BB283407	72772	Mm.133300.2	310.04	391.63	1.26	3.395	0.014951
1427047_at	Nup188: nucleoporin 188	BM208071	227699	Mm.23992.1	814.37	1022.97	1.26	3.506	0.012854
1443149_at	Mm.103034.1	AW553147		Mm.103034.1	143.3	179.16	1.25	2.731	0.034126
1438183_x_at	Sord: sorbitol dehydrogenase	AV253518	20322	Mm.104920.3	146.07	183.23	1.25	2.779	0.032372
1445611_at	Trappc9: trafficking protein particle complex 9	BB349535	76510	Mm.179878.1	157.21	196.35	1.25	2.705	0.04288
1444661_at	Gpr26: G protein-coupled receptor 26	BB247791	233919	Mm.124696.1	184.97	230.54	1.25	3.165	0.020774
1420727_a_at	Tmlhe: trimethyllysine hydroxylase, epsilon	AY033513	192289	Mm.139078.1	204.29	255.72	1.25	2.628	0.043153
1450286_at	Npr3: natriuretic peptide receptor 3	NM_008728	18162	Mm.57219.1	205.36	256.47	1.25	3.087	0.02147
1444244_at	Mm.152298.1	BM933750		Mm.152298.1	242.47	303.22	1.25	2.594	0.046791
1442310_at	Pip4k2a: Phosphatidylinositol-5-phosphate 4-kinase, type II, alpha	AI314891	18718	Mm.26910.1	258.83	324.1	1.25	3.734	0.014936
1460120_at	Ablim1: actin-binding LIM protein 1	AV079770	226251	Mm.45661.1	280.46	351.93	1.25	3.047	0.022619
1439359_x_at	Nrxn1: neurexin I	BF465348	18189	Mm.39843.2	281.46	351.37	1.25	2.917	0.027871
1446187_at	Mm.105013.1	AW536580		Mm.105013.1	289.35	360.26	1.25	3.156	0.022226
1452530_a_at	Runx1: runt related transcription factor 1	X97306	12394	Mm.4081.3	312.28	389.12	1.25	2.676	0.04079

1435938_at	Ckap2l: cytoskeleton associated protein 2-like	AA197362	70466	Mm.45502.1	371.79	463.76	1.25	3.889	0.010563
1438385_s_at	Gpt2: glutamic pyruvate transaminase (alanine aminotransferase) 2	BB068040	108682	Mm.29122.5	444.51	554.22	1.25	2.535	0.047714
1419346_a_at	Svs5: seminal vesicle secretory protein 5	NM_009301	20944	Mm.140154.1	520.1	647.98	1.25	3.326	0.016009
1457890_at	D6Ertd234e: DNA segment, Chr 6, ERATO Doi 234, expressed	C79485	52204	Mm.155606.1	143.84	178.61	1.24	2.481	0.047962
1433319_at	Sh3bgr: SH3-binding domain glutamic acid-rich protein	AK017399	50795	Mm.158694.1	177.18	220.11	1.24	3.242	0.017721
1444813_at	Mm.211147.1	BB521324		Mm.211147.1	182.58	227.18	1.24	3.196	0.025077
1439962_at	2310010J17Rik: RIKEN cDNA 2310010J17 gene	AA275039	78329	Mm.3212.1	200.52	248.33	1.24	3.052	0.02287
1417987_at	Btd: biotinidase	NM_025295	26363	Mm.142518.1	202.56	251.76	1.24	2.811	0.031341
1427093_at	Zfp707: zinc finger protein 707	BC026404	69020	Mm.41391.1	221.66	273.8	1.24	3.646	0.013711
1451318_a_at	Lyn: Yamaguchi sarcoma viral (v-yes-1) oncogene homolog	M57697	17096	Mm.1834.1	229.19	283.27	1.24	2.828	0.038108
1447264_at	Rab11fip1: RAB11 family interacting protein 1 (class I)	BB727442	75767	Mm.210458.1	232.59	288.11	1.24	3.708	0.010406
1447972_at	Kcnk15: potassium channel, subfamily K, member 15	AI504336	241769	Mm.31191.2	251.3	311.88	1.24	3.306	0.016936
1421930_at	Icos: inducible T-cell co-stimulator	AB023132	54167	Mm.42044.1	252.86	313.33	1.24	2.683	0.036968
1451427_a_at	Egfl7: EGF-like domain 7	BC024610	353156	Mm.46628.2	348.46	432.72	1.24	2.796	0.046426
1451215_at	Prrc1: proline-rich coiled-coil 1	BI155792	73137	Mm.29889.1	416.36	515.04	1.24	2.847	0.031057
1460623_at	Skap2: src family associated phosphoprotein 2	BB753881	54353	Mm.142867.1	621.52	768.96	1.24	2.642	0.039257
1417842_at	Caml: calcium modulating ligand	NM_007596	12328	Mm.2313.1	839.16	1039.78	1.24	2.595	0.044241
1455690_at	Mm.212612.1	BE956288		Mm.212612.1	150.59	184.49	1.23	2.998	0.027272
1432083_a_at	Lrrc23: leucine rich repeat containing 23	AK015011	16977	Mm.3207.2	185.15	227.91	1.23	2.62	0.042279
1450387_s_at	Ak4: adenylate kinase 4	NM_009647	11639	Mm.42040.1	191.97	236.64	1.23	2.889	0.02774
1446641_at	Mm.182654.1	AW549913		Mm.182654.1	228.68	280.83	1.23	2.734	0.034559
1420149_at	Mm.6159.1	AA673515		Mm.6159.1	263.64	323.79	1.23	3.582	0.01168
1442507_at	Whrn: whirlin	BG862377	73750	Mm.193579.1	282.51	346.44	1.23	2.635	0.04024
1434711_at	BC030867: cDNA sequence BC030867	AV094888	217216	Mm.33152.1	312.61	384.64	1.23	3.215	0.021051
1441260_a_at	Zfp771: zinc finger protein 771	BE947089	244216	Mm.101064.1	334.93	412.32	1.23	2.512	0.047745
1455518_at	Zdhhc18: zinc finger, DHHC domain containing 18	BB324402	503610	Mm.44482.1	347.31	428.13	1.23	2.671	0.047681
1426516_a_at	Lpin1: lipin 1	AK014526	14245	Mm.28548.2	380.98	466.84	1.23	2.586	0.041725
1440442_at	Map2k7: mitogen-activated protein kinase kinase 7	BE950627	26400	Mm.109956.1	446.22	548.84	1.23	3.22	0.018324
1421720_a_at	Dtx2: deltex 2 homolog (Drosophila)	NM_023742	74198	Mm.29343.1	490.19	602.82	1.23	3.039	0.0323
1436344_at	C2cd2: C2 calcium-dependent domain containing 2	BB005022	207781	Mm.1465.1	497.82	613.4	1.23	2.866	0.033106
1442348_at	Katnal1: katanin p60 subunit A-like 1	BB549862	231912	Mm.39996.1	886.1	1091.94	1.23	2.693	0.047153
1422190_at	C5ar1: complement component 5a receptor 1	NM_007577	12273	Mm.57044.1	139.46	170.79	1.22	3.203	0.01881
1457162_at	Ldlrap1: low density lipoprotein receptor adaptor protein 1	BB008111	100017	Mm.212646.1	156.36	191.4	1.22	3.859	0.010052
1440706_at	Bmp8b: bone morphogenetic protein 8b	BM210179	12164	Mm.214707.1	191.31	232.64	1.22	2.78	0.03294
1443974_at	Plcl1: phospholipase C-like 1	BB274799	227120	Mm.151246.1	204.9	250.27	1.22	2.97	0.02572
1455239_at	6330512M04Rik: RIKEN cDNA 6330512M04 gene	BM116861	320802	Mm.1898.1	228.85	278.29	1.22	2.58	0.042241
1448609_at	Tst: thiosulfate sulfurtransferase, mitochondrial	BC005644	22117	Mm.15312.1	237.95	290.71	1.22	3.409	0.01465
1452924_at	Fam83d: family with sequence similarity 83, member D	BF730742	71878	Mm.85162.1	265.8	324.23	1.22	3.9	0.011447
1419413_at	Ccl17: chemokine (C-C motif) ligand 17	NM_011332	20295	Mm.41988.1	285.09	346.92	1.22	3.207	0.020407
1450581_at	Galr3: galanin receptor 3	NM_015738	14429	Mm.57148.1	297.45	363.92	1.22	2.704	0.035412
1418782_at	Rxrg: retinoid X receptor gamma	NM_009107	20183	Mm.3475.1	298.5	364.18	1.22	3.73	0.014536
1419379_x_at	Fxyd2: FXYD domain-containing ion transport regulator 2	NM_052823	11936	Mm.22742.1	301.09	367.06	1.22	3.458	0.014396
1447608_x_at	Nacc2: nucleus accumbens associated 2, BEN and BTB (POZ) domain containing	BB286831	67991	Mm.133173.1	303.59	369.16	1.22	2.527	0.044876
1450325_at	Angpt4: angiopoietin 4	NM_009641	11602	Mm.89941.1	310.46	379.77	1.22	4.202	0.006598
1420460_a_at	Pex11b: peroxisomal biogenesis factor 11 beta	NM_011069	18632	Mm.20901.1	326.26	397.05	1.22	2.628	0.046692
1447878_s_at	Fgfrl1: fibroblast growth factor receptor-like 1	BB109694	116701	Mm.118450.1	395.77	483.97	1.22	2.468	0.049666
1416424_at	Plin3: perilipin 3	BC011116	66905	Mm.104975.1	404.95	494.05	1.22	2.689	0.047727
1427638_at	Zbtb16: zinc finger and BTB domain containing 16	Z47205	235320	Mm.100507.1	418.94	512.42	1.22	2.833	0.047083
1420911_a_at	Mfge8: milk fat globule-EGF factor 8 protein	NM_008594	17304	Mm.1451.1	438.69	536.05	1.22	3.302	0.020126
1451854_a_at	Shroom3: shroom family member 3	AF199422	27428	Mm.46014.2	522	639.22	1.22	2.699	0.036318
1454742_at	Rasgef1b: RasGEF domain family, member 1B	BB003229	320292	Mm.87466.1	671.26	819.81	1.22	3.163	0.028349
1429109_at	Msl2: male-specific lethal 2 homolog (Drosophila)	BB745314	77853	Mm.98082.1	758.75	924.96	1.22	3.237	0.026979
1448459_at	Kcnip1: Kv channel-interacting protein 1	NM_027398	70357	Mm.39745.1	888.49	1087.1	1.22	2.509	0.04805
1424516_at	B230354K17Rik: RIKEN cDNA B230354K17 gene	BB440272	320063	Mm.206588.1	936.27	1139.17	1.22	2.833	0.029967

1435867_at	Jhdm1d: jumonji C domain-containing histone demethylase 1 homolog D (S. cerevisiae)	BM244697	338523	Mm.30702.1	1376.07	1683.84	1.22	2.655	0.043688
1428074_at	Tmem158: transmembrane protein 158	BE981853	72309	Mm.8569.1	1447.13	1764.5	1.22	4.231	0.009907
1448254_at	Ptn: pleiotrophin	BC002064	19242	Mm.3063.1	2351.13	2870.13	1.22	2.87	0.043553
1430377_at	1300015D01Rik: RIKEN cDNA 1300015D01 gene	AK005014	74161	Mm.123157.1	147.75	178.87	1.21	2.745	0.033622
1451885_at	Mm.172457.1	BC019382		Mm.172457.1	156.99	190.16	1.21	2.67	0.037288
1447844_at	Mm.75540.1	AV077281		Mm.75540.1	163.97	198.92	1.21	2.669	0.041781
1437317_at	Uba7: ubiquitin-like modifier activating enzyme 7	BB735820	74153	Mm.1183.2	177.16	214.66	1.21	3.336	0.015721
1436287_at	Gm10664: predicted gene 10664	BF466943	1E+08	Mm.58847.1	177.76	214.68	1.21	3.3	0.020936
1449161_at	Edn2: endothelin 2	NM_007902	13615	Mm.1366.1	192.94	233.9	1.21	3.178	0.019374
1417441_at	Dnajc12: DnaJ (Hsp40) homolog, subfamily C, member 12	NM_013888	30045	Mm.32550.1	221.62	268.84	1.21	2.489	0.048589
1433715_at	Cpne7: copine VII	BB426433	102278	Mm.36434.1	226.43	274.86	1.21	2.808	0.033956
1431674_at	2610303G11Rik: RIKEN cDNA 2610303G11 gene	AK011970	70457	Mm.53530.1	236.39	285.65	1.21	2.501	0.04757
1445677_x_at	Slc35f2: solute carrier family 35, member F2	BB401264	72022	Mm.213330.1	241.81	292.37	1.21	2.653	0.041027
1444448_at	Gm10392: predicted gene 10392	BB206115	1E+08	Mm.212801.2	305.63	370.39	1.21	2.657	0.044135
1419003_at	Bves: blood vessel epicardial substance	NM_024285	23828	Mm.88374.1	337.92	407.25	1.21	2.571	0.042808
1421558_at	T2: brachyury 2	NM_013682	21331	Mm.12880.1	380.05	459.63	1.21	3.046	0.031833
1449970_at	Capn12: calpain 12	NM_021894	60594	Mm.81144.1	384.86	464.95	1.21	2.448	0.049905
1420807_a_at	Dlk2: delta-like 2 homolog (Drosophila)	NM_134120	106565	Mm.23633.1	481.62	582.82	1.21	3.553	0.020683
1451397_at	Gigyf2: GRB10 interacting GYF protein 2	BC027137	227331	Mm.23065.1	592.31	716.43	1.21	3.138	0.033991
1433551_at	Vat1l: vesicle amine transport protein 1 homolog-like (T. californica)	AV173683	270097	Mm.24704.1	711.68	860.32	1.21	2.954	0.04726
1426691_at	Tjap1: tight junction associated protein 1	AK002882	74094	Mm.25337.1	758.11	918.77	1.21	2.726	0.034524
1460724_at	Ap2a1: adaptor protein complex AP-2, alpha 1 subunit	NM_007458	11771	Mm.6877.1	1125.16	1358.19	1.21	2.839	0.034804
1437991_x_at	Rusc1: RUN and SH3 domain containing 1	BB145073	72296	Mm.27687.3	1158.92	1404.03	1.21	4.058	0.011071
1436026_at	Zfp703: zinc finger protein 703	BI558298	353310	Mm.204893.1	1670.21	2018.22	1.21	2.906	0.043829
1432331_a_at	Prrx2: paired related homeobox 2	AK019971	20204	Mm.1802.2	165.46	199.27	1.2	4.038	0.00827
1435338_at	Cdk6: cyclin-dependent kinase 6	BM238926	12571	Mm.31672.1	174.59	209.4	1.2	2.653	0.046182
1450240_a_at	Sytl1: synaptotagmin-like 1	NM_031393	269589	Mm.25660.1	182.33	219.54	1.2	2.822	0.031218
1451139_at	Slc39a4: solute carrier family 39 (zinc transporter), member 4	BC023498	72027	Mm.29483.1	182.8	218.61	1.2	2.518	0.048474
1419323_at	Padi1: peptidyl arginine deiminase, type I	NM_011059	18599	Mm.20854.1	195.41	235.32	1.2	2.688	0.047765
1450944_at	Cspg4: chondroitin sulfate proteoglycan 4	BB377873	121021	Mm.41329.1	206.13	248.15	1.2	3.042	0.022738
1429608_at	Adh6a: alcohol dehydrogenase 6A (class V)	AK007397	69117	Mm.46265.1	214.46	257.98	1.2	2.559	0.048285
1457118_at	Shc4: SHC (Src homology 2 domain containing) family, member 4	AV353605	271849	Mm.190005.1	226.21	271.95	1.2	2.622	0.039456
1440507_at	Gm10575: predicted gene 10575	BB059041	1E+08	Mm.80935.1	241.63	290.89	1.2	2.761	0.034966
1451119_a_at	Fbln1: fibulin 1	BC007140	14114	Mm.219663.2	244.93	295.01	1.2	2.921	0.033534
1448602_at	Pygm: muscle glycogen phosphorylase	NM_011224	19309	Mm.27806.1	249.77	298.57	1.2	2.577	0.044569
1456965_at	Mm.39772.1	BE949887		Mm.39772.1	260.38	311.82	1.2	3.093	0.021474
1415948_at	Creg1: cellular repressor of E1A-stimulated genes 1	BC027426	433375	Mm.459.1	283.62	338.95	1.2	2.997	0.026434
1433608_at	Scfd2: Sec1 family domain containing 2	BB821363	212986	Mm.24613.1	294.31	352.22	1.2	2.521	0.046351
1440366_at	Mm.122071.1	BB185168		Mm.122071.1	316.87	379.88	1.2	4.31	0.005415
1450981_at	Cnn2: calponin 2	BI663014	12798	Mm.21776.1	336.43	403.56	1.2	2.786	0.034638
1420304_x_at	LOC100503934: hypothetical LOC100503934	AV128236	1.01E+08	Mm.176758.1	342.88	412.65	1.2	2.575	0.042522
1428515_at	Zswim7: zinc finger, SWIM-type containing 7	AK010472	69747	Mm.141150.1	368.06	442.33	1.2	3.122	0.022047
1450235_at	Fgd3: FYVE, RhoGEF and PH domain containing 3	NM_015759	30938	Mm.20436.1	395.32	472.78	1.2	3.082	0.021791
1421306_a_at	Hdac9: histone deacetylase 9	NM_024124	79221	Mm.166423.1	413.39	496.19	1.2	3.101	0.022143
1450833_at	Chrm1: cholinergic receptor, muscarinic 1, CNS	NM_007698	12669	Mm.57200.1	434.5	522.12	1.2	4.47	0.004435
1449626_s_at	Acbd4: acyl-Coenzyme A binding domain containing 4	AI849317	67131	Mm.200110.1	473.81	567.39	1.2	3.402	0.016066
1416097_at	Lrrc4: leucine rich repeat containing 4	NM_138682	192198	Mm.40158.1	507.39	610.96	1.2	3.706	0.010483
1423074_at	Lman2: lectin, mannose-binding 2	AK004952	66890	Mm.38868.1	847.49	1015.64	1.2	3.338	0.017552
1432551_at	1700031F10Rik: RIKEN cDNA 1700031F10 gene	AK006579	73317	Mm.195664.1	156.12	186.45	1.19	2.669	0.045099
1420449_at	Heatr5b: HEAT repeat containing 5B	NM_028084	320473	Mm.46309.1	178.76	213.28	1.19	3.604	0.014624
1451807_at	Nr1i2: nuclear receptor subfamily 1, group I, member 2	AK018630	18171	Mm.8509.1	186.33	222.66	1.19	2.536	0.045089
1438290_x_at	Sftpc: Surfactant associated protein C	AV169310	20389	Mm.24040.2	188.42	224.04	1.19	2.73	0.03504
1425246_at	0610008F07Rik: RIKEN cDNA 0610008F07 gene	BC025862	68314	Mm.46190.1	199.85	237.37	1.19	2.931	0.02643
1441232_at	Mm.82607.1	BE957315		Mm.82607.1	213.12	254.57	1.19	3.616	0.015625

1422288_at	Htr1b: 5-hydroxytryptamine (serotonin) receptor 1B	NM_010482	15551	Mm.57047.1	216.2	256.78	1.19	2.921	0.027979
1419229_at	Rhox4a /// Rhox4b /// Rhox4c /// Rhox4d /// Rhox4e /// Rhox4f /// Rhox4g: reproductive homeobox 4A /// reproductive homeobox 4B /// reproductive homeobox 4C /// reproductive homeobox 4D /// reproductive homeobox 4E /// reproductive homeobox 4F /// reproductive homeobox 4G	NM_021300	194856 /434759 /57737 /636177 /664608 /664609 /664610	Mm.195896.1	227	270.54	1.19	2.485	0.048034
1447712_x_at	Ep400: E1A binding protein p400	BB345411	75560	Mm.131958.1	251.37	300.18	1.19	2.933	0.032256
1432197_at	4933417D19Rik: RIKEN cDNA 4933417D19 gene	AK016841	71186	Mm.158608.1	323.05	385.47	1.19	2.872	0.032071
1454229_a_at	Eri2: exoribonuclease 2	AK015831	71151	Mm.61240.2	395.87	469.3	1.19	2.497	0.04899
1451911_a_at	Ace: angiotensin I converting enzyme (peptidyl-dipeptidase A) 1	M55333	11421	Mm.754.1	469.61	559.58	1.19	3.122	0.021261
1450459_at	2010106G01Rik: RIKEN cDNA 2010106G01 gene	NM_023220	66552	Mm.218254.1	529.64	628.32	1.19	2.932	0.026212
1420557_at	Epha5: Eph receptor A5	NM_007937	13839	Mm.4466.1	562.35	669.3	1.19	3.178	0.022408
1442703_at	Greb1l: growth regulation by estrogen in breast cancer-like	BB820231	381157	Mm.213296.1	707.76	845.63	1.19	3.31	0.024033
1424425_a_at	Mtap: methylthioadenosine phosphorylase	BG075139	66902	Mm.28500.1	753.52	893.32	1.19	2.861	0.032703
1416160_at	Nr2f2: nuclear receptor subfamily 2, group F, member 2	AI463873	11819	Mm.16519.1	2747.4	3258.71	1.19	2.782	0.040141
1456408_x_at	4933439C10Rik: RIKEN cDNA 4933439C10 gene	AV205521	74476	Mm.17353.4	178.2	210.46	1.18	2.635	0.043009
1420762_a_at	Ybx2: Y box protein 2	NM_016875	53422	Mm.29286.1	182.1	214.8	1.18	2.5	0.046959
1460523_at	Gm9777: predicted gene 9777	AK019581	1E+08	Mm.195803.1	196.05	230.47	1.18	2.694	0.037095
1441029_at	Mm.153962.1	BI076737		Mm.153962.1	198.19	233.82	1.18	2.886	0.027831
1416552_at	Dppa5a: developmental pluripotency associated 5A	NM_025274	434423	Mm.139314.1	199.72	234.75	1.18	2.847	0.029781
1422890_at	Pcdh18: protocadherin 18	BM218630	73173	Mm.87246.1	200.86	237.32	1.18	3.119	0.025038
1416334_at	Wwox: WW domain-containing oxidoreductase	NM_019573	80707	Mm.33369.1	202.89	240.37	1.18	2.56	0.048064
1452308_a_at	Atp1a2: ATPase, Na+/K+ transporting, alpha 2 polypeptide	BB462665	98660	Mm.193539.2	223.02	262.62	1.18	2.503	0.048526
1421761_a_at	Barx2: BarH-like homeobox 2	NM_013800	12023	Mm.3508.1	261.76	309.65	1.18	2.639	0.038808
1440995_at	6430531B16Rik /// LOC100503791: RIKEN cDNA 6430531B16 gene /// hypothetical LOC100503791	BE946005	100503791 /// 381933	Mm.154402.1	270.03	319.18	1.18	2.737	0.040598
1454844_at	Mchr1: melanin-concentrating hormone receptor 1	AW049955	207911	Mm.23072.1	272.7	321.6	1.18	2.818	0.033808
1418904_at	Gfpt1: glutamine fructose-6-phosphate transaminase 1	AF334736	14583	Mm.19893.1	341.04	404.12	1.18	4.198	0.005698
1439883_at	Gm3620: Predicted gene 3620	AW049095	1E+08	Mm.103307.1	352.55	416.45	1.18	2.709	0.04141
1439995_at	Nhedc2: Na+/H+ exchanger domain containing 2	AV251613	97086	Mm.25081.1	379.59	446.51	1.18	2.862	0.033461
1433840_a_at	C330006K01Rik: RIKEN cDNA C330006K01 gene	BB499868	231855	Mm.78250.1	408.95	483.13	1.18	3.26	0.021669
1431831_at	2210009G21Rik: RIKEN cDNA 2210009G21 gene	AK010392	74243	Mm.116820.2	428.93	507.59	1.18	2.499	0.046627
1439020_at	AW146020: expressed sequence AW146020	AW146020	330361	Mm.27876.1	708.91	839.2	1.18	3.086	0.022416
1430526_a_at	Smarca2: SWI/SNF related, matrix associated, actin dependent regulator of chromatin, subfamily a, member 2	AK011935	67155	Mm.12184.3	866.5	1022.53	1.18	3.147	0.021146
1457248_x_at	Hsd17b7: hydroxysteroid (17-beta) dehydrogenase 7	BB554029	15490	Mm.215044.1	1141.15	1347.27	1.18	2.697	0.036563
1436923_at	Rab2b: RAB2B, member RAS oncogene family	BF466486	76338	Mm.32870.2	1287.66	1522.84	1.18	3.244	0.024627
1435805_at	Lin7a: lin-7 homolog A (C. elegans)	AV287586	108030	Mm.38592.1	1512.26	1788.44	1.18	3.35	0.017145
1422253_at	Col10a1: collagen, type X, alpha 1	NM_009925	12813	Mm.4837.1	173.06	203.24	1.17	3.662	0.010696
1433269_at	4930553M12Rik: RIKEN cDNA 4930553M12 gene	AK016108	75246	Mm.159476.1	208.93	244.49	1.17	2.478	0.049703
1419192_at	Il4i1 /// Nup62-il4i1: interleukin 4 induced 1 /// Nup62-Il4i1 protein	NM_010215	100328588 /// 14204	Mm.2565.1	222.06	260.5	1.17	3.295	0.01752
1422120_at	Eaf2: ELL associated factor 2	AY034479	106389	Mm.44970.1	225.02	264.23	1.17	2.954	0.027725
1428538_s_at	Rarres2: retinoic acid receptor responder (tazarotene induced) 2	BI328146	71660	Mm.28231.1	255.82	299.48	1.17	3.913	0.010512
1449611_at	Cd82: CD82 antigen	AI894122	12521	Mm.192736.1	256.74	301.61	1.17	2.726	0.035561
1434867_at	Slc4a11: solute carrier family 4, sodium bicarbonate transporter-like, member 11	AI503023	269356	Mm.31224.1	260.01	303.41	1.17	3.93	0.007823
1436752_at	Tbccd1: TBCC domain containing 1	BM229530	70573	Mm.23783.1	270.91	317.69	1.17	2.742	0.036873
1444761_at	Mm.33286.1	AI503482		Mm.33286.1	281.15	328.06	1.17	2.557	0.046345
1442133_at	Ado: 2-aminoethanethiol (cysteamine) dioxygenase	AI661805	211488	Mm.37989.1	287.49	337.1	1.17	2.651	0.048656
1418920_at	Cldn15: claudin 15	NM_021719	60363	Mm.87202.1	308.13	359.18	1.17	2.607	0.042019
1447449_at	Mm.151370.1	BE983114		Mm.151370.1	340.08	398.8	1.17	3.083	0.021631
1416433_at	Rpa2: replication protein A2	BC004578	19891	Mm.2870.1	370.05	434.78	1.17	2.896	0.030556
1447788_s_at	Tspyl3: TSPY-like 3	BB308532	241732	Mm.125632.1	410.23	478.69	1.17	2.595	0.041297
1449579_at	Sh3yl1: Sh3 domain YSC-like 1	NM_013709	24057	Mm.218624.1	571.5	669.76	1.17	3.656	0.010858
1419447_s_at	Tbc1d1: TBC1 domain family, member 1	BB501891	57915	Mm.56905.1	604.98	707.09	1.17	3.813	0.010691
1437419_at	Bmp2k: BMP2 inducible kinase	BB329439	140780	Mm.220302.1	725.68	846.97	1.17	2.944	0.026148

1437845_x_at	Pofut2: protein O-fucosyltransferase 2	BB027731	80294	Mm.203556.3	878.64	1031.65	1.17	2.735	0.045625
1426684_at	Cnot6: CCR4-NOT transcription complex, subunit 6	BM940481	104625	Mm.28824.1	883.62	1034.17	1.17	2.896	0.042772
1420885_a_at	Sez6: seizure related gene 6	NM_021286	20370	Mm.4727.1	900.18	1057.63	1.17	3.009	0.023729
1448865_at	Hsd17b7: hydroxysteroid (17-beta) dehydrogenase 7	NM_010476	15490	Mm.12882.1	938.97	1095.99	1.17	2.54	0.049906
1435510_at	Ppm1h: protein phosphatase 1H (PP2C domain containing)	BB283101	319468	Mm.134443.1	1063.15	1238.67	1.17	3.124	0.02988
1437206_at	Setd5: SET domain containing 5	BI739725	72895	Mm.99859.1	2053.88	2393.41	1.17	2.647	0.038301
1438329_at	Tlr12: toll-like receptor 12	BB745017	384059	Mm.212803.1	206.89	240.17	1.16	2.608	0.040238
1425982_a_at	Wrn: Werner syndrome homolog (human)	U97045	22427	Mm.15446.3	210.1	243.31	1.16	2.906	0.038385
1457194_at	Mm.214742.1	BB087681		Mm.214742.1	217.08	251.56	1.16	2.556	0.048216
1436642_x_at	AW047730: expressed sequence AW047730	BE993148	99870	Mm.23659.1	227.4	263.17	1.16	2.947	0.025724
1430559_at	Nt5c3l: 5'-nucleotidase, cytosolic III-like	BB402435	68106	Mm.28738.2	274.74	317.63	1.16	2.919	0.027431
1450836_at	Neurog1: neurogenin 1	NM_010896	18014	Mm.57230.1	286.62	332.05	1.16	2.561	0.04621
1436856_x_at	Tars2: threonyl-tRNA synthetase 2, mitochondrial (putative)	BB549252	71807	Mm.9945.4	346.73	402.06	1.16	2.621	0.042755
1422068_at	Pou3f1: POU domain, class 3, transcription factor 1	NM_011141	18991	Mm.1330.1	377.27	437.53	1.16	2.74	0.045879
1417701_at	Ppp1r14c: protein phosphatase 1, regulatory (inhibitor) subunit 14c	NM_133485	76142	Mm.23009.1	452.67	525.03	1.16	2.902	0.027545
1440168_x_at	Kctd7: potassium channel tetramerisation domain containing 7	BB252670	212919	Mm.74883.1	468.98	544.23	1.16	2.622	0.039546
1424991_s_at	Tyms /// Tyms-ps: thymidylate synthase /// thymidylate synthase, pseudogene	BC020139	22171 /// 22172	Mm.5879.1	623.19	721.46	1.16	2.86	0.029132
1417095_a_at	Hspa14: heat shock protein 14	NM_015765	50497	Mm.89341.1	623.54	725.58	1.16	2.993	0.025814
1453170_at	Mm.31537.1	AK005221		Mm.31537.1	646.47	748.42	1.16	2.474	0.048188
1424497_at	Tmem219: transmembrane protein 219	BC023442	68742	Mm.141925.1	758.96	877.41	1.16	2.665	0.040416
1418518_at	Furin: furin (paired basic amino acid cleaving enzyme)	NM_011046	18550	Mm.5241.1	874.77	1012.4	1.16	3.107	0.021287
1435795_at	Glb1: galactosidase, beta 1	BE956926	12091	Mm.76797.1	886.19	1030.11	1.16	2.648	0.038271
1415965_at	Scd1: stearoyl-Coenzyme A desaturase 1	NM_009127	20249	Mm.140785.1	926.83	1072.73	1.16	4.288	0.013462
1455244_at	Daam1: dishevelled associated activator of morphogenesis 1	BB794633	208846	Mm.30825.1	1614.1	1879.48	1.16	3.714	0.010222
1417724_at	Thoc4: THO complex 4	NM_011568	21681	Mm.1886.1	1667	1935.58	1.16	3.066	0.026139
1452762_at	Rbms3: RNA binding motif, single stranded interacting protein	AK018466	207181	Mm.99916.1	1911.76	2223.22	1.16	3.415	0.014305
1436938_at	Rbms3: RNA binding motif, single stranded interacting protein	BB053506	207181	Mm.133242.1	2975.39	3451.7	1.16	4.396	0.006044
1457541_at	Akap14: A kinase (PRKA) anchor protein 14	BB019018	434756	Mm.55422.1	200.87	231.11	1.15	2.609	0.040441
1436711_at	Actr5: ARP5 actin-related protein 5 homolog (yeast)	BB247665	109275	Mm.27747.1	326.63	375.07	1.15	2.849	0.030003
1427584_at	Amot: angiomotin	U80888	27494	Mm.215174.1	477.06	547.3	1.15	2.781	0.032015
1437381_x_at	Gpr172b: G protein-coupled receptor 172B	BB236260	52710	Mm.28597.3	480.57	554.05	1.15	2.541	0.045095
1437499_at	Ankrd39: ankyrin repeat domain 39	AV316495	109346	Mm.133378.1	487.34	560.92	1.15	2.976	0.028605
1453288_at	Atf6: activating transcription factor 6	AK020270	226641	Mm.153315.1	498.2	573.01	1.15	2.491	0.047153
1443990_at	Ntrk1: neurotrophic tyrosine kinase, receptor, type 1	AW124632	18211	Mm.80682.1	610.09	700.67	1.15	2.877	0.029585
1418004_a_at	Tmem176b: transmembrane protein 176B	NM_023056	65963	Mm.28385.1	616.64	706.9	1.15	2.738	0.040872
1452150_at	AU040320: expressed sequence AU040320	BG071197	100317	Mm.206206.1	669.13	771.23	1.15	3.646	0.010803
1425578_a_at	Gfra2: glial cell line derived neurotrophic factor family receptor alpha 2	BI134771	14586	Mm.41886.2	926.81	1061.29	1.15	2.542	0.044076
1426240_at	Chmp4b: chromatin modifying protein 4B	BC011429	75608	Mm.190436.1	969.6	1111.13	1.15	3.278	0.02041
1429509_at	Lsm12: LSM12 homolog (S. cerevisiae)	BB771548	268490	Mm.36280.1	1113.87	1286.39	1.15	2.61	0.040474
1431465_s_at	Fyttd1: forty-two-three domain containing 1	AK008130	69823	Mm.195995.1	1125.88	1300.01	1.15	2.911	0.028136
1458833_at	Nrcam: neuron-glia-CAM-related cell adhesion molecule	BB283553	319504	Mm.166553.1	1404.65	1613.07	1.15	2.783	0.036264
1441930_x_at	Vat1: Vesicle amine transport protein 1 homolog (T californica)	BB089991	26949	Mm.166455.1	1425.1	1640.03	1.15	4.721	0.010476
1423972_at	Etfa: electron transferring flavoprotein, alpha polypeptide	BC003432	110842	Mm.26949.1	2366.34	2711.27	1.15	3.775	0.012714
1434709_at	Nrcam: neuron-glia-CAM-related cell adhesion molecule	BB202655	319504	Mm.37263.1	2432.01	2787.89	1.15	3.257	0.017539
1416429_a_at	Cat: catalase	NM_009804	12359	Mm.4215.1	3851.07	4423.94	1.15	3.427	0.014494
1457456_at	Map3k10: mitogen-activated protein kinase kinase kinase 10	AI481735	269881	Mm.207692.1	216.29	247.54	1.14	2.484	0.0478
1417790_at	Dok1: docking protein 1	BC013066	13448	Mm.156.1	259.94	296.49	1.14	4.263	0.005607
1438437_a_at	4933439C10Rik: RIKEN cDNA 4933439C10 gene	AV205521	74476	Mm.17353.4	272.28	309.72	1.14	2.894	0.029093
1421413_a_at	Pdlim5: PDZ and LIM domain 5	NM_022554	56376	Mm.24839.1	287.22	326.98	1.14	2.943	0.025865
1455555_at	Vipr1: vasoactive intestinal peptide receptor 1	BF224468	22354	Mm.205513.1	301.66	345.17	1.14	2.694	0.048178
1447789_x_at	Ddx6: DEAD (Asp-Glu-Ala-Asp) box polypeptide 6	BB150520	13209	Mm.130899.1	325.86	372.64	1.14	2.967	0.028797
1439829_at	Adcy5: Adenylate cyclase 5	BE946363	224129	Mm.41137.1	413.66	473.11	1.14	2.769	0.033166
1450533_a_at	Plagl1: pleiomorphic adenoma gene-like 1	NM_009538	22634	Mm.220978.1	431.63	491.93	1.14	2.708	0.037033
1454367_at	Mm.78346.1	AV260466		Mm.78346.1	442.87	503.98	1.14	2.563	0.042771
1447703_x_at	Zfp593: zinc finger protein 593	AV214133	68040	Mm.177940.1	460.72	523.4	1.14	2.894	0.029966

1425474_a_at	Vps39: vacuolar protein sorting 39 (yeast)	BC007479	269338	Mm.29634.1	461.41	525.17	1.14	2.69	0.036757
1451464_at	Mfap3: microfibrillar-associated protein 3	BI661422	216760	Mm.30501.1	664.52	759.78	1.14	2.894	0.03161
1455409_at	Spire1: spire homolog 1 (Drosophila)	BM234794	68166	Mm.23853.1	854.31	976.85	1.14	2.796	0.031318
1425911_a_at	Fgfr1: fibroblast growth factor receptor 1	M65053	14182	Mm.3157.3	1026.74	1174.08	1.14	2.995	0.024181
1422227_at	Klf12: Kruppel-like factor 12	NM_010636	16597	Mm.42225.1	1141.03	1304.22	1.14	2.56	0.047528
1439460_a_at	Arfgap2: ADP-ribosylation factor GTPase activating protein 2	BB317953	77038	Mm.43636.3	1322.58	1512.04	1.14	3.693	0.010443
1435008_at	Slc9a6: solute carrier family 9 (sodium/hydrogen exchanger), member 6	BB611738	236794	Mm.17815.1	1819.01	2072.78	1.14	3.103	0.025093
1417733_at	Rnf146: ring finger protein 146	NM_026518	68031	Mm.28930.1	2222.96	2525.78	1.14	4.069	0.006842
1439084_at	Cxcl12: chemokine (C-X-C motif) ligand 12	BE986839	20315	Mm.39465.1	251.42	284.01	1.13	2.684	0.037749
1451384_at	Jmjd5: jumonji domain containing 5	BC024807	77035	Mm.33069.1	275.61	312.76	1.13	2.861	0.031486
1425133_s_at	Rab3il1: RAB3A interacting protein (rabin3)-like 1	BC020147	74760	Mm.200929.1	278.69	314.23	1.13	2.961	0.026704
1437864_at	Adipor2: adiponectin receptor 2	BE632137	68465	Mm.41916.1	469.1	530.07	1.13	2.931	0.027249
1423921_at	Ints3: integrator complex subunit 3	BC003209	229543	Mm.29529.1	588.77	663.91	1.13	3.232	0.019175
1428148_s_at	Coro7: coronin 7	BB203098	78885	Mm.41792.1	691.67	781.53	1.13	3.001	0.038804
1436917_s_at	Gpsm1: G-protein signalling modulator 1 (AGS3-like, C. elegans)	BB491018	67839	Mm.31239.4	986.95	1118.37	1.13	2.729	0.034287
1452878_at	Prkce: protein kinase C, epsilon	AK017901	18754	Mm.2013.1	1190.61	1343.6	1.13	2.527	0.044846
1426982_at	Flywch1: FLYWCH-type zinc finger 1	BB477613	224613	Mm.206621.1	1499.11	1699.89	1.13	3.518	0.012587
1428429_at	Rgmb: RGM domain family, member B	AK004310	68799	Mm.68556.1	1682.57	1902.6	1.13	3.404	0.016407
1435662_at	Nkap: NFKB activating protein	BB168118	67050	Mm.24089.1	2011.65	2278.4	1.13	3.261	0.017235
1424711_at	Tmem2: transmembrane protein 2	BC019745	83921	Mm.26702.1	4043.44	4554.23	1.13	3.374	0.018729
1424187_at	Ccdc80: coiled-coil domain containing 80	BG074158	67896	Mm.181074.1	250.68	281.59	1.12	2.572	0.043931
1441915_s_at	Plin5: perilipin 5	BB717485	66968	Mm.185311.1	254.08	285.76	1.12	2.459	0.04919
1441311_at	Rps6ka2: ribosomal protein S6 kinase, polypeptide 2	BG063083	20112	Mm.196198.1	261.87	293.61	1.12	2.86	0.033305
1456370_s_at	0610037L13Rik: RIKEN cDNA 0610037L13 gene	BB044881	74098	Mm.46638.2	350.43	393.65	1.12	2.63	0.039624
1454913_at	9930104L06Rik: RIKEN cDNA 9930104L06 gene	BE951725	194268	Mm.56193.1	351.72	394.13	1.12	2.589	0.041337
1424702_a_at	Atg2b: ATG2 autophagy related 2 homolog B (S. cerevisiae)	BC024533	76559	Mm.34412.1	400.12	446.17	1.12	3.181	0.020444
1456604_a_at	Pcmt1: protein-L-isoaspartate (D-aspartate) O-methyltransferase 1	BB315555	18537	Mm.25293.4	938.32	1054.33	1.12	3.369	0.020707
1453094_at	Foxn3: forkhead box N3	AK017346	71375	Mm.87594.1	1040.13	1165.49	1.12	2.948	0.027659
1418841_s_at	Cdk11b: cyclin-dependent kinase 11B	NM_007661	12537	Mm.4414.1	1558.28	1745.81	1.12	3.558	0.012139
1433655_at	Rnf141: ring finger protein 141	AV024351	67150	Mm.96867.1	2422.64	2711.1	1.12	2.727	0.034772
1423291_s_at	Hyou1: hypoxia up-regulated 1	BM231738	12282	Mm.116721.1	2835.9	3170.51	1.12	4.353	0.007782
1422431_at	Magee1: melanoma antigen, family E, 1	NM_053201	107528	Mm.24341.1	3001.34	3357.32	1.12	2.553	0.043579
1421881_a_at	Elavl2: ELAV (embryonic lethal, abnormal vision, Drosophila)-like 2 (Hu antigen B)	BB105998	15569	Mm.3823.1	3438.36	3843.87	1.12	2.666	0.04562
1423686_a_at	Prr13: proline rich 13	BC016234	66151	Mm.29865.1	5029.76	5616.16	1.12	3.1	0.021147
1435071_at	Zfyve1: zinc finger, FYVE domain containing 1	AV327165	217695	Mm.59257.1	309.72	344.29	1.11	3.488	0.013229
1426967_at	Axin1: axin 1	BB004060	12005	Mm.23684.1	361.87	401.41	1.11	2.522	0.045198
1417411_at	Nap1l5: nucleosome assembly protein 1-like 5	NM_021432	58243	Mm.41277.1	624.7	691.49	1.11	2.718	0.042143
1423265_at	Minpp1: multiple inositol polyphosphate histidine phosphatase 1	BB836564	17330	Mm.43580.1	638.02	705.92	1.11	3.052	0.030541
1425511_at	Mark1: MAP/microtubule affinity-regulating kinase 1	BM213279	226778	Mm.7445.1	644.94	714.33	1.11	3.059	0.023017
1446957_s_at	N4bp1: NEDD4 binding protein 1	C81621	80750	Mm.200132.1	694.48	768.88	1.11	2.659	0.043744
1439057_x_at	Zdhhc6: zinc finger, DHHC domain containing 6	BB143557	66980	Mm.202776.1	959.97	1064.04	1.11	2.661	0.039005
1455787_x_at	Minpp1: multiple inositol polyphosphate histidine phosphatase 1	AV339366	17330	Mm.43580.2	1139.02	1261.79	1.11	3.347	0.021866
1433973_at	Sephs1: selenophosphate synthetase 1	BB293127	109079	Mm.34329.1	1207.76	1342.78	1.11	3.471	0.013302
1426757_at	Ampd2: adenosine monophosphate deaminase 2	AK004759	109674	Mm.34758.1	1287.35	1430.44	1.11	2.717	0.039046
1439389_s_at	Myadm: myeloid-associated differentiation marker	BB500055	50918	Mm.29874.2	1333.33	1477.29	1.11	2.715	0.035144
1437908_a_at	Ergic1: endoplasmic reticulum-golgi intermediate compartment (ERGIC) 1	BB095626	67458	Mm.34244.2	3743.52	4150.64	1.11	2.592	0.047439
1451864_at	Cacng8: calcium channel, voltage-dependent, gamma subunit 8	AF361350	81905	Mm.214993.1	366.13	403.69	1.1	2.755	0.043609
1416704_at	Mapk14: mitogen-activated protein kinase 14	BC012235	26416	Mm.4437.1	498.81	549.48	1.1	2.584	0.046062
1440826_s_at	2610002I17Rik: RIKEN cDNA 2610002I17	BB285582	72341	Mm.200473.1	670.03	737.26	1.1	2.593	0.041464
1425803_a_at	Mbd2: methyl-CpG binding domain protein 2	AF072245	17191	Mm.322.2	884.33	974.06	1.1	2.492	0.04704
1436848_x_at	Impa1: inositol (myo)-1(or 4)-monophosphatase 1	AV348702	55980	Mm.183042.2	949.01	1046.31	1.1	3.597	0.011415
1439284_at	Epb4.1l5: erythrocyte protein band 4.1-like 5	AW537770	226352	Mm.147530.1	1179.89	1298.64	1.1	3.218	0.018197

REFERENCES

Adams, K. L., Rousso, D. L., Umbach, J. A., & Novitch, B. G. (2015). Foxp1-mediated programming of limb-innervating motor neurons from mouse and human embryonic stem cells. *Nat Commun, 6*, 6778. doi: 10.1038/ncomms7778

Billig, I., Foris, J. M., Enquist, L. W., Card, J. P., & Yates, B. J. (2000). Definition of neuronal circuitry controlling the activity of phrenic and abdominal motoneurons in the ferret using recombinant strains of pseudorabies virus. *J Neurosci, 20*(19), 7446-7454.

Butler, J., Cauwenbergs, P., & Cosmos, E. (1986). Fate of brachial muscles of the chick embryo innervated by inappropriate nerves: structural, functional and histochemical analyses. *J Embryol Exp Morphol, 95*, 147-168.

Carlstedt, T., Anand, P., Htut, M., Misra, P., & Svensson, M. (2004). Restoration of hand function and so called "breathing arm" after intraspinal repair of C5-T1 brachial plexus avulsion injury. Case report. *Neurosurg Focus, 16*(5), E7.

Dasen, J. S., De Camilli, A., Wang, B., Tucker, P. W., & Jessell, T. M. (2008). Hox repertoires for motor neuron diversity and connectivity gated by a single accessory factor, FoxP1. *Cell, 134*(2), 304-316. doi: 10.1016/j.cell.2008.06.019

Dasen, J. S., & Jessell, T. M. (2009). Hox networks and the origins of motor neuron diversity. *Curr Top Dev Biol, 88*, 169-200. doi: 10.1016/s0070-2153(09)88006-x

Dessaud, E., Yang, L. L., Hill, K., Cox, B., Ulloa, F., Ribeiro, A., . . . Briscoe, J. (2007). Interpretation of the sonic hedgehog morphogen gradient by a temporal adaptation mechanism. *Nature, 450*(7170), 717-720. doi: 10.1038/nature06347

Dobbins, E. G., & Feldman, J. L. (1994). Brainstem network controlling descending drive to phrenic motoneurons in rat. *J Comp Neurol, 347*(1), 64-86. doi: 10.1002/cne.903470106

Dubreuil, V., Thoby-Brisson, M., Rallu, M., Persson, K., Pattyn, A., Birchmeier, C., . . . Goridis, C. (2009). Defective respiratory rhythmogenesis and loss of central chemosensitivity in Phox2b mutants targeting retrotrapezoid nucleus neurons. *J Neurosci, 29*(47), 14836-14846. doi: 10.1523/jneurosci.2623-09.2009

Ellenberger, H. H., & Feldman, J. L. (1990). Brainstem connections of the rostral ventral respiratory group of the rat. *Brain Res, 513*(1), 35-42.

Ellenberger, H. H., Feldman, J. L., & Goshgarian, H. G. (1990). Ventral respiratory group projections to phrenic motoneurons: electron microscopic evidence for monosynaptic connections. *J Comp Neurol, 302*(4), 707-714. doi: 10.1002/cne.903020403

Ellenberger, H. H., Vera, P. L., Haselton, J. R., Haselton, C. L., & Schneiderman, N. (1990). Brainstem projections to the phrenic nucleus: an anterograde and retrograde HRP study in the rabbit. *Brain Res Bull, 24*(2), 163-174.

Feldman, J. L., Del Negro, C. A., & Gray, P. A. (2013). Understanding the rhythm of breathing: so near, yet so far. *Annu Rev Physiol, 75*, 423-452. doi: 10.1146/annurev-physiol-040510-130049

Feldman, J. L., Loewy, A. D., & Speck, D. F. (1985). Projections from the ventral respiratory group to phrenic and intercostal motoneurons in cat: an autoradiographic study. *J Neurosci, 5*(8), 1993-2000.

Fujito, Y., Kawasaki, H., & Aoki, M. (1989). Motor recovery after cross-reinnervation of a forelimb nerve by the phrenic nerve in cats. *Brain Res, 492*(1-2), 36-44.

Fukuhara, K., Imai, F., Ladle, D. R., Katayama, K., Leslie, J. R., Arber, S., . . . Yoshida, Y. (2013). Specificity of monosynaptic sensory-motor connections imposed by repellent Sema3E-PlexinD1 signaling. *Cell Rep, 5*(3), 748-758. doi: 10.1016/j.celrep.2013.10.005

Gerrits, P. O., Vodde, C., & Holstege, G. (2000). Retroambiguus projections to the cutaneus trunci motoneurons may form a pathway in the central control of mating. *J Neurophysiol, 83*(5), 3076-3083.

Gray, P. A., Hayes, J. A., Ling, G. Y., Llona, I., Tupal, S., Picardo, M. C., . . . Del Negro, C. A. (2010). Developmental origin of preBotzinger complex respiratory neurons. *J Neurosci, 30*(44), 14883-14895. doi: 10.1523/jneurosci.4031-10.2010

Greer, J. J., & Funk, G. D. (2005). Perinatal development of respiratory motoneurons. *Respir Physiol Neurobiol, 149*(1-3), 43-61. doi: 10.1016/j.resp.2005.03.017

Holstege, G., & Blok, B. F. (1989). Descending pathways to the cutaneous trunci muscle motoneuronal cell group in the cat. *J Neurophysiol, 62*(6), 1260-1269.

Holstege, G., van Neerven, J., & Evertse, F. (1987). Spinal cord location of the motoneurons innervating the abdominal, cutaneous maximus, latissimus dorsi and longissimus dorsi muscles in the cat. *Exp Brain Res, 67*(1), 179-194.

Jessell, T. M. (2000). Neuronal specification in the spinal cord: inductive signals and transcriptional codes. *Nat Rev Genet, 1*(1), 20-29. doi: 10.1038/35049541

Jung, H., Lacombe, J., Mazzoni, E. O., Liem, K. F., Jr., Grinstein, J., Mahony, S., . . . Dasen, J. S. (2010). Global control of motor neuron topography mediated by the repressive actions of a single hox gene. *Neuron, 67*(5), 781-796. doi: 10.1016/j.neuron.2010.08.008

Kam, K., Worrell, J. W., Janczewski, W. A., Cui, Y., & Feldman, J. L. (2013). Distinct inspiratory rhythm and pattern generating mechanisms in the preBotzinger complex. *J Neurosci, 33*(22), 9235-9245. doi: 10.1523/jneurosci.4143-12.2013

Lane, M. A. (2011). Spinal respiratory motoneurons and interneurons. *Respir Physiol Neurobiol, 179*(1), 3-13. doi: 10.1016/j.resp.2011.07.004

Li, C., & Wong, W. H. (2001). Model-based analysis of oligonucleotide arrays: expression index computation and outlier detection. *Proc Natl Acad Sci U S A, 98*(1), 31-36. doi: 10.1073/pnas.011404098

Machado, C. B., Kanning, K. C., Kreis, P., Stevenson, D., Crossley, M., Nowak, M., . . . Lieberam, I. (2014). Reconstruction of phrenic neuron identity in embryonic stem cell-derived motor neurons. *Development, 141*(4), 784-794. doi: 10.1242/dev.097188

Malessy, M. J., van Dijk, J. G., & Thomeer, R. T. (1993). Respiration-related activity in the biceps brachii muscle after intercostal-musculocutaneous nerve transfer. *Clin Neurol Neurosurg, 95 Suppl*, S95-102.

Mantilla, C. B., & Sieck, G. C. (2008). Key aspects of phrenic motoneuron and diaphragm muscle development during the perinatal period. *J Appl Physiol (1985), 104*(6), 1818-1827. doi: 10.1152/japplphysiol.01192.2007

Mellen, N. M., Janczewski, W. A., Bocchiaro, C. M., & Feldman, J. L. (2003). Opioid-induced quantal slowing reveals dual networks for respiratory rhythm generation. *Neuron, 37*(5), 821-826.

Merrell, A. J., & Kardon, G. (2013). Development of the diaphragm -- a skeletal muscle essential for mammalian respiration. *FEBS J, 280*(17), 4026-4035. doi: 10.1111/febs.12274

Merrill, E. G., & Lipski, J. (1987). Inputs to intercostal motoneurons from ventrolateral medullary respiratory neurons in the cat. *J Neurophysiol, 57*(6), 1837-1853.

Novitch, B. G., Chen, A. I., & Jessell, T. M. (2001). Coordinate regulation of motor neuron subtype identity and pan-neuronal properties by the bHLH repressor Olig2. *Neuron, 31*(5), 773-789.

Novitch, B. G., Wichterle, H., Jessell, T. M., & Sockanathan, S. (2003). A requirement for retinoic acid-mediated transcriptional activation in ventral neural patterning and motor neuron specification. *Neuron, 40*(1), 81-95.

Pecho-Vrieseling, E., Sigrist, M., Yoshida, Y., Jessell, T. M., & Arber, S. (2009). Specificity of sensory-motor connections encoded by Sema3e-Plxnd1 recognition. *Nature, 459*(7248), 842-846. doi: 10.1038/nature08000

Qiu, K., Lane, M. A., Lee, K. Z., Reier, P. J., & Fuller, D. D. (2010). The phrenic motor nucleus in the adult mouse. *Exp Neurol, 226*(1), 254-258. doi: 10.1016/j.expneurol.2010.08.026

Road, J. D., Ford, T. W., & Kirkwood, P. A. (2013). Connections between expiratory bulbospinal neurons and expiratory motoneurons in thoracic and upper lumbar segments of the spinal cord. *J Neurophysiol, 109*(7), 1837-1851. doi: 10.1152/jn.01008.2012

Rose, D., Larnicol, N., & Duron, B. (1984). An HRP study of the cat's spinal respiratory motoneurones during postnatal development. *Exp Brain Res, 56*(3), 458-467.

Rose, M. F., Ren, J., Ahmad, K. A., Chao, H. T., Klisch, T. J., Flora, A., . . . Zoghbi, H. Y. (2009). Math1 is essential for the development of hindbrain neurons critical for perinatal breathing. *Neuron, 64*(3), 341-354. doi: 10.1016/j.neuron.2009.10.023

Rousso, D. L., Gaber, Z. B., Wellik, D., Morrisey, E. E., & Novitch, B. G. (2008). Coordinated actions of the forkhead protein Foxp1 and Hox proteins in the columnar organization of spinal motor neurons. *Neuron, 59*(2), 226-240. doi: 10.1016/j.neuron.2008.06.025

Rousso, D. L., Pearson, C. A., Gaber, Z. B., Miquelajauregui, A., Li, S., Portera-Cailliau, C., . . . Novitch, B. G. (2012). Foxp-mediated suppression of N-cadherin regulates neuroepithelial character and progenitor maintenance in the CNS. *Neuron, 74*(2), 314-330. doi: 10.1016/j.neuron.2012.02.024

Sanes, J. R., & Lichtman, J. W. (2001). Induction, assembly, maturation and maintenance of a postsynaptic apparatus. *Nat Rev Neurosci, 2*(11), 791-805. doi: 10.1038/35097557

Sanes, J. R., & Yamagata, M. (2009). Many paths to synaptic specificity. *Annu Rev Cell Dev Biol, 25*, 161-195. doi: 10.1146/annurev.cellbio.24.110707.175402

Smith, J. C., Ellenberger, H. H., Ballanyi, K., Richter, D. W., & Feldman, J. L. (1991). Pre-Botzinger complex: a brainstem region that may generate respiratory rhythm in mammals. *Science, 254*(5032), 726-729.

Spyer, K. M., & Gourine, A. V. (2009). Chemosensory pathways in the brainstem controlling cardiorespiratory activity. *Philos Trans R Soc Lond B Biol Sci, 364*(1529), 2603-2610. doi: 10.1098/rstb.2009.0082

Stornetta, R. L. (2009). Neurochemistry of bulbospinal presympathetic neurons of the medulla oblongata. *J Chem Neuroanat, 38*(3), 222-230. doi: 10.1016/j.jchemneu.2009.07.005

Stornetta, R. L., Schreihofer, A. M., Pelaez, N. M., Sevigny, C. P., & Guyenet, P. G. (2001). Preproenkephalin mRNA is expressed by C1 and non-C1 barosensitive bulbospinal neurons in the rostral ventrolateral medulla of the rat. *J Comp Neurol, 435*(1), 111-126.

Stornetta, R. L., Sevigny, C. P., & Guyenet, P. G. (2003). Inspiratory augmenting bulbospinal neurons express both glutamatergic and enkephalinergic phenotypes. *J Comp Neurol, 455*(1), 113-124. doi: 10.1002/cne.10486

Surmeli, G., Akay, T., Ippolito, G. C., Tucker, P. W., & Jessell, T. M. (2011). Patterns of spinal sensory-motor connectivity prescribed by a dorsoventral positional template. *Cell, 147*(3), 653-665. doi: 10.1016/j.cell.2011.10.012

Swift, T. R. (1994). The breathing arm. *Muscle Nerve, 17*(1), 125-129. doi: 10.1002/mus.880170122

Tripodi, M., Stepien, A. E., & Arber, S. (2011). Motor antagonism exposed by spatial segregation and timing of neurogenesis. *Nature, 479*(7371), 61-66. doi: 10.1038/nature10538

Tupal, S., Huang, W. H., Picardo, M. C., Ling, G. Y., Del Negro, C. A., Zoghbi, H. Y., & Gray, P. A. (2014). Atoh1-dependent rhombic lip neurons are required for temporal delay between independent respiratory oscillators in embryonic mice. *Elife, 3*, e02265. doi: 10.7554/eLife.02265

Vrieseling, E., & Arber, S. (2006). Target-induced transcriptional control of dendritic patterning and connectivity in motor neurons by the ETS gene Pea3. *Cell, 127*(7), 1439-1452. doi: 10.1016/j.cell.2006.10.042

Wichterle, H., Lieberam, I., Porter, J. A., & Jessell, T. M. (2002). Directed differentiation of embryonic stem cells into motor neurons. *Cell, 110*(3), 385-397.

Yates, B. J., Smail, J. A., Stocker, S. D., & Card, J. P. (1999). Transneuronal tracing of neural pathways controlling activity of diaphragm motoneurons in the ferret. *Neuroscience, 90*(4), 1501-1513.

Zhang, Y., Li, S., Yuan, L., Tian, Y., Weidenfeld, J., Yang, J., . . . Morrisey, E. E. (2010). Foxp1 coordinates cardiomyocyte proliferation through both cell-autonomous and nonautonomous mechanisms. *Genes Dev, 24*(16), 1746-1757. doi: 10.1101/gad.1929210

Zlatic, M., Li, F., Strigini, M., Grueber, W., & Bate, M. (2009). Positional cues in the Drosophila nerve cord: semaphorins pattern the dorso-ventral axis. *PLoS Biol, 7*(6), e1000135. doi: 10.1371/journal.pbio.1000135

CHAPTER FOUR – Essential roles of Pou3f1 in phrenic and thoracic respiratory motor circuit maintenance

Terrestrial organisms require respiration to sustain life. Recent attention has come to a POU domain transcription factor, Pou3f1, to be a possible master regulator in respiratory motor neuron development. Pou3f1 is selectively expressed in phrenic motor neurons and the medial-half of intercostal motor neurons. When Pou3f1 is removed, the phrenic motor neuron population and the intercostal motor neuron population are generated in normal numbers. In addition, the removal of Pou3f1 did not alter the expression of other phrenic-specific molecules that were hypothesized to be downstream of Pou3f1. Preliminary electrophysiological recording showed that Pou3f1 mutant pups may exhibit some defects in respiratory activity through the ventral roots. In addition, Pou3f1 mutant diaphragms show partial innervation of the sternal portion of the diaphragm. In the thoracic spinal cord, misexpression of Pou3f1 led to a concomitant decrease of the lateral thoracic RMC motor pool identified by Bcl11b. The converse experiment revealed that Bcl11b can suppress the expression of Pou3f1 in the medial thoracic RMC motor pool as well. I conclude that Pou3f1 is involved in multiple aspects of respiratory motor circuit development of axon growth. Future studies should delineate the role of Pou3f1 in supraspinal oscillating microcircuits and axonal growth.

INTRODUCTION

Respiratory motor column (RMC) motor neurons (MNs) innervate the body wall muscles throughout the rostrocaudal axis (Kanning, Kaplan, & Henderson, 2010). These muscles include but are not limited to the diaphragm, cutaneous maximus, intercostal, and abdominal muscles (Chapter 3). The RMC motor pools have been attributed with molecular markers that are selectively but not uniquely expressed. For example, POU Class 3 Homeobox 1 transcription factor (Pou3f1; also known as Oct6 or Tst-1) was shown to be expressed in phrenic MNs, ETS translocation variant 1 (Etv1) and Pou3f1 in subsets of intercostal MNs, and ETS translocation variant 4 (Etv4) in cutaneous maximus MNs (Dasen, De Camilli, Wang, Tucker, & Jessell, 2008; Livet et al., 2002; Rousso, Gaber, Wellik, Morrisey, & Novitch, 2008). However, there is still a considerable gap of understanding of their role in RMC MN development and maturation.

The phrenic MNs provide efferent output to the diaphragm, which is the only muscle responsible for inspiration at rest. Phrenic MNs are located at C3-6 spinal levels in the mouse in a very tight nuclei of neurons (Qiu, Lane, Lee, Reier, & Fuller, 2010). Before entering the brachial plexus, the phrenic motor axons from C3-6 spinal levels join together and descend down to the ribcage and the diaphragm medially as shown in **Fig 4-1A** (Laskowski & Sanes, 1987). Once the phrenic motor axons contact developing diaphragmatic myotubes, at least three diaphragmatic branches emerge from the point of contact as summarized in **Fig 4-1B** (Mantilla & Sieck, 2008a). The final innervation of the diaphragm results in a topographic organization of the diaphragm as summarized in **Fig 4-1B** (Laskowski & Sanes, 1987). Pou3f1 uniquely identifies the phrenic motor neurons at mid-cervical levels, although at caudal cervical levels forearm flexor-

innervating MNs also express Pou3f1. Interestingly, homozygous removal of Pou3f1 in mice results in neonatal death and slow respiratory rate in rare survivors (Bermingham et al., 1996). Conditional removal of Pou3f1 from Schwann cells were demonstrated to be fully viable, which suggests that the respiratory insufficiency comes from defects other than from peripheral neural conduction (Ghazvini et al., 2002). Furthermore, forced overexpression of Pou3f1 in in differentiating MNs from embryonic stem cells resulted in up-regulation of other related molecules suggesting that Pou3f1 may be sufficient for phrenic motor identity (Machado et al., 2014). Thus, in this chapter I decided to explore the possible defect in the respiratory motor circuitry in the Pou3f1 mice.

Pou3f1 was shown to be important for proper maturation and transition of promyelin cells to myelinating cells during axonal wrapping (Bermingham et al., 1996; Jaegle et al., 1996). Confirming this hypothesis, promyelinating Schwann cells were shown to express the highest amount of Pou3f1 both in developing and regenerating nerves (Arroyo, Bermingham, Rosenfeld, & Scherer, 1998). The absence of Pou3f1 results in delayed expression of Krox20 (Ghazvini et al., 2002). The up-regulation of Pou3f1 follows and requires the NFκB signaling pathway, although the necessity of NFκB signaling of Pou3f1 up-regulation has been disputed (Morton et al., 2013; Nickols, Valentine, Kanwal, & Carter, 2003). Overexpression of Pou3f2 (a.k.a Brn2) in the Pou3f1 mutant sciatic nerve showed a partial rescue showing that the two transcription factors might be functionally redundant (Jaegle et al., 2003).

In this chapter, I asked whether Pou3f1 is necessary for proper maturation and innervation of the diaphragm. Also, I ask whether Pou3f1 overexpression can redirect MNs from other cell fates to the respiratory phenotype *in vivo.* I have evidence that the

removal of Pou3f1 in the developing mouse spinal cord results in maintained markers of phrenic MN development, but the sternal branch of the diaphragm stalls before reaching the target. However, many alternate markers of phrenic MNs remain with the removal of Pou3f1, which suggest that Pou3f1 is required for specific stages of maturation rather than during birth or differentiation of MNs. In the thoracic spinal cord, Pou3f1 and Bcl11b exhibited a mutually repressive relationship as when one was misexpressed the other displayed reduced expression levels. Thus, Pou3f1 may be sufficient for the inspiratory motor phenotype but not necessary only for certain aspects of motor innervation defects.

MATERIALS AND METHODS

Animal preparation

All animal protocols were approved by the Animal Research Committee of the University of California, Los Angeles. A Pou3f1$^{Lacz/+}$ mouse line was generated and generously shared by Dies Meijer (Jaegle et al., 1996). The mouse colony was maintained with Pou3f1$^{Lacz/+}$ heterozygote mice with food and water *ad libitum*. The mouse colony also included some Pou3f1$^{Lacz/+}$ heterozygote mice crossed with an Hb9::GFP MN-reporter mouse strain to visualize the axons (Wichterle, Lieberam, Porter, & Jessell, 2002). Although the data is not shown, when possible neuron-specific class III beta-tubulin was co-localized with GFP in the diaphragm, which was always shown in absolute co-localization. Mating cages were checked every morning for mating plugs, in which that day was denoted as e0.5.

In ovo electroporation

Fertilized eggs were purchased from McIntyre Farms (Lakeside, CA) and stored at 55°F until the desired time. Eggs were put in the egg incubator, which was denoted as time 0. The eggs were removed from the incubator at day 2.5. A small window was created for the experimental set up. Plasmids were diluted to the concentration of 0.5 µg/µL for Hb9(3.6kb)::Cre and 1.5 µg/µL for CMV::flox-stop-flox mcs, Pou3f1 or Bcl11b followed by IRES-EGFP (this was denoted as pMN). The plasmid mix was subsequently electroporated into the chick spinal cord. CMF solution and penicillin/streptomycin mixture was dropped on top of the embryos to provide moisture and suppress antibiotic growth.

Plasmid construction

Most of the plasmids were constructed using the three-way Tol2 transposase system (Invitrogen). The Hb9 promoter fragment was provided by Fred Gage. The Hb9 promoter was inserted into the p5E vector by Ken Yamauchi. The flox-stop-flox insert (termination sequence flanked by loxP sequences) driven by cytomegalovirus ubiquitous promoter was removed from an Ai9 construct (Invitrogen) and placed into the p5E-mcs sequence. The IRES-eGFP was cloned into the p3E-mcs sequence. The chicken version of Pou3f1 was generously provided by Dies Meijer. The mouse version of Bcl11b was cloned using the primers targeting the beginning and the end of coding sequence.

Tissue processing

Pregnant dams at defined ages were collected at noon and fixed in 4% paraformaldehyde (PFA) in phosphate buffered saline (PBS) at 4-degrees. The embryos were washed in PBS three times. The embryos were then cryoprotected in 30% sucrose overnight, and the tissues were subsequently mounted in OCT after removing as much sucrose as possible (Tissue tek). The mounted blocks were stored at -80°C in sealed plastic bags to resist ice crystals. The mounted blocks were eventually sectioned at thicknesses appropriate for different ages.

Immunohistochemistry

After sectioning of the mounted blocks, the slides were dried and blocked in antibody blocking solution for one hour (0.1% Triton-X, 1% heat-inactivated horse

serum, and 0.05% sodium azide in PBS). The slides were incubated with the primary antibodies in the humidifying chamber overnight. The following day, the slides were washed with 0.1% Triton-X in PBS (PBS-T0.1) three times, five minutes each. The slides were then incubated with secondary antibodies that matched the species of antibody origin for two hours. After the incubation, the slides were washed three times with PBS-T five minutes each, and mounted with ProLong Gold Antifade Mountant (Invitrogen).

The antibodies used in this study include guinea pig Foxp1 antibody (Rousso et al., 2008), rabbit Pou3f1 (generous gift from Dies Meijer), goat Pou3f1 (Santa Cruz Biotechnology, Inc.), and goat Islet-1 (R&D Systems). Alpha-bungarotoxin conjugated to Alexa647 (αBTX-A647; Invitrogen) was used to label the end plate of the diaphragm. The secondary antibodies used in this study were purchased from Jackson Laboratories.

In situ hybridization

To visualize the location of the mRNA transcripts for certain genes, I generated anti-sense RNA probes to perform *in situ* hybridization experiments. Briefly, primers were designed to surround a 400-bp segment of the transcript of interest. The 400-bp segment was amplified by polymerase chain reaction with a GoTaq 2X mix. Subsequently, the probe was synthesized with this cDNA using T3 RNA polymerase (Invitrogen) and DIG-labeling mix.

For the in situ hybridization, tissue slides were post-fixed with 4% PFA, washed with PBS, and then acetylated with acetyl acetate and triethanolamine mix. The slides were then washed with PBS. The slides were covered with hybridization buffer and

placed inside the humidifying chamber at 68°C overnight. The slides underwent rounds of stringent washes. Anti-DIG antibody (Roche) was placed for 80 minutes, and subsequently developed using NBT/BCIP solution (Roche).

Diaphragm whole mount

The diaphragm was dissected as an intact preparation from the ribcage. The diaphragm was fixed and washed with 1% Triton-X in PBS. The diaphragm was incubated in primary antibody overnight, washed with PBS-T three times, and placed in secondary antibodies overnight. The preparation was washed with PBS-T three times. The diaphragm was mounted with ProLong Gold Antifade Mountant (Invitrogen) and dried before imaging.

Confocal microscopy

All images were collected on a Zeiss LSM700 microscope system. Stained slides were imaged as described previously (Adams, Rousso, Umbach, & Novitch, 2015). Diaphragm wholemount preparations were imaged with a 10x objective with z-stack interval recommended by the Zeiss Zen 2012 software (Zeiss). The z-stack confocal images were tiled and stitched using the Zen software as well.

"En bloc" brainstem-spinal cord preparation and recording

We used wild type and mutant neonatal C57BL/6 mice (P0) of either sex for experiments *in vitro*, and the experimenter was blinded to the genotype. The brainstem and spinal cord were dissected out as described previously (Mellen, Janczewski,

Bocchiaro, & Feldman, 2003; Rose et al., 2009; Tupal et al., 2014). Briefly, following deep anesthesia with isoflurane, a complete thoracotomy and coronal transection at the level of the bregma was performed, followed by dorsal laminectomy, and an intracollicular transection. The preparation was then placed ventral side up and the ventral surface of the brain was exposed and the cranial nerves cut. A ventral laminectomy revealed the ventral surface of the cord and ventral spinal nerves. Spinal nerves were visualized and then cut. The spinal cord was severed caudal to T6, and the pons was left attached. The preparation was dissected in artificial cerebrospinal fluid (ACSF) containing (in mM): 124 NaCl, 3 KCl, 1.5 $CaCl_2$, 1 $MgSO_4$, 25 $NaHCO_3$, 0.5 NaH_2PO_4, and 30 D-glucose, equilibrated with 95% O_2 and 5% CO_2 (27°C, pH=7.4).

En bloc preparations were perfused with 27°C ACSF at 4 ml/min in a 0.5 ml chamber mounted rostral side up in a fixed-stage DMLFS (Leica Microsystems, Buffalo Grove, IL, USA) microscope, and were allowed to equilibrate for 30 minutes. Respiratory activity reflecting suprathreshold action potential (AP) firing from populations of spinal motor neurons was simultaneously recorded from spinal nerves (C4, C6, C7, C8) using suction electrodes, amplified with a MultiClamp 700B (Molecular Devices, Sunnyvale, CA, USA) and a Model 1700 differential AC amplifier (A-M Systems, Sequim, WA, USA), filtered at 2–4 kHz, and digitized at 10 kHz. Activity was full-wave rectified and digitally integrated with a Paynter filter with a time constant of 20 ms.

Data analysis and statistics

Digitized data were analyzed off-line using custom procedures written for IgorPro (Wavemetrics, Portland, OR, USA) (Kam, Worrell, Janczewski, Cui, & Feldman,

2013). Semi-automated event detection was executed using custom procedures that used multiple criteria, including slope and amplitude thresholds, to select events automatically, which were then confirmed visually by the experimenter.

Unlike intracellular recordings, suction electrode recordings lack a scale that allows comparisons across experiments, and the value of nerve discharge signals, i.e., measured voltage, varied significantly in absolute value between experiments. Therefore, for comparisons across experiments, the baseline was subtracted and the signal scaled to the maximum peak amplitude in the control condition for each experiment. The amplitude was then measured from the scaled signal. A peak-detection algorithm defined event amplitude as the difference between peak and baseline. The period was calculated as the time between the peaks of two consecutive events.

Data are represented as mean ± standard deviation (SD). Statistical significance was uniformly set at a minimum of $p<0.05$. For statistical comparisons of more than two groups, an ANOVA was first performed. In most cases, a two-way repeated measures ANOVA was used for comparisons of various parameters in different conditions and for making comparisons across different events. If the null hypothesis (equal means) was rejected, post-hoc paired t-tests were then used for pairwise comparisons of interest. Individual p-values are reported, but Holm-Bonferroni analysis for multiple comparisons was conducted to correct for interactions between the multiple groups. For one-way and two-way ANOVAs, post-hoc significance for pairwise comparisons was analyzed using Tukey-Kramer analysis.

RESULTS

Pou3f1 is expressed in the phrenic motor neurons and medial intercostal motor neurons

The expression pattern of Pou3f1 was assessed in the developing spinal cord of the mouse and the chick. Pou3f1 is expressed in the diaphragm-projecting phrenic MNs at the brachial level as previously described **(Fig 4-2A)** (Bermingham et al., 1996; Machado et al., 2014; Rousso et al., 2008). Pou3f1 is also expressed in human fetal spinal cord showing that the expression of Pou3f1 is conserved between mouse and human **(Fig 4-2B)**.

In the thoracic spinal cord, Pou3f1 is also expressed by a subpopulation of the thoracic hypaxial MNs that innervate the intercostal muscles (Chapter 3). Other markers including Etv1, Nr2f2, and a nuclear receptor family-related protein Bcl11b is also found in the thoracic MNs (Chapter 3). There is a general medial-lateral segregation of these motor neurons as described before (Chapter 3). Avian species including chickens lack a diaphragm and use different mechanics of breathing involving air sacs. Nevertheless, the avian thoracic spinal cord also express Pou3f1 at the thoracic level, and this expression is conserved between mouse and chick. In both species, there are prominent dorsal and ventral branches of the intercostal nerves, which can be retrogradely labeled. The Pou3f1+ intercostal MNs exclusively projects to the limbs compared to the other branch as shown in Figure 2A, whereas the other branch innervates the internal intercostal branch (Chapter 3).

Pou3f1 is not required for generation and initial projection of phrenic MNs

In previous studies and our own microarray experiment, multiple molecules have been identified in the phrenic motor neurons other than Pou3f1 (Chapter 3) (Machado et al., 2014). Most notably, the phrenic MN markers were upregulated by forced expression of Pou3f1 in motor neurons differentiated from embryonic stem cells. Thus, we hypothesized that Pou3f1 may also be necessary for the alternate marker expression. We first looked at markers such as Pleiotrophin (Ptn), Del1 and Pappa. Contrary to our initial expectation, I found that Ptn is expressed in the phrenic MNs at e12.5 even in the absence of Pou3f1 **(Fig 4-2D, 2G)**. The other markers Del1 and Pappa were also expressed in phrenic MNs at e12.5 in the absence of Pou3f1 (**Fig 4-2E, 2H**; data not shown for Pappa). In addition, the number of phrenic MNs and intercostal MNs did not change with the removal of Pouf1 **(Fig 4-2I, 2J, 2K)**. Thus, I conclude that Pou3f1 is not necessary for up-regulation of these phrenic MN markers at e12.5.

Pou3f1 is necessary for proper growth of the primary phrenic nerve branch

Next, I looked at the phrenic nerve branches by diaphragm wholemount of Pou3f1 mutants. MNs reach their muscle target by e13.5 (rat; ~e11.5 mouse), and begin to form contact with the differentiating muscle fibers (Greer, Allan, Martin-Caraballo, & Lemke, 1999; Mantilla & Sieck, 2008a). The phrenic nerve reaches the diaphragm bilaterally at the center of the two hemidiaphragms, then forms three branches dorsally, ventrally and medially. When the costal branch was assessed at e16.5 and e18.5, the costal branch of the diaphragm was much shorter in Pou3f1 mutants **(Fig 4-3A-3E)**. The differences in length were greatest at e18.5, where it was 2.595 mm **(Fig 4-3F)** ($p = 3.84E-5$, *Student's t*

test). Comparing the lengths of sternal branch between Pou3f1$^{Lacz/Lacz}$ between e16.5 and e18.5 diaphragm, the most growth of diaphragm length supports the idea that the branching defect is due to slow growth of these axons rather than retraction of the axons.

It is still questionable whether this phrenic nerve defect would be sufficient for the immediate death of the neonatal homozygous mutants. Indeed, through my study, I unexpectedly encountered two survivors that were homozygous mutants. Both pups were small, exhibited extreme tremor, and died prior to P15. Unfortunately, any respiratory parameters or recording was not performed due to their sudden death at P15. It is yet unclear what allows the escapers to survive beyond usual time of death.

Misexpression of Pou3f1 can suppress markers of expiratory RMC MNs

In the thoracic RMC, at least three different MN populations exist that are organized into respiratory motor pools when retrogradely labeled from intercostal branches (Chapter 3). Two predominant motor pools are Pou3f+ RMC motor pool and Bcl11b+ RMC motor pool. I was interested in whether misexpression of Pou3f1 or Bcl11b might influence the cell fate specification. First I misexpressed the control vector pMN-mcs **(Fig 4-4A, 4B)**, experimental vector pMN-cPou3f1 **(Fig 4-4C, 4D)**, and another experimental vector Bcl11b **(Fig 4-4E, 4F)**. Then I assessed the impact of misexpression of Pou3f1 on Bcl11b expression. The number of Bcl11b+GFP+ MNs were counted and normalized by the number of MNs. The pMN-cPou3f1 electroporation decreased 12.88% of proportion of Bcl11b+GFP+ MNs (**Fig 4-4G**; $p = 0.0128$; *Student's t-test*). The un-electroporated Bcl11b+ MNs did not change in proportion (**Fig 4-4G**; $p = 0.5614$; *Student's t-test*).

To study the reciprocal repression by the two vectors, pMN-mBcl11b was electroporated into the chick spinal cord. When quantifying the number of Pou3f1+ MNs, the experimental condition with pMN-mBcl11b construct had 4.595% reduced proportion of Pou3f1+ MNs compared to control (**Fig 4-4H**; p = 0.0377; *Student's t-test*). The un-electroporated population also did not have any significant difference (**Fig 4-4H**; p = 7097; *Student's t-test*).

En bloc recording of cervical and thoracic ventral motor roots

The diaphragm branching phenotype was significant and severe, it did not seem intuitive to us that some Pou3f1$^{Lacz/Lacz}$ did not even take the first breath upon birth. Thus, we utilized the brain stem-spinal cord "en bloc" preparation to obtain ventral root recording of C4 and T2 nerves in wild type and Pou3f1$^{Lacz/Lacz}$ e18.5 embryos. In the control preparations, we noticed robust activity in C4 and T2 ventral roots **(Fig 4-5A)**. However, the same ventral root recording in Pou3f1$^{Lacz/Lacz}$ mice showed irregular burst frequency and amplitude **(Fig 4-5B)**. Thus, neural defect that arise from defects in Pou3f1 mutation is not likely to be due to the diaphragmatic defect alone, but also supraspinal respiratory areas could be involved in the respiratory insufficiency phenotype of Pou3f1$^{Lacz/Lacz}$.

DISCUSSION

Respiratory MN cell fate determination does not require Pou3f1

MN cell fate determination and axon trajectory requires a balance of multiple secreted and membrane-bound factors to influence cellular identity during development. Removal of critical proteins such as Hox5 resulted in severe defects in axon branching (Philippidou, Walsh, Aubin, Jeannotte, & Dasen, 2012). Furthermore, defects in proper axon guidance to the diaphragm by removal of Unc5C results in a reduced or absent phrenic nerve to the diaphragm (Burgess, Jucius, & Ackerman, 2006). In this study, I showed that removal of Pou3f1 neither affects the genesis of phrenic and intercostal MNs nor fails to upregulate alternate phrenic markers. However, we observed delayed phrenic motor axon growth to the distal-most sternal diaphragm that can be seen as early as e16.5 **(Fig 4-4A)**.

The molecular signaling cascade that confers respiratory MN cell fate is not yet clear. Machado and colleagues showed that Notch influence from V2 interneuron population is sufficient for up-regulation of Pou3f1 (Machado et al., 2014). The Wnt signaling pathway was also studied for its influence on segmental cell fate determination between MMC and HMC (Agalliu, Takada, Agalliu, McMahon, & Jessell, 2009). It may be possible that HMC is a ground-state that MNs proceed to develop in the absence of other cell non-autonomous influence for cell fate commitment (Dasen & Jessell, 2009). Future studies should be aimed at elucidating the roles of these signaling pathways on respiratory cell fate determinant.

Pou3f1 is required for proper phrenic nerve branching outgrowth

The phrenic nerve phenotype in Pou3f1 mutants resemble that of Hox5 mutants and Unc5C mutants. Hox5 alters the segmental identity of cervical levels in which phrenic MNs are born, therefore influencing downstream molecules important for phrenic nerve arborization (Philippidou et al., 2012). Removal of HoxC9 results in extension of LMC down to the thoracic spinal cord (Jung et al., 2010). Thus, Hox molecules play a critical role that establishes a context for proper MN development. The nature of Unc5C mutants are less clear. The Unc5C phenotype is observed in a stochastic and strain-dependent manner (Burgess et al., 2006). Because the Unc5C phenotype was observed in a C57/B6 background, Pou3f1 phenotype might be also more severe in this background. The underlying nature of the Pou3f1 mutant is likely due to an inability to respond to various trophic factors expressed in the developing diaphragm myotubes. The diaphragm myotubes and Schwann cells are known to express a variety of trophic factors including neurotrophins and adhesion molecules that might be critical for innervation (Mantilla & Sieck, 2008b).

In addition, the diaphragm is innervated by the phrenic MNs in a topographical manner, where the ventral-most diaphragm is innervated by rostral-most phrenic MNs (Laskowski & Sanes, 1987). This study did not examine the number of phrenic MNs at later stages in development, and the first place that should be assessed should be the rostral-most spinal cord **(Fig 4-1A)**. As the alternate phrenic markers such as Ptn and Del1 are expressed through later in development, any changes of levels of expression of these markers by qPCR or RNA-sequencing techniques may shed light in understanding the diaphragm phenotype of Pou3f1 mutant embryos.

Pou3f1 and Bcl11b co-repress each other in the developing thoracic spinal cord

In this study, I demonstrated that the misexpression of Pou3f1 resulted in a reduced number of Bcl11b+ MNs and vice versa. This is a surprising finding because the thoracic spinal cord of Pou3f1 mutant or Bcl11b mutant embryos do not show altered cell fates (i.e. Bcl11b+ MNs do not increase in Pou3f1 mutant and vice versa; data not shown). It is possible that other agents such as Pou3f1 and Bcl11b could play a role in consolidating MN identity. Indeed, Pou3f1 and Bcl11b are found in the LMC MNS, sometimes co-localizing in certain motor pools.

The cross-suppressive ability may be a context dependent phenomenon. It is important to know that the breathing mechanics are slightly different in avian species, where the animals use air sacs for active inspiration and active expiration. Hypaxial MNs have been also been described in the chick species where they are positioned more laterally compared to epaxial MNs of the medial motor column (MMC) (Gutman, Ajmera, & Hollyday, 1993). Although intercostal muscle innervation is shared between chick and the mouse, the premotor networks innervating these MNs are likely very different. Thus, species-specific features should be expected when analyzing the roles of Pou3f1 and Bcl11b.

There are other regions of the central nervous system that express Pou3f1 and Bcl11b. Bcl11b (a.k.a. Ctip2) is expressed in corticothalamic neurons of layer V, and Pou3f1 is expressed in subcerebral-projecting neurons of layer V (Molyneaux, Arlotta, Menezes, & Macklis, 2007). It is already known that Bcl11b mutants suffer from defects in corticospinal tract formation (Arlotta et al., 2005). Future studies should assess

whether Pou3f1+ or Bcl11b+ cortical neurons make up circuitry with Pou3f1+ or Bcl11b+ MNs as the final output.

CONCLUSION

Pou3f1 is expressed in human and mouse phrenic motor neurons during development as well as the intercostal motor neurons of the chick and the mouse. Removal of Pou3f1 does not alter the early cell fate specification. However, Pou3f1 plays a critical role in proper innervation of the distal-most areas of the diaphragm. In addition to the defects in innervation, the ventral root activity show irregular rhythm that suggest dysregulation of supraspinal respiratory areas. Thoracic respiratory MNs exhibit a co-repressive behavior where misexpression of Pou3f1 results in lower levels of Bcl11b and Bcl11b suppressing Pou3f1 when Bcl11b is misexpressed. However, other molecules must act upstream of Pou3f1 or Bcl11b as removal of either markers do not show any prominent shift in territories of respiratory motor neurons.

FIGURES

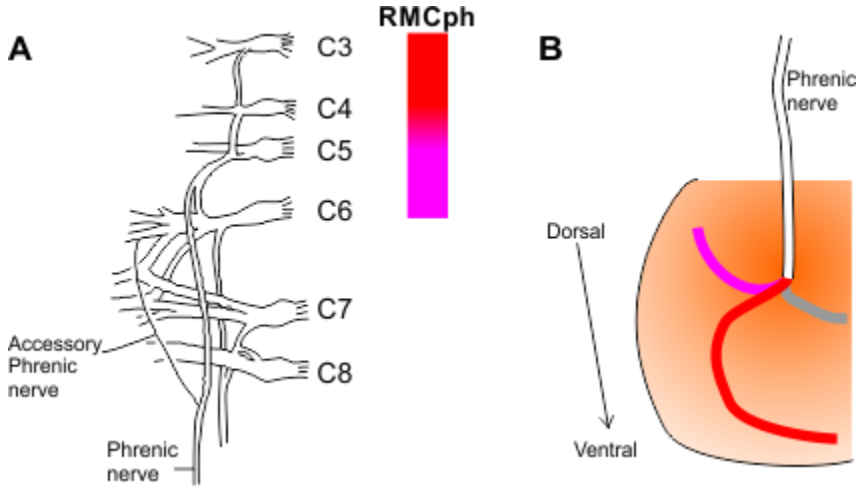

Figure 4-1. Anatomical origins of the phrenic nerve in the mouse

(A) Phrenic nerve originates from C3-6 ventral roots in the mouse and projects down to the primordial diaphragm without intersecting the brachial plexus. Adapted from Laskowski and colleagues (Laskowski & Sanes, 1987).

(B) At the primordial diaphragm, the phrenic nerve branches into three separate branches dorsally, ventrally and medially innervating three separate muscles that make up the diaphragm muscle.

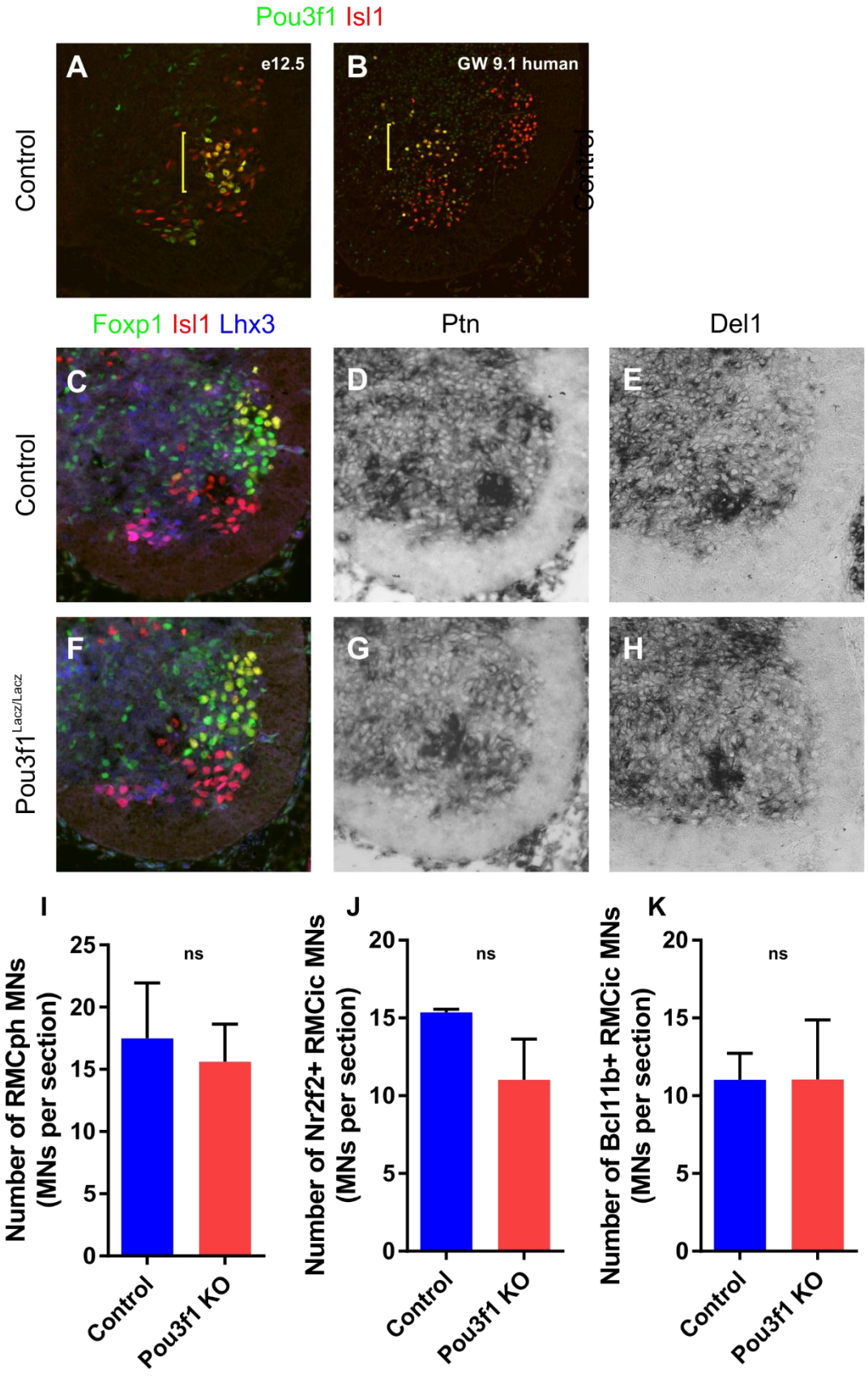
Pou3f1 Isl1
A
e12.5
B
GW 9.1 human
Control
Control
Foxp1 Isl1 Lhx3
Ptn
Del1
C
D
E
Control
F
G
H
Pou3f1Lacz/Lacz
I
J
K
Number of RMCph MNs (MNs per section)
Number of Nr2f2+ RMCic MNs (MNs per section)
Number of Bcl11b+ RMCic MNs (MNs per section)
ns
ns
ns
25
20
15
10
5
0
Control
Pou3f1 KO

Figure 4-2. Expression of the phrenic MN markers in the developing human and mouse spinal cord

(A) Expression of Pou3f1 and Isl1 in the mid-cervical spinal cord of e12.5 mouse embryos.

(B) Expression of POU3F1 and ISL1 in the mid-cervical spinal cord of GW 9.1 human fetus.

Expression of Foxp1, Isl1, and Lhx3 in the mid-cervical spinal cord of e12.5 control (C) and Pouf1$^{Lacz/Lacz}$ (F) mouse embryos.

Expression of Ptn (D, G) and Del1 (E, H) in Control (D, E) and Pouf1$^{Lacz/Lacz}$ (G, H) mouse embryos.

Quantification of phrenic (I), inspiratory RMC (i.e. Nr2f2+; J), expiratory RMC (i.e. Bcl11b; K) of control and Pouf1$^{Lacz/Lacz}$ e12.5 mouse embryos.

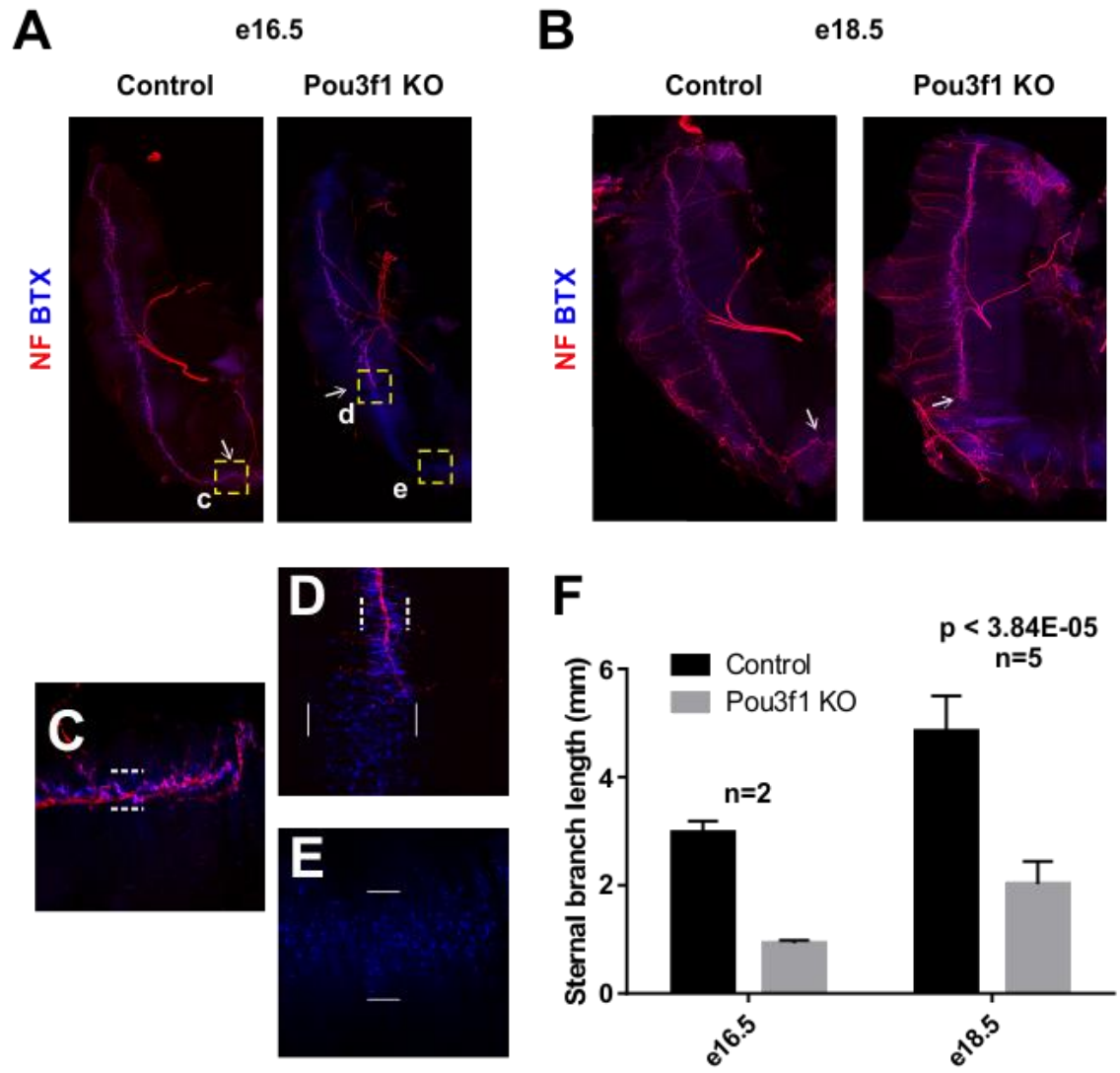

Figure 4-3. Phrenic nerve projection in the diaphragm at late embryonic stages

(A) The projection patterns of diaphragm braches in control and Pouf1$^{Lacz/Lacz}$ e16.5 mouse embryos.

(B) The projection patterns of diaphragm branches in control and Pouf1$^{Lacz/Lacz}$ e18.5 mouse embryo.

Zoomed view of the distal-most sternal branch of the phrenic branch in the control (C) and Pouf1$^{Lacz/Lacz}$ (D).

(E) The areas that were not innervated by the phrenic nerve branch still show presence of motor endplates revealed by alpha-bungarotoxin staining.

(F) Quantification of the sternal branch at e16.5 and e18.5 time point in control and Pouf1$^{Lacz/Lacz}$.

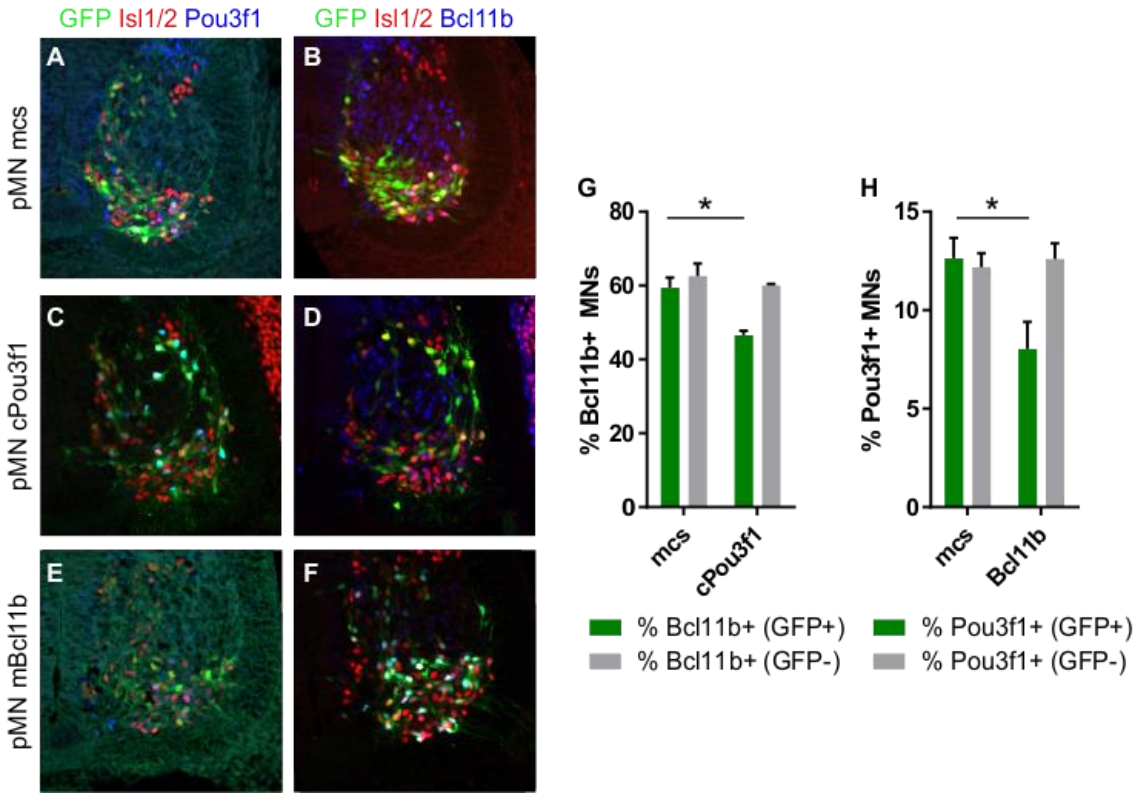

Figure 4-4 Misexpression of POU3F1 and BCL11B have suppressive reaction to one another

Expression of GFP, ISL1/2 and POU3F1 (A) and GFP, ISL1/2 and BCL11B (B) in the thoracic spinal cord of e5.5 chick embryo that was electroporated with pMN-mcs. Expression of GFP, ISL1/2 and POU3F1 (C) and GFP, ISL1/2 and BCL11B (D) in the thoracic spinal cord of e5.5 chick embryo that was electroporated with pMN-POU3F1. Expression of GFP, ISL1/2 and POU3F1 (E) and GFP, ISL1/2 and Bcl11b/BCL11B (F) in the thoracic spinal cord of e5.5 chick embryo that was electroporated with pMN-Bcl11b.

(G) Quantification of BCL11B/Bcl11b+ MNs when pMN-POU3F1 was electroporated.

(H) Quantification of POU3F1+ MNs when pMN-Bcl11b was electroporated.

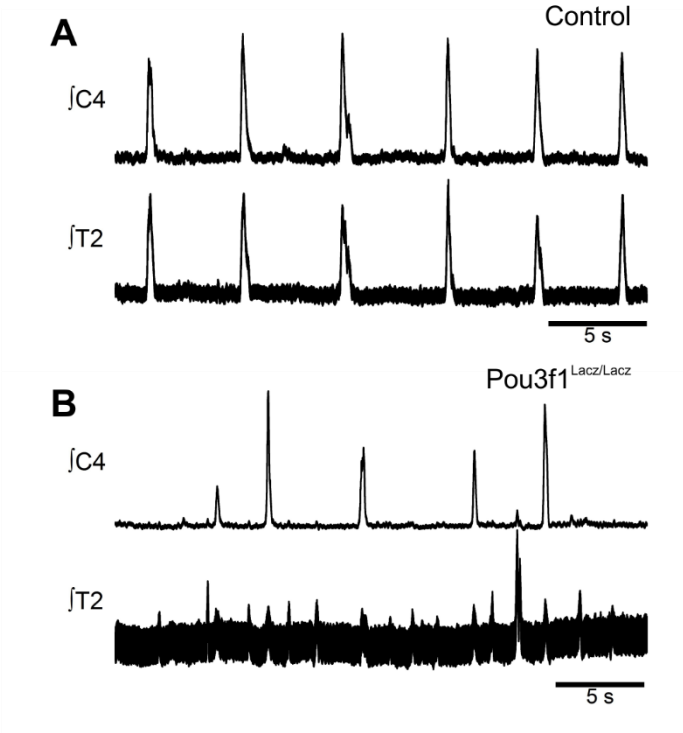

Figure 4-5. "En bloc" recording of C4 and T2 ventral roots of control and Pou3f1$^{Lacz/Lacz}$ e18.5 mouse embryos

(A) Integrated C4 and T2 nerve activity from an e18.5 wild type mouse brainstem-spinal cord ("en bloc") preparation, showing rhythmic inspiratory bursts.

(B) Integrated C4 and T2 nerve activity from an e18.5 Pou3f1 -/- mouse brainstem-spinal cord ("en bloc") preparation with irregular burst frequency and amplitude.

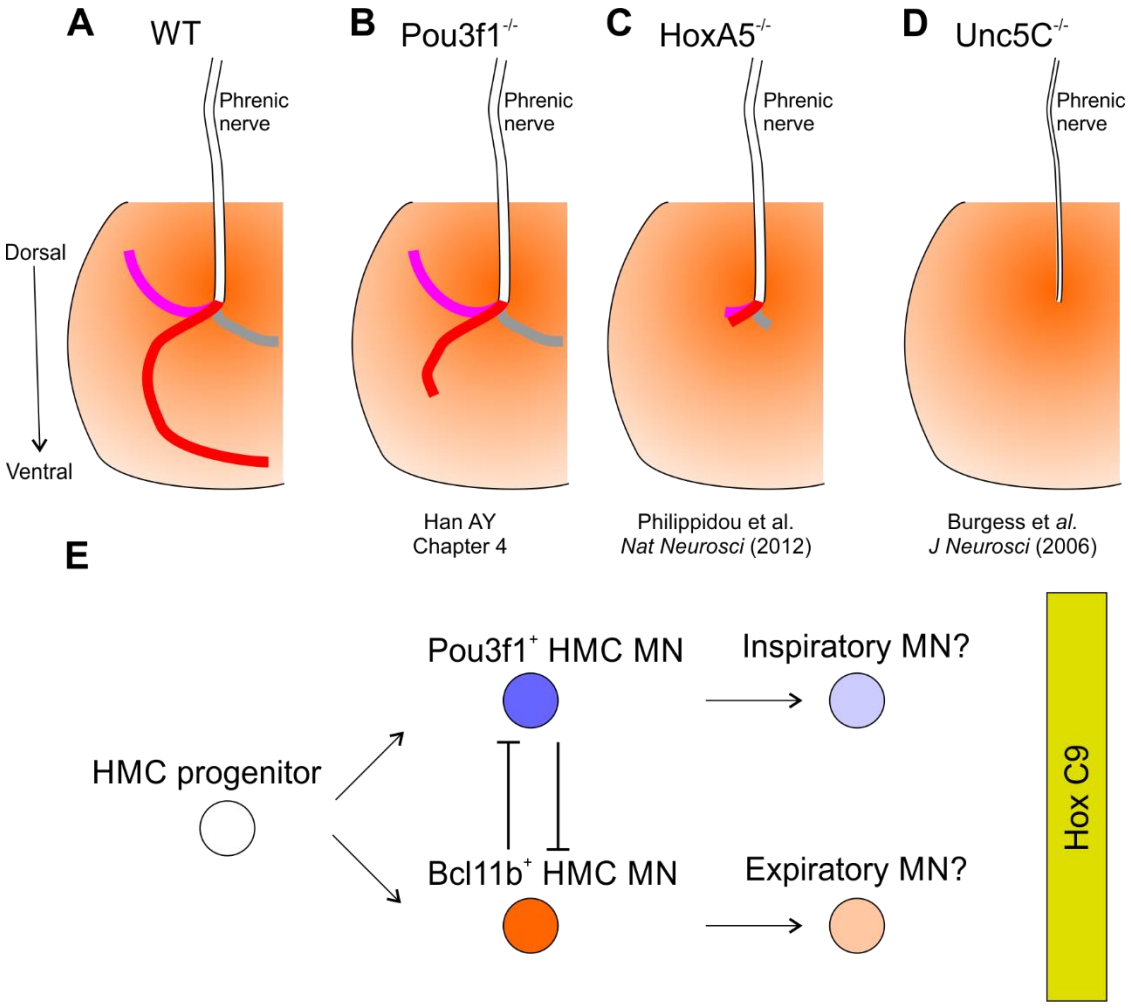

Figure 4-6 Model of the different roles molecules critical for diaphragm innervation

(A) Illustration of the normal anatomy of the phrenic nerve branching.

(B) Summary of the sternal branch defect seen in Pou3f1 mutant mouse embryos.

(C) Summary of the general phrenic branch defect seen in Hox5 mutant mouse embryos.

(D) Summary of the phrenic nerve projection defect of Unc5C mutant mouse embryos.

(E) Model of Pou3f1-Bcl11b cross-repression in the thoracic HMC MNs that may consolidate their identity into inspiratory vs. expiratory MNs.

REFERENCES

Adams, K. L., Rousso, D. L., Umbach, J. A., & Novitch, B. G. (2015). Foxp1-mediated programming of limb-innervating motor neurons from mouse and human embryonic stem cells. *Nat Commun, 6*, 6778. doi: 10.1038/ncomms7778

Agalliu, D., Takada, S., Agalliu, I., McMahon, A. P., & Jessell, T. M. (2009). Motor neurons with axial muscle projections specified by Wnt4/5 signaling. *Neuron, 61*(5), 708-720. doi: 10.1016/j.neuron.2008.12.026

Arlotta, P., Molyneaux, B. J., Chen, J., Inoue, J., Kominami, R., & Macklis, J. D. (2005). Neuronal subtype-specific genes that control corticospinal motor neuron development in vivo. *Neuron, 45*(2), 207-221. doi: 10.1016/j.neuron.2004.12.036

Arroyo, E. J., Bermingham, J. R., Jr., Rosenfeld, M. G., & Scherer, S. S. (1998). Promyelinating Schwann cells express Tst-1/SCIP/Oct-6. *J Neurosci, 18*(19), 7891-7902.

Bermingham, J. R., Jr., Scherer, S. S., O'Connell, S., Arroyo, E., Kalla, K. A., Powell, F. L., & Rosenfeld, M. G. (1996). Tst-1/Oct-6/SCIP regulates a unique step in peripheral myelination and is required for normal respiration. *Genes Dev, 10*(14), 1751-1762.

Burgess, R. W., Jucius, T. J., & Ackerman, S. L. (2006). Motor axon guidance of the mammalian trochlear and phrenic nerves: dependence on the netrin receptor Unc5c and modifier loci. *J Neurosci, 26*(21), 5756-5766. doi: 10.1523/jneurosci.0736-06.2006

Dasen, J. S., De Camilli, A., Wang, B., Tucker, P. W., & Jessell, T. M. (2008). Hox repertoires for motor neuron diversity and connectivity gated by a single accessory factor, FoxP1. *Cell, 134*(2), 304-316. doi: 10.1016/j.cell.2008.06.019

Dasen, J. S., & Jessell, T. M. (2009). Hox networks and the origins of motor neuron diversity. *Curr Top Dev Biol, 88*, 169-200. doi: 10.1016/s0070-2153(09)88006-x

Ghazvini, M., Mandemakers, W., Jaegle, M., Piirsoo, M., Driegen, S., Koutsourakis, M., . . . Meijer, D. (2002). A cell type-specific allele of the POU gene Oct-6 reveals Schwann cell autonomous function in nerve development and regeneration. *EMBO J, 21*(17), 4612-4620.

Greer, J. J., Allan, D. W., Martin-Caraballo, M., & Lemke, R. P. (1999). An overview of phrenic nerve and diaphragm muscle development in the perinatal rat. *J Appl Physiol (1985), 86*(3), 779-786.

Gutman, C. R., Ajmera, M. K., & Hollyday, M. (1993). Organization of motor pools supplying axial muscles in the chicken. *Brain Res, 609*(1-2), 129-136.

Jaegle, M., Ghazvini, M., Mandemakers, W., Piirsoo, M., Driegen, S., Levavasseur, F., . . . Meijer, D. (2003). The POU proteins Brn-2 and Oct-6 share important functions in Schwann cell development. *Genes Dev, 17*(11), 1380-1391. doi: 10.1101/gad.258203

Jaegle, M., Mandemakers, W., Broos, L., Zwart, R., Karis, A., Visser, P., . . . Meijer, D. (1996). The POU factor Oct-6 and Schwann cell differentiation. *Science, 273*(5274), 507-510.

Jung, H., Lacombe, J., Mazzoni, E. O., Liem, K. F., Jr., Grinstein, J., Mahony, S., . . . Dasen, J. S. (2010). Global control of motor neuron topography mediated by the repressive actions of a single hox gene. *Neuron, 67*(5), 781-796. doi: 10.1016/j.neuron.2010.08.008

Kam, K., Worrell, J. W., Janczewski, W. A., Cui, Y., & Feldman, J. L. (2013). Distinct inspiratory rhythm and pattern generating mechanisms in the preBotzinger complex. *J Neurosci, 33*(22), 9235-9245. doi: 10.1523/jneurosci.4143-12.2013

Kanning, K. C., Kaplan, A., & Henderson, C. E. (2010). Motor neuron diversity in development and disease. *Annu Rev Neurosci, 33*, 409-440. doi: 10.1146/annurev.neuro.051508.135722

Laskowski, M. B., & Sanes, J. R. (1987). Topographic mapping of motor pools onto skeletal muscles. *J Neurosci, 7*(1), 252-260.

Livet, J., Sigrist, M., Stroebel, S., De Paola, V., Price, S. R., Henderson, C. E., . . . Arber, S. (2002). ETS gene Pea3 controls the central position and terminal arborization of specific motor neuron pools. *Neuron, 35*(5), 877-892.

Machado, C. B., Kanning, K. C., Kreis, P., Stevenson, D., Crossley, M., Nowak, M., . . . Lieberam, I. (2014). Reconstruction of phrenic neuron identity in embryonic stem cell-derived motor neurons. *Development, 141*(4), 784-794. doi: 10.1242/dev.097188

Mantilla, C. B., & Sieck, G. C. (2008a). Key aspects of phrenic motoneuron and diaphragm muscle development during the perinatal period. *J Appl Physiol (1985), 104*(6), 1818-1827. doi: 10.1152/japplphysiol.01192.2007

Mantilla, C. B., & Sieck, G. C. (2008b). Trophic factor expression in phrenic motor neurons. *Respir Physiol Neurobiol, 164*(1-2), 252-262. doi: 10.1016/j.resp.2008.07.018

Mellen, N. M., Janczewski, W. A., Bocchiaro, C. M., & Feldman, J. L. (2003). Opioid-induced quantal slowing reveals dual networks for respiratory rhythm generation. *Neuron, 37*(5), 821-826.

Molyneaux, B. J., Arlotta, P., Menezes, J. R., & Macklis, J. D. (2007). Neuronal subtype specification in the cerebral cortex. *Nat Rev Neurosci, 8*(6), 427-437. doi: 10.1038/nrn2151

Morton, P. D., Dellarole, A., Theus, M. H., Walters, W. M., Berge, S. S., & Bethea, J. R. (2013). Activation of NF-kappaB in Schwann cells is dispensable for myelination in vivo. *J Neurosci, 33*(24), 9932-9936. doi: 10.1523/jneurosci.2483-12.2013

Nickols, J. C., Valentine, W., Kanwal, S., & Carter, B. D. (2003). Activation of the transcription factor NF-kappaB in Schwann cells is required for peripheral myelin formation. *Nat Neurosci, 6*(2), 161-167. doi: 10.1038/nn995

Philippidou, P., Walsh, C. M., Aubin, J., Jeannotte, L., & Dasen, J. S. (2012). Sustained Hox5 gene activity is required for respiratory motor neuron development. *Nat Neurosci, 15*(12), 1636-1644. doi: 10.1038/nn.3242

Qiu, K., Lane, M. A., Lee, K. Z., Reier, P. J., & Fuller, D. D. (2010). The phrenic motor nucleus in the adult mouse. *Exp Neurol, 226*(1), 254-258. doi: 10.1016/j.expneurol.2010.08.026

Rose, M. F., Ren, J., Ahmad, K. A., Chao, H. T., Klisch, T. J., Flora, A., . . . Zoghbi, H. Y. (2009). Math1 is essential for the development of hindbrain neurons critical for perinatal breathing. *Neuron, 64*(3), 341-354. doi: 10.1016/j.neuron.2009.10.023

Rousso, D. L., Gaber, Z. B., Wellik, D., Morrisey, E. E., & Novitch, B. G. (2008). Coordinated actions of the forkhead protein Foxp1 and Hox proteins in the columnar organization of spinal motor neurons. *Neuron, 59*(2), 226-240. doi: 10.1016/j.neuron.2008.06.025

Tupal, S., Huang, W. H., Picardo, M. C., Ling, G. Y., Del Negro, C. A., Zoghbi, H. Y., & Gray, P. A. (2014). Atoh1-dependent rhombic lip neurons are required for temporal delay between independent respiratory oscillators in embryonic mice. *Elife, 3*, e02265. doi: 10.7554/eLife.02265

Wichterle, H., Lieberam, I., Porter, J. A., & Jessell, T. M. (2002). Directed differentiation of embryonic stem cells into motor neurons. *Cell, 110*(3), 385-397.

CHAPTER FIVE – Relevance of respiratory motor circuit development on regenerative medicine

In my dissertation, I explored different aspects of the respiratory motor circuit assembly. In Chapter 2, I assessed the organization of motor pools in respiratory cranial motor nuclei of the brainstem. In Chapter 3, I demonstrated that motor neurons (MNs) of all cervical segments have the ability to provide respiratory output but Foxp1 suppresses this potential. I also identified a number of molecules expressed in the phrenic and other respiratory MNs that might be critical in different stages of MN maturation. In Chapter 4, I studied the anatomical defects resulting from the removal of Pou3f1 during development, which supported the hypothesis that Pou3f1 is required for proper innervation of the diaphragm. In this chapter, the information that I gathered from my dissertation studies is summarized, synthesized, and the remaining questions are discussed.

Cranial motor neuron organization and relevance to communication

One salient observation from Chapter 2 is the conservation of molecules utilized in cell fate determination and motor axon trajectory between cranial MNs and spinal MNs. Although this idea is not new, cranial motor systems have not received much attention compared to the extensive studies done on spinal motor systems. Another key feature of the cranial MNs is their proximity to one another in the brainstem. MNs belonging to a specific motor pool seldom act alone. Groups of homonymous muscles or

muscles of shared function contract together in concert to achieve the desired motor behavior, which are mediated by a number of circuits made up of diverse interneuron populations. Similarly, cranial MNs are activated in sequence or in specific rhythm for feeding, vomiting, breathing, coughing, and vocalization **(Fig 5-1A)**. Indeed, recent investigators of whisking movement proposed the idea that all rhythmic orofacial movement originates from the respiratory rhythm (Kleinfeld, Deschenes, Wang, & Moore, 2014; Moore et al., 2013; Moore, Kleinfeld, & Wang, 2014). Due to this importance of respiratory rhythm and the existence of cardiorespiratory centers in the brainstem, congenital or acquired injury due to stroke or cerebral edema result in extremely high probability of death. The inability to properly execute certain motor behaviors, such as speech or gesture, may also lead to diminished quality of life especially in patients.

Higher vertebrates communicate using sophisticated command of the written and spoken language. The evolution of the faculty of language has been a very controversial topic even today (Bolhuis, Tattersall, Chomsky, & Berwick, 2014; Lieberman, 2015). However, rodents can still serve as a useful model for generation of specific vocalizations for communication. These include separation calls by pups, mating solicitation calls by females, and distress calls (Fischer & Hammerschmidt, 2011; Lahvis, Alleva, & Scattoni, 2011; Scattoni, Crawley, & Ricceri, 2009). Proper vocalization involves coordinated contraction of the muscles of the face, tongue, and the vocal cord with the diaphragm. The somatic locations of the motor neurons that innervate these muscles have been largely characterized by classic retrograde labeling (Ashwell, 1982; McClung & Goldberg, 2000). However, in contrast with the spinal cord, the molecular organization of

the cranial MNs are now receiving more attention (Yoshikawa et al., 2015). In addition, the exact premotor circuitry that underlie the sophisticated vocal control is not yet well characterized. To date, only a handful of studies have explored this pathway that involves multiple medullary interneurons (Bass, 2014; Bass, Gilland, & Baker, 2008; Dobbins & Feldman, 1995; Stanek, Cheng, Takatoh, Han, & Wang, 2014). Congenital and acquired speech disorders may result from incorrect assembly and/or regeneration of damaged motor axons. Thus, understanding the molecular mechanisms of cranial MNs and principles of circuit assembly serve an important clinical interest.

Similar to other motor behaviors, vocalization behavior can receive modulation from areas of higher cognition such as the neocortex. It would be extremely interesting to study which of these modulations is governed by the cortical influence and what others are mediated by local circuitry. Being able to produce speech sound is a sensorimotor phenomenon, and each speech sound (phoneme: the smallest unit of spoken language) must be learned for articulation. Indeed, patients with cochlear implants can begin to modify their motor programs for clear articulation after surgery (Nasir & Ostry, 2008). Furthermore, expressive language is often coupled with appropriate facial expression to enhance communication (Fridlund, 1994).

The speech and gesture producing circuitry may be linked with considerable overlap especially in the areas of higher cognitive function (Goldin-Meadow & Alibali, 2013; Willems, Ozyurek, & Hagoort, 2007). In non-human primates, recent studies promote the idea that speech rhythm may have originated from rhythmic facial motion in a specific frequency range such as lip smacking (Ghazanfar & Takahashi, 2014). It is yet unknown how much of this phenomena is conserved in rodent animals, but this would

provide an interesting insight into the rudimentary circuitry underlying speech and gesture. It would be of great challenge or may even be an impossible feat to study aspects of language that are unique to humans. However, with novel techniques of using stem cell-derived organoid cultures, multiple labs including our own are seeking out ways to define the origins of the key players and initial wiring of circuits using layered human cortical organoid culture systems (Eiraku & Sasai, 2012; Sasai, 2013).

It is of a special interest that multiple case reports identify FOXP1 as the culprit in patients with a syndrome of language impairment and mental retardation. Homozygous mutation of FOXP1 would likely result in defects in heart development similar to what occurs mouse (Rousso, Gaber, Wellik, Morrisey, & Novitch, 2008). However, FOXP1 haploinsufficiency phenotype has been reported in humans. Patients with FOXP1 mutation tended to have specific facial features in addition to specific impairment of expressive language (Hamdan et al., 2010; Horn et al., 2010). In Chapter 2, I demonstrated that Foxp1 is expressed in MNs that control the movement of the face and the tongue in the developing mouse. I predict that some aspects of language impairment result from the inability to move these muscles critical for communication in addition to other defects in the central nervous system such as the neocortex that may result from the FOXP1 mutation.

Vocalization pathways in the cranial motor circuitry

The laryngeal muscles serve as particular muscles of interest among the muscles innervated by cranial MNs as they have both voluntary and involuntary actions (Berke & Long, 2010). These muscles are used in vocalization, swallowing, the cough reflex, and

the gag reflex (Shiba, 2010). During swallowing, the elevation of the hyoid bone pulls the larynx up so that the epiglottis can assume a horizontal position to block the trachea. Furthermore, congenital or acquired vocal cord paralysis can be severely debilitating to affected patients (Cunningham, Eavey, & Shannon, 1985; Kenn & Balkissoon, 2011). Laryngeal muscles are innervated by the nucleus ambiguus in rats, cats and monkeys **(Fig 5-1B, 1C)** (Gacek, 1975; Portillo & Pasaro, 1988; Yoshida, Mitsumasu, Hirano, & Kanaseki, 1985). Although species-specific variations do exist significant differences have been noted between rats and cats/monkeys where cricothyroid MNs and intrinsic laryngeal muscles were organized in two large groups in cats and monkeys (Portillo & Pasaro, 1988). Laryngeal electromyography has been demonstrated to be useful for the diagnosis of the underlying causes of vocal fold symptoms (Simpson, Sternman, Graves-Wright, & Sanders, 1993). Understanding the pathophysiology of vocal cord condition would be extremely important for designing appropriate rehabilitation strategies.

Regenerative therapy to repair diseased respiratory or vocal motor pathways

Recent advances in methods of generating embryonic stem cell- and induced pluripotent stem cell-derived motor neurons opened new avenues for potential applications into repairing diseased or injured motor neurons (Adams, Rousso, Umbach, & Novitch, 2015; Umbach, Adams, Gundersen, & Novitch, 2012; Wichterle, Lieberam, Porter, & Jessell, 2002). Forcefully expressing a critical limb-innervating motor neuron program resulted in directed differentiation of embryonic stem cell-derived motor neuron that successfully innervated the limbs (Adams et al., 2015). Although spinal MNs and

cranial MNs are placed in a different rostrocaudal (i.e. Hox) context, a similar approach may be used to direct diffentiation of stem cells to a specific cranial MN character.

Multiple studies have hypothesized that the RMC (or hypaxial motor column-HMC) is evolutionally more ancient compared to the limb-innervating lateral motor column (Dasen, De Camilli, Wang, Tucker, & Jessell, 2008; Dasen & Jessell, 2009; Jung et al., 2010; Jung et al., 2014; Rousso et al., 2008). It is likely that for this reason that RMC MNs are more compatible with many other muscles in the developing nervous system. Previous thoracic transplantation studies into the brachial spinal cord resulted in innervation followed by massive denervation of wing-associated muscles in the developing chick embryo (Butler, Cauwenbergs, & Cosmos, 1986). However, Butler et al did not examine the distal nerves of the forelimbs as I have done in Chapter 3. It may be possible that only the proximal muscles have been affected by this transplantation experiment in the thoracic transplantation into the brachial spinal cord.

Considerable compatibility exists between phrenic and limb-projecting MNs even in adults. In brachial plexus injury or peripheral nerve grafts, the phrenic MNs inadvertently innervate the forelimb muscles to provide respiratory drive, which have been documented as the "breathing arm" phenomena (Carlstedt, Anand, Htut, Misra, & Svensson, 2004; Swift, 1994). Furthermore, many collateral descending inputs into the phrenic MNs exist in the developing and adult central nervous system that allows for respiratory innervation of the MNs. Thus, due to the flexibility of the respiratory motor circuit, I predict that transplantation of MNs in patients of spinal cord injury may not require as stringent molecular and physiological specificity as that of the limb-innervating MNs.

Molecular basis of respiratory cell fate determination

Previous studies analyzing the roles of HoxA5 and Pou3f1 in phrenic MN development reported that the two transcription factors work in conjunction for proper development of phrenic MNs (Machado et al., 2014; Philippidou, Walsh, Aubin, Jeannotte, & Dasen, 2012). Multiple markers of the phrenic MNs and the respiratory motor column (RMC) have been suggested in these papers, but from my findings in Chapter 4 many of these molecules can be expressed even in the absence of Pou3f1. Furthermore, the phrenic-associated markers are not unique to phrenic MNs but pervade throughout the respiratory MNs in the brainstem and the thoracic RMC. My findings in Chapter 3 also showed that not only is the respiratory phenotype suppressed by Foxp1 upon induction into the LMC phenotype, but the potential for the assembly of respiratory circuitry as a whole is suppressed as well.

Combining together my findings in Chapter 2 where Pou3f1 can be found in all MNs that innervate muscles critical for rhythmic behaviors and appearance of rhythmic activity with Pou3f1+ RMC-like population by removal of Foxp1 suggest that Pou3f1 might be involved in establishment of rhythmic circuitry in the central nervous system. Indeed, Pou3f1 expression is prominent in the facial nucleus involved in whisking behavior, and the recent studies of this circuitry concluded that the pre-Bötzinger is the critical master oscillator in rhythmic activity including whisking behavior in rodents (Moore et al., 2013). I believe Pou3f1 expression correlates or even may play an aspect in the circuit assembly of relaying this rhythmic activity from the rhythm generators.

Molecular basis of respiratory motor circuit assembly

In Chapter 3, I demonstrated that the limb-innervating MNs in the absence of Foxp1 receive respiratory drive. This is yet more evidence that the respiratory motor circuit assembly is protected by many redundancies and multiple plasticity mechanisms during development to ensure the correct circuit layout. When a hemisection or lateral contusion is performed in the adult spinal cord rostral to the location of phrenic MNs, the contralateral phrenic MNs can receive the respiratory drive as demonstrated by the transection of the contralateral phrenic nerve **(Fig 5-2A-2C)**. This finding, named cross phrenic phenomena (CPP), was originally documented in 1895 by Porter in dogs and rabbits, and subsequently explored in possible therapeutic options for restoring respiratory abilities in patients with SCI (Goshgarian, 2009). While it had been debated whether it was the dendrites of the phrenic MNs or the axons extending from the contralateral rostral ventral respiratory group (rVRG), it was demonstrated that the prevailing input is due to the rVRG input from the contralateral medulla that crosses the midline to form contact with phrenic MNs present in the ipsilateral side to the injury (Moreno, Yu, & Goshgarian, 1992). Furthermore, the process in which that the respiratory motor circuit can rewire takes hours, although this process is instantaneous in neonatal pups showing that the crossed fibers are functional during development (Minor, Akison, Goshgarian, & Seeds, 2006; Zimmer & Goshgarian, 2005). CPP could be demonstrated using local plasticity elicited by light-induced channelrhodopsins, which can induce CPP in an NMDA-dependent manner (Alilain et al., 2008). As breathing is

undeniably the most important life-sustaining behavior, CPP is only one of the multiple mechanisms that repairs and guards to preserve the function of this circuitry.

My findings that the respiratory drive can extend to respiratory converted limb-innervating brachial MNs open up a series of new questions that would help us understand the developmental dynamics of the respiratory motor circuit organization. First, where and what are the origins of respiratory premotor neurons in the brainstem and the spinal cord? Classical anterograde and retrograde labeling experiments with tracers from various respiratory center and transynaptic viruses in respiratory muscles have documented the existence the location of these interneurons (Billig, Foris, Card, & Yates, 1999; Billig, Foris, Enquist, Card, & Yates, 2000; Billig, Hartge, Card, & Yates, 2001; Dobbins & Feldman, 1994; Yates, Smail, Stocker, & Card, 1999). Although the morphology and projection patterns have been meticulously documented by early pioneers, now we have the molecular and genetic tools to trace the developmental lineage of these neurons. Indeed, several reports have now demonstrated that the medullary oscillator Pre-Bötzinger complex originates from the *Dbx1*-lineage (Bouvier et al., 2010; Gray et al., 2010; Wang et al., 2014). Furthermore, the advent of light-induced channelrhodopsins has provided an unprecedented opportunities where specific interneuron classes can be now activated for their contributions in modulation of respiratory MN activity or forging of the connections (Chang, Strochlic, Williams, Umans, & Liberles, 2015; Sherman, Worrell, Cui, & Feldman, 2015).

Secondly, what is the developmental mechanism that allows for correct anatomical layout of the respiratory motor circuitry? In Chapter 3, I have identified the Semaphorin family as possible candidates for attracting respiratory motor fibers and

repelling fibers that do not contribute to respiratory functions. The identification of new families of guidance molecules and previously identified molecules that have been revisited for guidance functions-such as the bone morphogenetic protein family- may contribute to the proper assembly of motor circuits (Yamauchi, Phan, & Butler, 2008). It would be exciting to understand what specific molecules are the key players in the wiring process. Due to the similarities found in CPP and respiratory conversion phenotype of extending the respiratory premotor fibers beyond their usual target of innervation, it would be useful to screen for CPP in mutant pups of different Semaphorin or other guidance cue mutations to see their roles in medio-lateral extension of the respiratory drive, and then generating a Foxp1-mutant mouse with the mutation of the specific guidance protein to assess their roles in extension of respiratory drive rostrocaudally.

Finally, CPP and respiratory conversion could result from a purely activity-dependent plasticity phenomenon. Since the initial observation by Hubel and Wiesel of the optical columns in the visual cortex, it is known that early passive sensory experience has tremendous influence in circuit assembly in sensory areas (Hubel & Wiesel, 1962; Recanzone, Schreiner, & Merzenich, 1993). Even in motor systems, the elimination of neuromuscular junction and spontaneous motor activity are intricately related, where increased motor activity enhances the elimination of the neuromuscular junction (Thompson, 1983). Thus, it would be ideal to study the respiratory motor circuit assembly at the earliest time point when rVRG has made contact with respiratory MNs and interneurons and the system has not yet had any opportunity of alteration by presence or absence of motor activity. A related important feature of MNs that the field needs to explore is the intrinsic difference of different types of MNs. It is widely accepted that

MNs are excited by glutamate transmission and inhibited by gamma-aminobutyric acid. However, the MN receives much more including monoamine and peptide neurotransmitters- epinephrine, norepinephrine, enkephalin, and serotonin to name a few.

Similar to the MN-muscle matching process, it is likely that ligand/receptor specificity is also present that could gate the specificity of activation or specificity in circuit assembly; furthermore, the sensitivity of the MNs to the ligands and the physiological cascade of ion channel opening resulting from the initial spike also needs to be explored (Rekling, Funk, Bayliss, Dong, & Feldman, 2000). In the developing spinal cord, multiple morphogens work in a gradient-dependent manner to assign progenitor cell fates (Dessaud et al., 2007). Premotor afferents may reuse similar concentration-dependent mechanisms for other ligands/receptor pairs. I predict that phrenic MNs would be much more sensitive to excitatory inputs compared to the limb- or axial-musculature innervating MNs as phrenic MNs serve life-sustaining function. Currently, multiple laboratories around the world including our lab are working together to delineate the molecular recipe for generation of phrenic MNs and molecules that are required for proper innervation of the respiratory motor circuit, which will ultimately be translated to clinical therapy that will impact the quality of life of patients suffering from multiple disorders involving breathing pathways.

CONCLUSION

The diversity of cranial and spinal MNs involved in respiration and other reflexive behavior has been characterized in my dissertation. My study demonstrates that the respiratory drive can extend to limb-innervating brachial MN populations that normally do not receive respiratory drive. The respiratory conversion phenotype resembles the crossed phrenic phenomenon, in which respiratory drive innervates respiratory MNs beyond their usual territory of innervation. In addition, as now we have a better understanding of the organization of the diversity of cranial MNs, it would be of high clinical interest to assess their molecular organization in disease or injury models or to study the mechanisms that underlie the proper wiring of microcircuits that is important for coughing and vocalization.

FIGURES

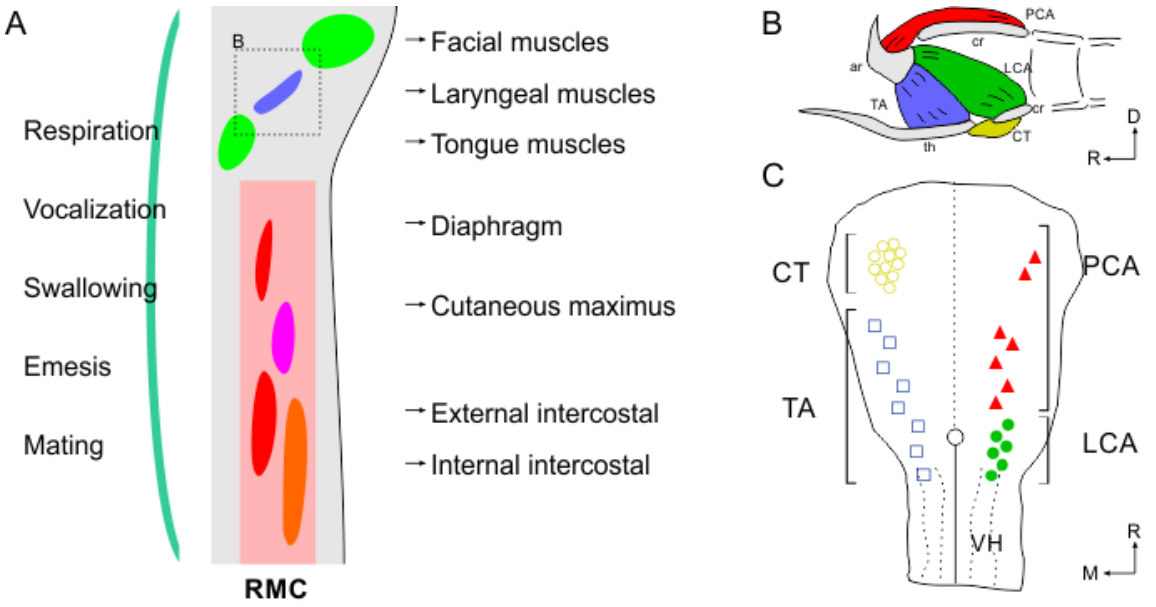

Figure 5-1. Behavioral relevance of respiratory motor neurons in the brainstem and the spinal cord

(A) Summary of respiratory motor neuron organization in the brainstem into respiratory motor nuclei and in the spinal cord into respiratory motor columns. Motor behaviors that these motor neurons activate in concert are listed on the left.

(B, C) Musculotopic innervation pattern of the laryngeal muscles in the rat. Adapted from Portillo and Pasaro, 1988; ar = Arytenoid cartilage; cr = cricoid cartilage; th = thyroid cartilage; CT = cricohyoid muscle; TA = thyroarytenoid muscle; PCA = posterior cricoarytenoid muscle; LCA = lateral cricoarytenoid muscle.

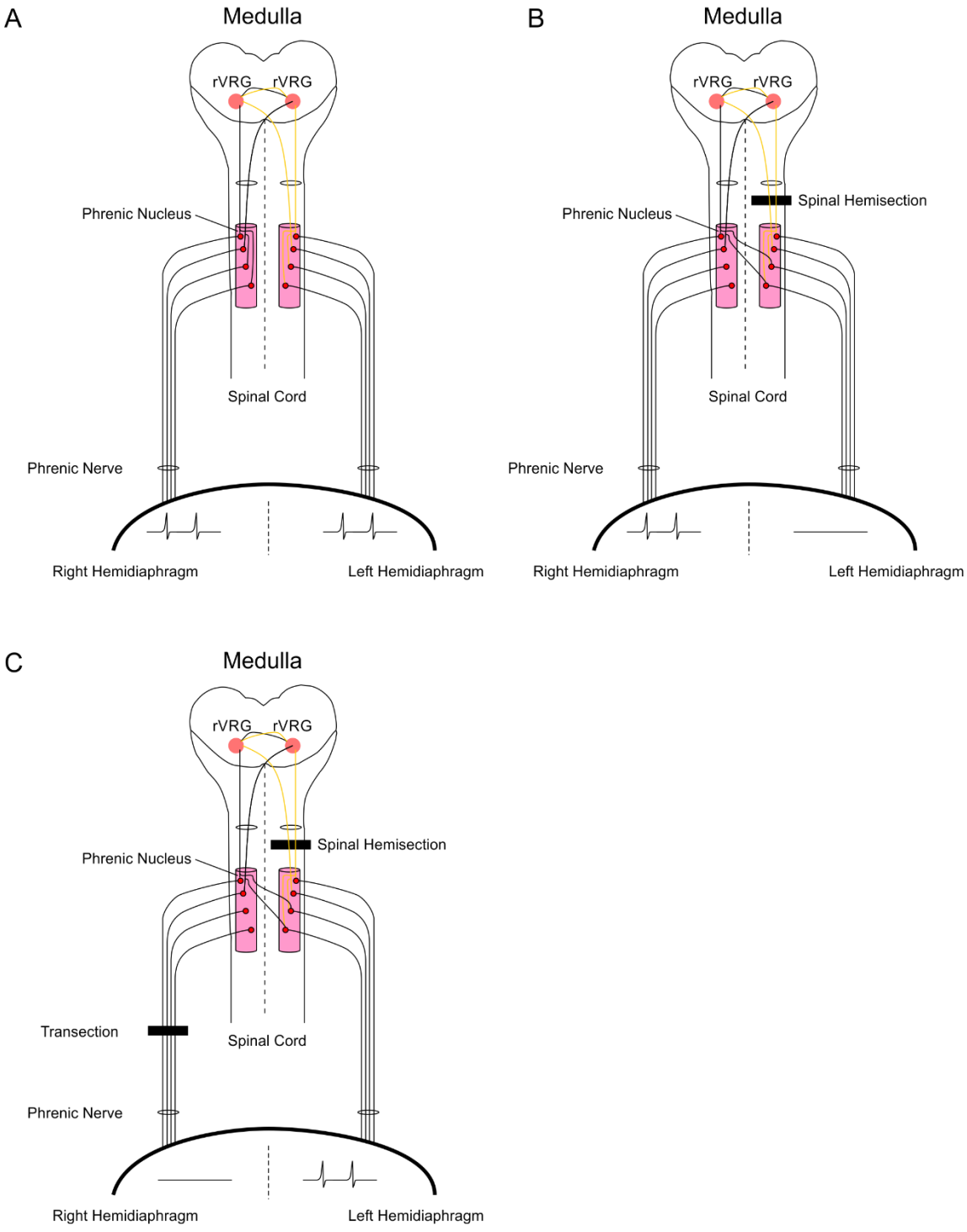

Figure 5-2. Crossed phrenic phenomenon illustrated in sequence of events

(A) Innervation of the respiratory motor circuit.

(B) Descending respiratory premotor fibers cross the midline in the spinal cord after spinal hemisection.

(C) The transection of the contralateral phrenic nerve results in preserved diaphragm activity in the injured animal.

REFERENCES

Adams, K. L., Rousso, D. L., Umbach, J. A., & Novitch, B. G. (2015). Foxp1-mediated programming of limb-innervating motor neurons from mouse and human embryonic stem cells. *Nat Commun, 6*, 6778. doi: 10.1038/ncomms7778

Alilain, W. J., Li, X., Horn, K. P., Dhingra, R., Dick, T. E., Herlitze, S., & Silver, J. (2008). Light-induced rescue of breathing after spinal cord injury. *J Neurosci, 28*(46), 11862-11870. doi: 10.1523/jneurosci.3378-08.2008

Ashwell, K. W. (1982). The adult mouse facial nerve nucleus: morphology and musculotopic organization. *J Anat, 135*(Pt 3), 531-538.

Bass, A. H. (2014). Central pattern generator for vocalization: is there a vertebrate morphotype? *Curr Opin Neurobiol, 28*, 94-100. doi: 10.1016/j.conb.2014.06.012

Bass, A. H., Gilland, E. H., & Baker, R. (2008). Evolutionary origins for social vocalization in a vertebrate hindbrain-spinal compartment. *Science, 321*(5887), 417-421. doi: 10.1126/science.1157632

Berke, G. S., & Long, J. L. (2010). Chapter 10.1 - Functions of the larynx and production of sounds. In M. B. Stefan (Ed.), *Handbook of Behavioral Neuroscience* (Vol. Volume 19, pp. 419-426): Elsevier.

Billig, I., Foris, J. M., Card, J. P., & Yates, B. J. (1999). Transneuronal tracing of neural pathways controlling an abdominal muscle, rectus abdominis, in the ferret. *Brain Res, 820*(1-2), 31-44.

Billig, I., Foris, J. M., Enquist, L. W., Card, J. P., & Yates, B. J. (2000). Definition of neuronal circuitry controlling the activity of phrenic and abdominal motoneurons in the ferret using recombinant strains of pseudorabies virus. *J Neurosci, 20*(19), 7446-7454.

Billig, I., Hartge, K., Card, J. P., & Yates, B. J. (2001). Transneuronal tracing of neural pathways controlling abdominal musculature in the ferret. *Brain Res, 912*(1), 24-32.

Bolhuis, J. J., Tattersall, I., Chomsky, N., & Berwick, R. C. (2014). How could language have evolved? *PLoS Biol, 12*(8), e1001934. doi: 10.1371/journal.pbio.1001934

Bouvier, J., Thoby-Brisson, M., Renier, N., Dubreuil, V., Ericson, J., Champagnat, J., . . . Fortin, G. (2010). Hindbrain interneurons and axon guidance signaling critical for breathing. *Nat Neurosci, 13*(9), 1066-1074. doi: 10.1038/nn.2622

Butler, J., Cauwenbergs, P., & Cosmos, E. (1986). Fate of brachial muscles of the chick embryo innervated by inappropriate nerves: structural, functional and histochemical analyses. *J Embryol Exp Morphol, 95*, 147-168.

Carlstedt, T., Anand, P., Htut, M., Misra, P., & Svensson, M. (2004). Restoration of hand function and so called "breathing arm" after intraspinal repair of C5-T1 brachial plexus avulsion injury. Case report. *Neurosurg Focus, 16*(5), E7.

Chang, R. B., Strochlic, D. E., Williams, E. K., Umans, B. D., & Liberles, S. D. (2015). Vagal Sensory Neuron Subtypes that Differentially Control Breathing. *Cell, 161*(3), 622-633. doi: 10.1016/j.cell.2015.03.022

Cunningham, M. J., Eavey, R. D., & Shannon, D. C. (1985). Familial vocal cord dysfunction. *Pediatrics, 76*(5), 750-753.

Dasen, J. S., De Camilli, A., Wang, B., Tucker, P. W., & Jessell, T. M. (2008). Hox repertoires for motor neuron diversity and connectivity gated by a single accessory factor, FoxP1. *Cell, 134*(2), 304-316. doi: 10.1016/j.cell.2008.06.019

Dasen, J. S., & Jessell, T. M. (2009). Hox networks and the origins of motor neuron diversity. *Curr Top Dev Biol, 88*, 169-200. doi: 10.1016/s0070-2153(09)88006-x

Dessaud, E., Yang, L. L., Hill, K., Cox, B., Ulloa, F., Ribeiro, A., . . . Briscoe, J. (2007). Interpretation of the sonic hedgehog morphogen gradient by a temporal adaptation mechanism. *Nature, 450*(7170), 717-720. doi: 10.1038/nature06347

Dobbins, E. G., & Feldman, J. L. (1994). Brainstem network controlling descending drive to phrenic motoneurons in rat. *J Comp Neurol, 347*(1), 64-86. doi: 10.1002/cne.903470106

Dobbins, E. G., & Feldman, J. L. (1995). Differential innervation of protruder and retractor muscles of the tongue in rat. *J Comp Neurol, 357*(3), 376-394. doi: 10.1002/cne.903570305

Eiraku, M., & Sasai, Y. (2012). Mouse embryonic stem cell culture for generation of three-dimensional retinal and cortical tissues. *Nat Protoc, 7*(1), 69-79. doi: 10.1038/nprot.2011.429

Fischer, J., & Hammerschmidt, K. (2011). Ultrasonic vocalizations in mouse models for speech and socio-cognitive disorders: insights into the evolution of vocal communication. *Genes Brain Behav, 10*(1), 17-27. doi: 10.1111/j.1601-183X.2010.00610.x

Fridlund, A. J. (1994). *Human facial expression : an evolutionary view*. San Diego: Academic Press.

Gacek, R. R. (1975). Localization of laryngeal motor neurons in the kitten. *Laryngoscope, 85*(11 pt 1), 1841-1861. doi: 10.1288/00005537-197511000-00007

Ghazanfar, A. A., & Takahashi, D. Y. (2014). Facial expressions and the evolution of the speech rhythm. *J Cogn Neurosci, 26*(6), 1196-1207. doi: 10.1162/jocn_a_00575

Goldin-Meadow, S., & Alibali, M. W. (2013). Gesture's role in speaking, learning, and creating language. *Annu Rev Psychol, 64*, 257-283. doi: 10.1146/annurev-psych-113011-143802

Goshgarian, H. G. (2009). The Crossed Phrenic Phenomenon and Recovery of Function Following Spinal Cord Injury. *Respiratory physiology & neurobiology, 169*(2), 85-93. doi: 10.1016/j.resp.2009.06.005

Gray, P. A., Hayes, J. A., Ling, G. Y., Llona, I., Tupal, S., Picardo, M. C., . . . Del Negro, C. A. (2010). Developmental origin of preBotzinger complex respiratory neurons. *J Neurosci, 30*(44), 14883-14895. doi: 10.1523/jneurosci.4031-10.2010

Hamdan, F. F., Daoud, H., Rochefort, D., Piton, A., Gauthier, J., Langlois, M., . . . Michaud, J. L. (2010). De novo mutations in FOXP1 in cases with intellectual disability, autism, and language impairment. *Am J Hum Genet, 87*(5), 671-678. doi: 10.1016/j.ajhg.2010.09.017

Horn, D., Kapeller, J., Rivera-Brugues, N., Moog, U., Lorenz-Depiereux, B., Eck, S., . . . Strom, T. M. (2010). Identification of FOXP1 deletions in three unrelated patients with mental retardation and significant speech and language deficits. *Hum Mutat, 31*(11), E1851-1860. doi: 10.1002/humu.21362

Hubel, D. H., & Wiesel, T. N. (1962). Receptive fields, binocular interaction and functional architecture in the cat's visual cortex. *The Journal of Physiology, 160*(1), 106-154.102.

Jung, H., Lacombe, J., Mazzoni, E. O., Liem, K. F., Jr., Grinstein, J., Mahony, S., . . . Dasen, J. S. (2010). Global control of motor neuron topography mediated by the repressive actions of a single hox gene. *Neuron, 67*(5), 781-796. doi: 10.1016/j.neuron.2010.08.008

Jung, H., Mazzoni, E. O., Soshnikova, N., Hanley, O., Venkatesh, B., Duboule, D., & Dasen, J. S. (2014). Evolving Hox activity profiles govern diversity in locomotor systems. *Dev Cell, 29*(2), 171-187. doi: 10.1016/j.devcel.2014.03.008

Kenn, K., & Balkissoon, R. (2011). Vocal cord dysfunction: what do we know? *Eur Respir J, 37*(1), 194-200. doi: 10.1183/09031936.00192809

Kleinfeld, D., Deschenes, M., Wang, F., & Moore, J. D. (2014). More than a rhythm of life: breathing as a binder of orofacial sensation. *Nat Neurosci, 17*(5), 647-651. doi: 10.1038/nn.3693

Lahvis, G. P., Alleva, E., & Scattoni, M. L. (2011). Translating mouse vocalizations: prosody and frequency modulation. *Genes Brain Behav, 10*(1), 4-16. doi: 10.1111/j.1601-183X.2010.00603.x

Lieberman, P. (2015). Language did not spring forth 100,000 years ago. *PLoS Biol, 13*(2), e1002064. doi: 10.1371/journal.pbio.1002064

Machado, C. B., Kanning, K. C., Kreis, P., Stevenson, D., Crossley, M., Nowak, M., . . . Lieberam, I. (2014). Reconstruction of phrenic neuron identity in embryonic stem cell-derived motor neurons. *Development, 141*(4), 784-794. doi: 10.1242/dev.097188

McClung, J. R., & Goldberg, S. J. (2000). Functional anatomy of the hypoglossal innervated muscles of the rat tongue: a model for elongation and protrusion of the mammalian tongue. *Anat Rec, 260*(4), 378-386.

Minor, K. H., Akison, L. K., Goshgarian, H. G., & Seeds, N. W. (2006). Spinal cord injury-induced plasticity in the mouse--the crossed phrenic phenomenon. *Exp Neurol, 200*(2), 486-495. doi: 10.1016/j.expneurol.2006.02.125

Moore, J. D., Deschenes, M., Furuta, T., Huber, D., Smear, M. C., Demers, M., & Kleinfeld, D. (2013). Hierarchy of orofacial rhythms revealed through whisking and breathing. *Nature, 497*(7448), 205-210. doi: 10.1038/nature12076

Moore, J. D., Kleinfeld, D., & Wang, F. (2014). How the brainstem controls orofacial behaviors comprised of rhythmic actions. *Trends Neurosci, 37*(7), 370-380. doi: 10.1016/j.tins.2014.05.001

Moreno, D. E., Yu, X. J., & Goshgarian, H. G. (1992). Identification of the axon pathways which mediate functional recovery of a paralyzed hemidiaphragm following spinal cord hemisection in the adult rat. *Exp Neurol, 116*(3), 219-228.

Nasir, S. M., & Ostry, D. J. (2008). Speech Motor Learning in Profoundly Deaf Adults. *Nature neuroscience, 11*(10), 1217-1222. doi: 10.1038/nn.2193

Philippidou, P., Walsh, C. M., Aubin, J., Jeannotte, L., & Dasen, J. S. (2012). Sustained Hox5 gene activity is required for respiratory motor neuron development. *Nat Neurosci, 15*(12), 1636-1644. doi: 10.1038/nn.3242

Portillo, F., & Pasaro, R. (1988). Location of motoneurons supplying the intrinsic laryngeal muscles of rats. Horseradish peroxidase and fluorescence double-labeling study. *Brain Behav Evol, 32*(4), 220-225.

Recanzone, G. H., Schreiner, C. E., & Merzenich, M. M. (1993). Plasticity in the frequency representation of primary auditory cortex following discrimination training in adult owl monkeys. *J Neurosci, 13*(1), 87-103.

Rekling, J. C., Funk, G. D., Bayliss, D. A., Dong, X. W., & Feldman, J. L. (2000). Synaptic control of motoneuronal excitability. *Physiol Rev, 80*(2), 767-852.

Rousso, D. L., Gaber, Z. B., Wellik, D., Morrisey, E. E., & Novitch, B. G. (2008). Coordinated actions of the forkhead protein Foxp1 and Hox proteins in the columnar organization of spinal motor neurons. *Neuron, 59*(2), 226-240. doi: 10.1016/j.neuron.2008.06.025

Sasai, Y. (2013). Cytosystems dynamics in self-organization of tissue architecture. *Nature, 493*(7432), 318-326. doi: 10.1038/nature11859

Scattoni, M. L., Crawley, J., & Ricceri, L. (2009). Ultrasonic vocalizations: a tool for behavioural phenotyping of mouse models of neurodevelopmental disorders. *Neurosci Biobehav Rev, 33*(4), 508-515. doi: 10.1016/j.neubiorev.2008.08.003

Sherman, D., Worrell, J. W., Cui, Y., & Feldman, J. L. (2015). Optogenetic perturbation of preBotzinger complex inhibitory neurons modulates respiratory pattern. *Nat Neurosci, 18*(3), 408-414. doi: 10.1038/nn.3938

Shiba, K. (2010). Chapter 9.1 - Functions of larynx in breathing, vocalization and airway protective reflexes. In M. B. Stefan (Ed.), *Handbook of Behavioral Neuroscience* (Vol. Volume 19, pp. 373-381): Elsevier.

Simpson, D. M., Sternman, D., Graves-Wright, J., & Sanders, I. (1993). Vocal cord paralysis: clinical and electrophysiologic features. *Muscle Nerve, 16*(9), 952-957. doi: 10.1002/mus.880160911

Stanek, E. t., Cheng, S., Takatoh, J., Han, B. X., & Wang, F. (2014). Monosynaptic premotor circuit tracing reveals neural substrates for oro-motor coordination. *Elife, 3*, e02511. doi: 10.7554/eLife.02511

Swift, T. R. (1994). The breathing arm. *Muscle Nerve, 17*(1), 125-129. doi: 10.1002/mus.880170122

Thompson, W. (1983). Synapse elimination in neonatal rat muscle is sensitive to pattern of muscle use. *Nature, 302*(5909), 614-616.

Umbach, J. A., Adams, K. L., Gundersen, C. B., & Novitch, B. G. (2012). Functional neuromuscular junctions formed by embryonic stem cell-derived motor neurons. *PLoS One, 7*(5), e36049. doi: 10.1371/journal.pone.0036049

Wang, X., Hayes, J. A., Revill, A. L., Song, H., Kottick, A., Vann, N. C., . . . Del Negro, C. A. (2014). Laser ablation of Dbx1 neurons in the pre-Botzinger complex stops inspiratory rhythm and impairs output in neonatal mice. *Elife, 3*, e03427. doi: 10.7554/eLife.03427

Wichterle, H., Lieberam, I., Porter, J. A., & Jessell, T. M. (2002). Directed differentiation of embryonic stem cells into motor neurons. *Cell, 110*(3), 385-397.

Willems, R. M., Ozyurek, A., & Hagoort, P. (2007). When language meets action: the neural integration of gesture and speech. *Cereb Cortex, 17*(10), 2322-2333. doi: 10.1093/cercor/bhl141

Yamauchi, K., Phan, K. D., & Butler, S. J. (2008). BMP type I receptor complexes have distinct activities mediating cell fate and axon guidance decisions. *Development, 135*(6), 1119-1128. doi: 10.1242/dev.012989

Yates, B. J., Smail, J. A., Stocker, S. D., & Card, J. P. (1999). Transneuronal tracing of neural pathways controlling activity of diaphragm motoneurons in the ferret. *Neuroscience, 90*(4), 1501-1513.

Yoshida, Y., Mitsumasu, T., Hirano, M., & Kanaseki, T. (1985). Somatotopic representation of the laryngeal motoneurons in the medulla of monkeys. *Acta Otolaryngol, 100*(3-4), 299-303.

Yoshikawa, M., Hirabayashi, M., Ito, R., Ozaki, S., Aizawa, S., Masuda, T., . . . Shiga, T. (2015). Contribution of the Runx1 transcription factor to axonal pathfinding and muscle innervation by hypoglossal motoneurons. *Dev Neurobiol*. doi: 10.1002/dneu.22285

Zimmer, M. B., & Goshgarian, H. G. (2005). Spontaneous crossed phrenic activity in the neonatal respiratory network. *Exp Neurol, 194*(2), 530-540. doi: 10.1016/j.expneurol.2005.03.013